THE ACTIVITIES OF Cu_2O and NiO IN SILICATE SLAGS

A THESIS

by

JEFFREY RICHARD TAYLOR

Department of Metallurgy,

Imperial College.

September 1973.

SYNOPSIS

Activities of $CuO._5$ and NiO have been measured in iron silicate slags varying in composition from about 38 wt% SiO_2 (silica saturation) to 13 wt% SiO_2, over a range of temperatures from 1300°C to 1500°C, and oxygen partial pressures from 10^{-10} to 10^{-6} atm.

A levitation melting technique was used in which powdered slag was added to molten copper/gold and copper/nickel alloys, levitated in a gas stream of known CO/CO_2 ratio.

Activity coefficients of $CuO._5$ and NiO were not greatly affected by changes in slag composition over the range of conditions studied. At low copper slag contents, $\gamma_{CuO._5}$ changed from 2.96 to 2.74 as the silica content decreased from 38 wt% to 12 wt% (at constant copper activity of 0.96). γ_{NiO} changed from 1.33 at silica saturation to 1.17 in a 13% silica slag.

TABLE OF CONTENTS

SYMBOLS USED

aNiO	indicates activity of e.g. nickel oxide.
N NiO	indicates mol. fraction of e.g. nickel oxide.
γ	indicates activity coefficient.
( )	indicates a liquid phase,or occasionally, a component in a slag phase.
[ ]	indicates a solid phase, or occasionally, a component in a matte phase.

CHAPTER 1.

1. INTRODUCTION

The pyrometallurgical treatment of concentrated copper ores leads to a recovery in the order of over 97% of the copper.

This suggests the processes involved are extremely efficient,but to judge by the amount of research, both in industry and Universities, applied to the problem of copper losses, it is clear that there is considerable incentive to raise the recovery figure even higher.

Most of the unrecovered metal is lost in the slags discarded from the process. It is thought that a knowledge and understanding of the chemical and physical properties of such slags will aid the running of the process and the recovery of the metal. In this present work, activities of copper and nickel oxide in iron silicate slags are measured over a wide range of conditions.

This first chapter is intended as a background to the main part of the thesis and gives an outline of the pyrometallurgical treatment of copper and nickel ores, a review of the nature of slags, a literature survey of other relevant work, and a description of the aims of this work.

2. THE PYROMETALLURGICAL EXTRACTION OF COPPER AND NICKEL

(a) Copper Extraction

Most copper is today extracted from ores in which copper is associated with sulphur, and usually iron. The important minerals are chalcopyrite $CuFeS_2$, chalcocite Cu_2S, bornite Cu_5FeS_4, and more complex minerals associated with compounds of zinc, arsenic, antimony, bismuth and precious metals. The copper content of the ore is usually under 5% and often under 2%. Oxidised copper ores, produced by natural weathering of sulphide ores, are metallurgically attractive since they can be directly reduced to copper, but for this reason, most deposits have been used up many years ago.

Generally,copper ores are crushed, concentrated by flotation methods using Xanthates, and then roasted in order to adjust the sulphur content to produce a suitable matte. Too much sulphur results in a lower grade matte, high in iron content. Roasting also removes some impurities, such as arsenic and antimony, as volatile oxides.

The roasted concentrates are melted in a reverberatory or electric arc furnace. The main purpose is to produce a molten matte (1200-1300°C). This approximates to a mixture of Cu_2S and FeS, usually slightly deficient in sulphur. A slag is formed above the matte from the 'gangue' i.e. from iron and other oxides (CaO, MgO, Al_2O_3) and silica associated with the floated concentrate. Extra silica can be added as necessary, to form a fluid layer with a low melting point (about 1100-1200°C). This slag is usually the only slag discarded from the process, so it is essential that the copper content should be as low as possible. Typical discard slag analyses are given in Table 1.1, pg 4. Slags from later stages are commonly returned to this smelting stage, where slag copper oxides are reduced to matte copper sulphides by the oxidation of FeS from the matte to FeO in the slag. This preferential oxidation of FeS to FeO, and eventual formation of Cu rather than Cu_2O on oxidation of Cu_2S, is a vital part of this method of copper production and deserves further consideration.

The stability of FeS and Cu_2S at about 1100-1200°C are very similar, so the free energy changes for the formation of Cu and Fe by blowing oxygen are also very similar.

i.e. $Cu_2S + O_2 = 2Cu + SO_2$ $\quad \Delta G^\circ_{1100^\circ C}$ -40 Kcal

$FeS + O_2 = Fe + SO_2$ $\quad \Delta G^\circ_{1100^\circ C}$ -42 Kcal

Reverberatory furnace discard slags and matte grades reported for various smelters Table 1.1

Analyses in wt%

	Wet Concentrate, side-charged								Calcine-charged		
Slag	Mufulira	Luanshya	San Manuel	Morenci	Chino	Hayden	Gaspé	Noranda	Noranda	Douglas	Braden
Cu	0.56	0.66	0.40	0.44	0.56	0.34	0.27	0.34	0.37	0.35	0.88
FeO	32.5	32.8	42.9	44.6	47.8	39.9	44.0	42.8	45.1	42.0	54.5
SiO_2	40.6	37.3	36.4	38.7	35.1	37.6	39.0	37.9	38.1	41.7	27.4
CaO	15.5	13.1	5.5	4.6	4.3	3.5	7.0	1.8	1.1	5.6	0.7
Al_2O_3	5.7	9.0	7.1	6.5	8.3	9.6	3.2	7.7	6.5	4.6	11.9
MgO	2.7	2.4	-	0.7	-	-	1.6	1.0	-	-	0.6
S	0.3	0.9	-	0.9	0.8	1.3	0.8	1.6	1.3	0.9	1.2
Matte											
Cu	57.6	47.0	32.0	31.0	40.5	27.2	33.0	28.6	24.4	25.5	50.3
Fe	17.5	24.0	37.9	37.5	29.5	40.7	35.0	36.3	42.2	42.2	-
S	23.7	23.8	30.0	27.7	24.9	-	28.0	27.8	25.8	25.1	-

Converter Slag Analyses, wt%

	Cu	SiO_2	FeO	S	Al_2O_3	CaO
Gaspé	1.5	31.6	52.5	-	-	4.7
Morenci	5.7	27.4	57.8	2.0	3.0	-
Douglas	5.6	23.0	63.0	1.7	2.3	-
Chino	4.01	25.1	60.0	0.7	10.5	0.9

On this basis, oxidation of a matte bath should produce a mixture of iron and copper. This does not happen, of course, and the determining factor in the process is the relative stabilities of the oxides of S, Cu and Fe.

As can be seen from the free energy diagram Fig. 1.1, pg 6, the stable phase in contact with SO_2 for iron is FeO, whilst for copper it is Cu, and not Cu_2O. Fig. 1.2, page 7, (from ref. 1) shows the effect of changing oxygen pressure on the FeS system. At low sulphur levels, iron is oxidised to FeO preferentially to sulphur being oxidised to SO_2. As the sulphur content increases towards FeS composition, SO_2 and FeO are formed simultaneously. In the Cu_2S system, Fig. 1.3, page 7, SO_2 forms preferentially to Cu_2O even at relatively low sulphur levels. This does not mean, of course, that no Cu_2O is formed from the oxidation of a matte bath, but the activity it can reach in the presence of substantial quantities of Fe and S is severely limited. The same arguements apply to nickel sulphide in mattes as apply to cuprous sulphide, although the tendency to form nickel oxide will be somewhat greater.

The molten matte from the melting process is charged into converters, where conversion to copper takes place in two stages. Air is first blown into the matte to oxidise the iron sulphide to SO_2, and iron oxide, which is fluxed with silica to form a slag, leaving almost pure Cu_2S, or white metal. The slag is run off and returned to the reverbatory smelting stage, further matte is added and the process repeated until sufficient white metal is formed to warrant running the second stage of the process. In the second stage, air is blown into the white metal and copper is produced as a second, more dense phase, collecting underneath the Cu_2S phase. Converters are arranged so air is blown into the upper sulphide phase rather than the lower copper phase. The overall reaction is

$$Cu_2S + O_2 = Cu + SO_2$$

The product of the converters is blister copper, about 98-99% pure. Typical converter slag analyses are given in Table 1.1, page 4.

A recent copper smelting innovation is to compress the melting and converting stages into a 'one step' process.[2,3] The principle of the process is that prepared concentrate and flux are fed into a furnace under very turbulent conditions created by air or oxygen lancing of the bath. The concentrates are melted and oxidised to the degree that iron and sulphur form oxides, but copper metal collects as a pool at the bottom of the furnace. The slag formed at this point will contain considerable quantities

FIG.1.1

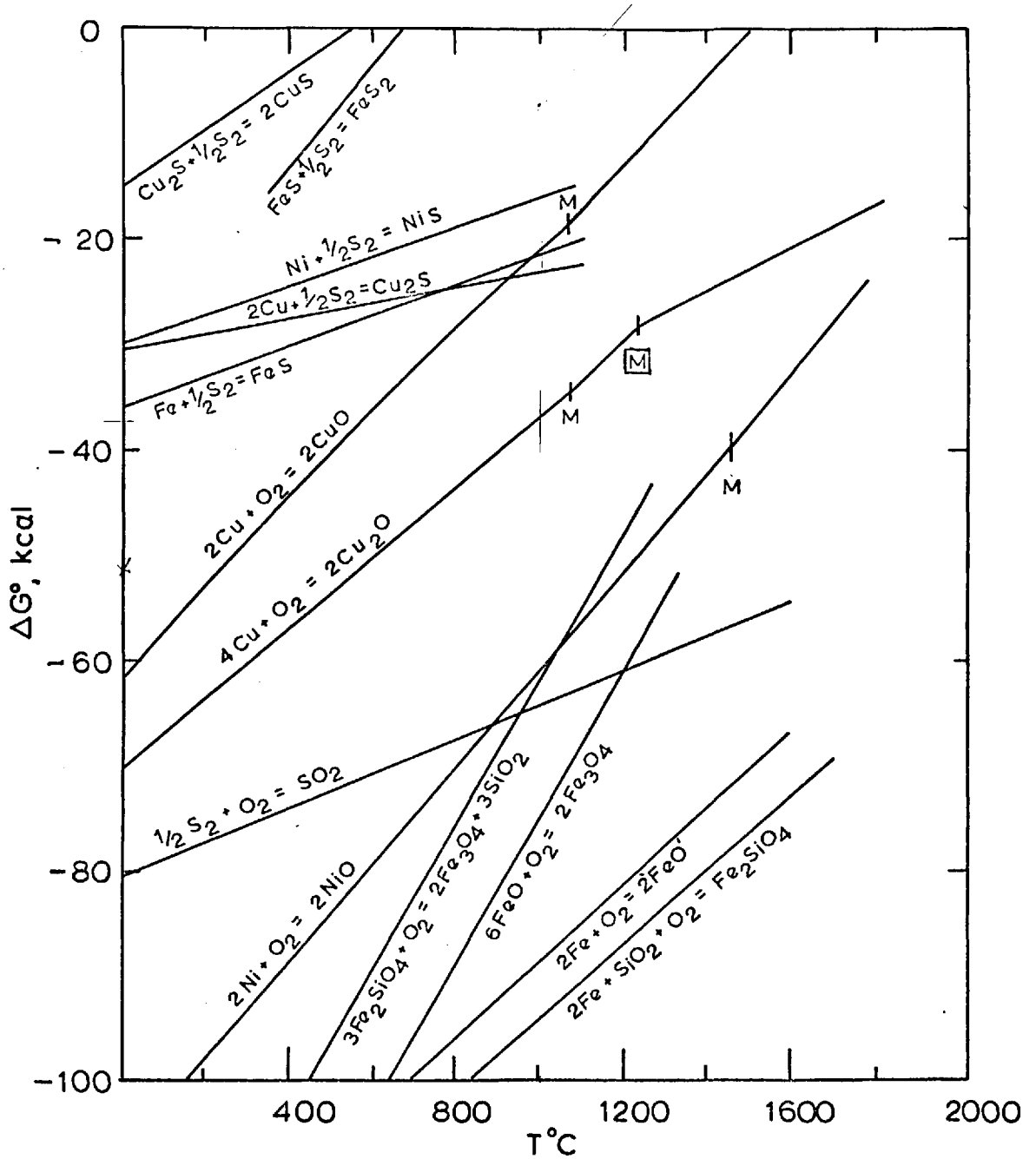

STANDARD FREE ENERGIES OF FORMATION OF OXIDES AND SULPHIDES OF IRON, COPPER AND NICKEL

FIG.1.2

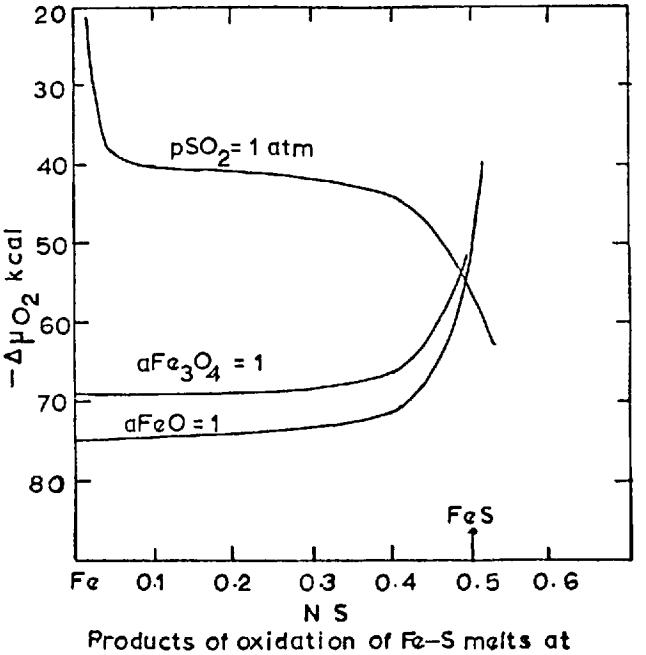

Products of oxidation of Fe–S melts at 1350 °C

FIG.1.3

Products of oxidation of Cu–S melts at 1350 °C

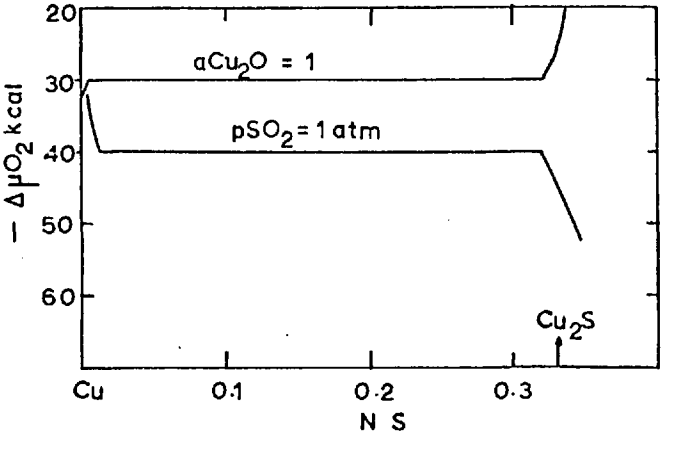

of copper, both as oxidised metal and entrapped sulphide matte. It is necessary either to allow the slag to run to a quieter part of the furnace where reduction by reducing flame and settling out of the matte can occur, or to recover copper from the discarded slag by further treatment, to produce a copper discard comparable with conventional reverbatory furnace procedure.

(b) Nickel Extraction

The majority of world nickel comes from the pentlandite ores, (Ni,Cu,Fe)S, from Sudbury,Ontario. Selective treatment of the crushed ore allows the nickel to be collected as a copper-nickel concentrate, producing a matte low in iron.[4]

The problem of separating the copper from the nickel has been tackled in various ways. For instance, roasting the matte to form a copper and nickel oxide mixture from which the copper can be preferentially leached with sulphuric acid. In the Orford Process, the matte is remelted with coke and sodium sulphate, producing a sodium-copper sulphide 'top' and a nickel sulphide 'bottom' as two immiscible layers. A more recent process[4] relies on the fact that Cu_2S and Ni_3S_2 are almost completely immiscible in the solid state. Molten matte is thus cooled over a period of several days, allowing large crystals of nickel sulphide to form, which can be separated by flotation after crushing.

Sulphur-free nickel silicate ores do not lend themselves to direct reduction smelting, and sulphur is usually added to produce a nickel matte.

Production of nickel from nickel sulphide can be effected by roasting the matte to an oxide, and then reducing the oxide to nickel metal at high temperatures in reverbatory or electric arc furnaces using a carbonaceous reducing agent. Alternatively, water gas or natural gas can be used as a reductant at $300^{o}C$. It is also possible to cast the nickel sulphide into anodes for electrolytic extraction.

Direct conversion of nickel sulphide matte to nickel metal by oxygen blowing has not proved feasible until recently.[5] The process is more difficult than copper converting because of the greater free energy of formation of NiO compared with Cu_2O, and the refractory nature of NiO, formation of which is aggravated by the need to blow into a matte of decreasing sulphur content rather than a sulphide phase of constant composition as in the copper case. These problems have been largely solved by using a top blown rotary Kaldo converter in which turbulent

conditions are created by oxygen lancing and the rotary motion of the converter. The high degree of turbulence ensures that NiO does not build up until most of the sulphur has been removed.

Purification of the metal can be done by electrolytic means, or by the Mond carbonyl process, in which nickel reacts with carbon monoxide at atmospheric pressure and about 60°C to form nickel carbonyl. The reaction reverses on heating to 150°C, depositing high purity nickel. A recently developed high pressure carbonyl process, operating at 180°C and 70 atm., allows formation of iron, cobalt and nickel carbonyls, which can be separated and then decomposed at higher temperatures and atmospheric pressure.

Nickel is not always required as a pure metal, and low grade lateritic ores (1-2% Ni), free from sulphur, but containing iron, are often used to produce ferronickel rather than pure nickel.[6,7] Ferronickel is quite acceptable to the steel industry, for instance, in the production of stainless steel. Typically, the ore is crushed and prepared, but not concentrated, then fed to an electric arc furnace where heating takes place. A reductant is added which reduces the nickel oxide to nickel and part of the iron oxides to iron. The ore usually contains sufficient silica to form a fluid slag. The reductant could be coke breeze, ferro-silicon or a portion of pre-reduced ore which contains metallic iron. The grade of ferronickel can be controlled by the ratio of reductant to ore. The higher the nickel metal content, the greater will be the nickel slag loss. Overall nickel recoveries are quoted at about 91%,[6(a)] 90%,[6(b)] 92-97%,[6(c)] and 97-98%.[7] Most of the losses being in the discard slag.

3. THE NATURE OF SLAGS

Slags are essentially mixtures of metal oxides and silica which are usually homogenous and fluid at the temperatures at which they are formed.

The traditional view of slags was of melts in which the constituents existed as discrete molecular compounds, dissociating into component oxides to varying extents under differing conditions, (e.g. ref. 8).

However, measurement of various physical properties of silicate melts such as electrical conductivity, transport properties, viscosity and surface tension in the early fifties resulted in a view that the melts were ionic in nature. A metal oxide added to the melt would dissociate into charged cations and anions rather than remain as discrete molecules.

(a) Binary Silicates

In pure crystalline silica, each silicon ion (Si^{4+}) forms directional bonds with four oxygen ions, forming an SiO_4^{4-} unit of regular tetrahedral shape, with an oxygen ion at each corner. Each corner oxygen ion is shared by one other Si^{4+} ion, building a three-dimensional crystal of overall formula SiO_2.

Liquid silica is thought to be structurally similar, but with some distortion and loss of regularity. On addition of a divalent oxide, the oxygen ion enters the lattice and breaks into a Si-O-Si bond, forming two O^- 'ends', with which the cation remains associated.

$$Si\text{-}O\text{-}Si + M^{2+} + O^{2-} \longrightarrow Si\text{-}O^- \cdots M^{2+} \cdots O^-\text{-}Si$$

Continued addition of oxide causes progressive breakdown of the silicate lattice, forming a series of silicate anions, the average size of which decreases with increasing basicity of the melt. At orthosilicate composition ($2MO.SiO_2$) there are sufficient oxygen ions for all the silicon to be present as SiO_4^{4-} ions. Early studies of silicates considered further addition of metal oxide resulted in an increase in M^{2+} and O^{2-} ions, the silica remaining as SiO_4^{4-}. (Further breakdown of the SiO_4^{4-} ions to Si^{4+} and O^{2-} is considered probable only at temperatures approaching the boiling point of silica). In the approach outlined above, it was considered that free oxygen ions were unlikely to exist in melts more acid than the orthosilicate composition. For a fuller discussion of much of the above, see refs. 9,10,11.

From considerations of the minimum in the free energy of mixing and other thermodynamic measurements, Richardson [12,13] suggested that substantial proportions of O^{2-} ions could exist in melts between the metasilicate ($MO.SiO_2$) and orthosilicate compositions. Fincham and Richardson[14] recognised three types of oxygen ions in any silicate melt; those bonded to two silicon atoms Si-O-Si those bonded to one silicon atom and associated with a metal atom, e.g. $Si\text{-}O^-.....\frac{1}{2}Ca^{2+}$ and those independant of silica and associated with metal atoms only $O^{2-}\text{-}Ca^{2+}$. They suggested an equilibrium would be set up between these three oxygen types, represented as:

$$2(Si\text{-}O^-) \rightleftharpoons O^{2-} + Si\text{-}O\text{-}Si \ , \quad K = \frac{(O^{2-})\ (Si\text{-}O\text{-}Si)}{(Si\text{-}O^-)^2}$$

and that proportions of the three anion types would depend on the melt composition and the character of the metal cation. In highly siliceous melts, there would be very few O^{2-} ions and in very basic melts, very few oxygens bonded to two silicon atoms. Oxides with large negative free energies of interaction with silica would give low values of K.

This equilibrium between the anionic species of the melt was put on a more quantitative basis by Toop and Samis.[15,16] If the three forms of oxygen are designated O^- for single bonded, O^o for double bonded and O^{2-} for free oxygen ions, then:

$$2O^- \rightleftharpoons O^o + O^{2-} \qquad -(1)$$

and

$$k = \frac{(O^o)\ (O^{2-})}{(O^-)^2} \qquad -(2)$$

k is a constant at a given temperature and is characteristic of the cation present. From considerations of stoichiometry, ionic charge balance and material balance, it is possible to determine values of O^o, O^{2-} and O^- at a given melt composition and assumed value of k. Fig. 1.4, page 12 shows equilibrium values of O^o, O^- and O^{2-} for k = 0.06.

Since oxygen in the pure metal oxide is in the form O^{2-} and in pure silica as O^o, then equation (1) represents the reaction of one mole of divalent oxide with one mole of silica to form 2 moles of binary silicate. The standard free energy change ΔG^o should be given by

$$\frac{\Delta G^o}{4.575\ T} = \log k$$

However, in the formation of one mole of liquid silicate, the number of oxygen ions that have actually reacted in the melt is $\frac{O^-}{2}$, so

FIG. 1.4 Values of O^{2-}, O^- and O° for k = 0.06

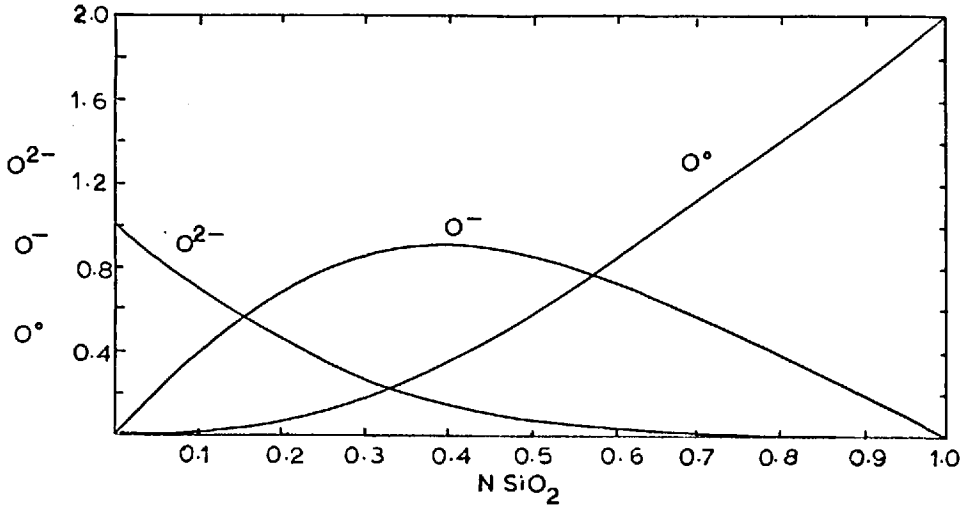

FIG. 1.5

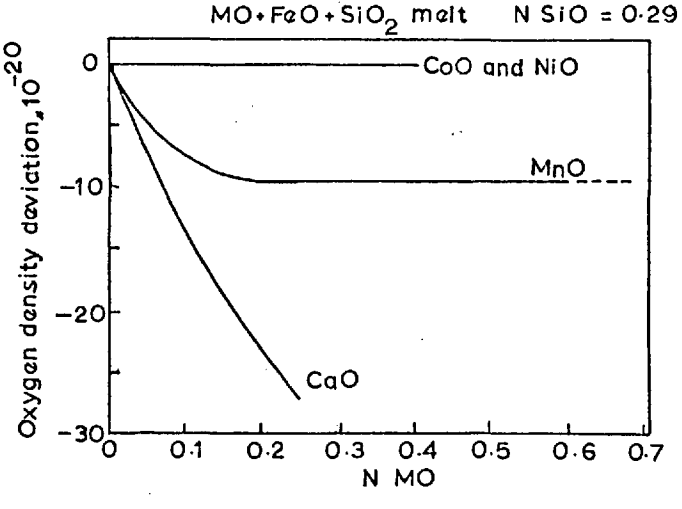

$$\frac{\Delta G \text{ mix}}{4.575\ T} = \frac{O^-}{2} \log k \qquad \text{is suggested.}$$

Curves plotted using various values of k and the corresponding values of O^- show a marked similarity in shape to measured free energy of mixing curves, even though k is expressed in concentration terms rather than activities of the species aO^{2-}, aO^{o} and aO^{-}. The implication is that the free energy of mixing of a binary silicate may arise entirely from the interaction of oxygen ions and silica. A further implication is that in the expression for the free energy of mixing of a binary silicate

$$(1-N\ SiO_2).\log aMO + N\ SiO_2.\log aSiO_2 = \frac{\Delta Gmix}{4.575\ T}$$

aMO may be replaced by aO^{2-}. Since

$$aMO = aO^{2-}.\ aM^{2+}$$

then in a binary silicate, $aM^{2+} = 1$.

Toop and Samis investigated this conclusion by defining the standard state for metal ions such that $aM^{2+} = 1$ when $N\ M^{2+} = 1$, i.e., in pure liquid melts of MO and SiO_2 in all proportions. $N\ M^{2+}$ is the Temkin[17] ion fraction defined as

$$N\ M^{2+} = \frac{\text{number of } M^{2+} \text{ ions}}{\text{sum of positive ions}}$$

Taking Elliott's[18] values for $aSiO_2$ in the ternary $CaO-FeO-SiO_2$, a ternary Gibbs Duhem integration was performed in terms of aFe^{2+}, aCa^{2+} and aO^{2-}. The standard state for O^{2-} ions was the binary oxide where $aO^{2-} = N\ O^{2-} = 1$. The derived values of aFe^{2+}, aCa^{2+} and aO^{2-} gave activities of FeO and CaO which are completely consistent with any other method of ternary integration.

Although this model implies the degree of polymerization of the melt, no conclusions can be drawn concerning the distribution of discrete species without further assumptions.

The approach of Masson[19] to the interpretation of binary silicate structures is a limited extension of the Toop and Samis approach. It is less general in its assumptions, but allows a distribution of individual ions to be calculated.

Masson considered a highly basic $MO-SiO_2$ melt in which depolymerization is virtually complete. On addition of increasing amounts of silica, the degree of polymerization increases by a series of reactions, each involving the SiO_4^{4-} ion, to produce higher members in a series of linear

polyanionic chains, with elimination of an oxygen ion at each condensation step.

$$SiO_4^{4-} + SiO_4^{4-} \rightleftharpoons Si_2O_7^{6-} + O^{2-} \qquad (k_{11})$$

$$SiO_4^{4-} + Si_2O_7^{6-} \rightleftharpoons Si_3O_{10}^{8-} + O^{2-} \qquad (k_{12})$$

$$SiO_4^{4-} + Si_3O_{10}^{8-} \rightleftharpoons Si_4O_{13}^{10-} + O^{2-} \qquad (k_{13})$$

etc.

The assumption is made that $k_{11} = k_{12} = k_{13} = ...= k$. This implies that all the silicate anions are equally reactive. The assumption of Toop and Samis was that k was constant for all condensation steps in which an oxygen ion was eliminated. Masson's assumption is for reactions in which the SiO_4^{4-} ion takes part. Meadowcroft and Richardson[20] studied anionic distributions in phosphate melts, and showed the anionic chain distribution could be expressed by a series of equilibria of the form

$$2(P_nO_{3n+1})^{(n+2)^-} = (P_{n+1}O_{3n+4})^{(n+3)^-} + (P_{n-1}O_{3n-2})^{(n+1)^-}$$

with an equilibrium constant k_n. In practice, k_n approaches unity for n greater than about 2-5. Applying the same equilibria to silicate melts, it can be seen that

Masson's $k_{11} = k_1$ of Meadowcroft and Richardson

" $k_{12} = k_1.k_2$ of Meadowcroft and Richardson

" $k_{13} = k_1.k_2.k_3$ of Meadowcroft and Richardson

Thus Masson's $k_{11} = k_{12} = k_{13} =.....= k$ is valid only if k_1 is the only constant of Meadowcroft and Richardson's equilibria not equal to unity. However, this does appear to be reasonable for silicate melts.[21]

The main limitation of Masson's theory given here is that only linear chain anions are considered to be present. No allowance is made for condensations between pairs of singly bonded oxygen atoms attached to the same polyanion, leading to the formation of ring structures or networks, although it is possible to allow for branching of the chains.[22] This modification need not concern us here.

At a fixed value of k, the ion fraction of all anionic species, including $N\ O^{2-}$, may be calculated as a function of melt composition. Plots of $N\ O^{2-}$ against mole fraction of silica for selected values of k give good approximations to the measured oxide activity curves of various binary silicates. Values of $N\ O^{2-}$ are related to activities by the Temkin equation

$$aMO = N\ M^{2+} . N\ O^{2-}$$

Since N M^{2+} = 1 then aMO = N O^{2-}. The model suggests that metal oxide activities may be approximately related to the oxygen ion fraction. Knowledge of aMO at one composition allows the prediction of aMO at all other compositions (above N MO = 0.5).

The melt, then, consists of M^{2+} cations, O^{2-} anions and an array of silicate anions which can be calculated from the chosen value of k. The melt structure and degree of polymerization, and hence the value of k, is determined by the nature of the cation. Cations which interact strongly with silicate anions, e.g. Ca^{2+}, may be expected to exert a 'shielding' effect on the reactive groups in the silicate anions and inhibit polycondensation. Such cations will have low k values and corresponding low N O^{2-} values and metal oxide activities. Free oxygen ions in the melt, as well as silicate anions attract the cation, however, so the overall degree of polymerization is likely to be governed by the relative magnitude of these two effects. The enthalpy of mixing will depend on the number of O^- bonds formed, and the energy difference between M^{2+}- O^{2-} and M^{2+}-O^--Si bonds. Gaskell[23] has shown that the configurational entropy for a melt of orthosilicate composition is a maximum at N O^{2-} = 0.5. The degree of polymerization and the number of N O^{2-} ions will be such that $\Delta H^m - T\Delta S^m = \Delta G^m$ is a minimum.

The polymerization models discussed above were developed mainly from considerations of thermodynamic properties of the melt. There is little supporting physical evidence. However, chromatographic studies on phosphate systems[20] have allowed individual anionic species to be identified. Results confirm the presence of a range of anionic species in the melts. Much progress has been made in recent years in applying a chromatographic technique to the study of silicate minerals and glasses. The method involves leaching discrete silicate anions from the solid and simultaneously blocking of reactive sites by trimethylsilylation. The method was originally introduced by Lentz[24] and developed further by Masson and co-workers, mainly to minimise side reactions which interfere with the anions produced. Results once again show a range of anionic species, with SiO_4^{4-} ions the most abundant silicate species. This is in agreement with the predictions of the Masson model.

Results of density measurements of ternary silicate melts[26] have been interpreted in terms of a polymerization model as will be discussed later.

(b) Ternary Silicate Melts

Little experimental data on activities in ternary melts is available and several models have been proposed to predict activities in ternary melts.

According to Temkin,[27] the activity of a component A_XB_Y in an ideal ionic melt is related to its ion fractions N A and N B by the equation

$$aA_XB_Y = N\,A^X \,.\, N\,B^Y$$

The ion fractions are defined as

$$N\,A = \frac{\text{number of A cations}}{\text{total number of cations}}$$

$$N\,B = \frac{\text{number of B anions}}{\text{total number of anions}}$$

No account is taken of the ionic charge of the species present. The assumption here is that there is random mixing of cations with cations and anions with anions, but no cation/anion mixing. Other models have been proposed which assume cation/anion mixing[28] or make allowances for differences in valency of ionic species, giving equivalent ion fractions.[29] With the Temkin model, in an ideal mixture of A_2Y and B_2Y, $aA_2Y = (N\,A_2Y)^2$, where $N\,A_2Y$ is the mol. fraction of A_2Y in the melt.

In view of the difference in energies of mixing between different binary silicate melts, the assumption of ideal mixing is unlikely to hold in ternary melts. Flood et al have proposed a model where cations and anions are still assumed to mix randomly (on an equivalent ion fraction basis), but different energies of interaction between cation and anion are allowed.[29] The interactions are presented in terms of all exchange reactions in which the component may take part. Thus for a slag containing Fe^{2+}, Ca^{2+}, Mg^{2+}, SiO_4^{4-}, O^{2-} ions etc.

$$RT\ln aFeO = RT\ln N'Fe^{2+}.N'O^{2-} + RT\ln {}^{Y}\!Fe^{2+}.{}^{Y}\!O^{2-} + N'Ca^{2+}.N'SiO_4^{4-}.\Delta G_{11} + N'Mg^{2+}.N'SiO_4^{4-}.\Delta G_{12} + N'Ca^{2+}.N'PO_4.\Delta G_{21}.....$$

where ΔG_{11} is the standard free energy for the reaction

$$FeO + \tfrac{1}{2}\,Ca_2SiO_4 = \tfrac{1}{2}\,Fe_2SiO_4 + CaO$$

ΔG_{12} for

$$FeO + \tfrac{1}{2}\,Mg_2SiO_4 = \tfrac{1}{2}\,Fe_2SiO_4 + MgO$$

etc.

The term $RT\ln\gamma_{Fe^{2+}}.\gamma_{O^{2-}}$ cannot be evaluated from existing data and is usually ignored. Results are fairly good for basic slags, but the equation cannot be applied to slags more acid than orthosilicate since $N_{O^{2-}}$ becomes zero. Attempts to extend this treatment to more silica-rich slags require the use of empirical constants.[30,31]

Lumsden proposed that the $FeO-FeO_{1.5}-SiO_2$ system showed regular solution behaviour.[32] From knowledge of binary systems and assumptions of regular solution behaviour, interaction parameters were obtained which could be applied in a simple manner to ternary and more complex melts. This approach predicted properties of the $FeO-FeO_{1.5}-SiO_2$ system close to measured values. Prediction of ZnO activities in the $ZnO-FeO-FeO_{1.5}-SiO_2$ system were close to measured values.[33]

From consideration of phase diagrams and thermal data for mixtures of metasilicates of divalent oxides (e.g. mixtures of $MgSiO_3$ and $FeSiO_3$), and mixtures of some orthosilicates (e.g. Mg_2SiO_4 and Fe_2SiO_4), Richardson[34] suggested that the heat of mixing would be small, and that activities could be calculated in terms of configurational entropy changes, provided the basic structure of the melt remained unchanged. If it is further assumed that the configuration of the anions remains constant between the limits of melt composition, then the only configurational change will be mixing of cations. Mixing of two orthosilicates, then, is equivalent to an ideal Temkin mixing of compounds A_2Y and B_2Y. $aA_2Y = N^2_{A_2Y}$, so that

$$a(Ma_2SiO_4,\ Mb_2SiO_4) = N^2(Ma_2SiO_4,\ Mb_2SiO_4)$$

In the more general case of a binary liquid silicate of composition $(xMaO.SiO_2)$ being mixed with a binary silicate of composition $(xMbO.SiO_2)$

$$a(xMaO.SiO_2) = N^x(xMaO.\ SiO_2) \qquad \text{then}$$

$$a(xMaO.SiO_2) = \frac{a^x(MaO).aSiO_{2\ \text{ternary}}}{a^x(MaO).aSiO_{2\ \text{binary}}} = N^x(xMaO.SiO_2)$$

$aSiO_{2\ \text{ternary}}$ is evaluated by linear interpolations of log $aSiO_2$ between the two binary limits. Thus if activities in the two binary silicates are known, aMaO in the ternary can be evaluated.

The calculated activities agree well with measured values at metasilicate composition, and for some systems at orthosilicate composition. In the $CaO-FeO-SiO_2$ system around orthosilicate composition, however, there are marked negative deviations from Richardson's 'ideal' laws for the activity of FeO. Measured values of aFeO in this system show that the

activity of FeO is increased by additions of CaO, but the 'ideal solution' model predicts much larger positive deviations.

Richardson[35,36] suggests that these 'negative' deviations might arise from interactions between different cations, from better packing resulting from the presence of different cations of different sizes, or from structural changes in the silicate matrix arising from the presence of two different cations. With respect to this latter possibility, it was suggested that there could be a tendency for the solution to unmix by such a reaction as

$$Ca_2SiO_4 + Fe_2SiO_4 = 2CaSiO_3 + 2FeO$$

This would tend to give more 'free' FeO in the melt, but it was calculated that the free energy of mixing would become more negative by this means and thus the activity of FeO could fall below the 'ideal' mixing curve.

Gaskel et al[26] argued that any increased tendency for orthosilicate ions to polymerize to an $Si_2O_7^{6-}$ ion due to the influence of Ca^{2+} ions was contrary to the polymerization models discussed earlier. Gaskel et al measured the effect on melt density of replacing FeO in a binary SiO_2-FeO melt with increasing amounts of CaO, MnO, CoO and NiO. Results are expressed in terms of oxygen density, which is the number of oxygen atoms of any form per c.c. of melt. High oxygen densities suggest efficient oxygen packing and hence large silicate molecules and high degrees of polymerization. The effect of small differences in cation size are assumed to be negligible. Along lines of constant silica content, changes in oxygen density suggest changes in anionic configuration. (Fig. 1.5, page 12).

Addition of CaO and MnO which have k values lower than FeO, results in a decrease in density, suggesting a decrease in the degree of polymerization. By analogy with the MnO line, the effect of replacing FeO with oxides of higher k values (CoO and NiO) might not be seen until much higher CoO and NiO concentrations. The density decrease is greater for CaO than for MnO, which agrees with the lower k value for CaO than MnO.

As suggested earlier, the degree of polymerization may depend on the degree of preference of the metal for the M^{2+}-O^{2-} bond or the M^{2+}-O^- silicate bond, as indicated by the k value and the free energy of mixing. The polymerization theory explanation for the increase in FeO activity on adding CaO to an FeO-SiO_2 melt is that the Ca^{2+} ions tend to associate with the silicate anions and depolymerize the melt, while the Fe^{2+} ions try to maintain their hold on the decreasing numbers of O^{2-} ions, increasing the activity of the FeO.

It can be seen that one of the basic assumptions of Richardson's theory is that anionic configuration is the same for two different binary systems at the same silica content, whilst the polymerization theory assumes different cations produce different anionic distributions.

4. LITERATURE SURVEY

(a) Copper in Slags

The copper content of discard slags from the reverbatory furnace is in the order of 0.5wt%. This copper loss is thought to arise from two sources, mechanical entrapment of matte particles, and a soluble copper loss, where copper is in solution in the slag as Cu^{+} ions. The proportions of mechanical to soluble losses have been the subject of much research, with little agreement between researchers. The proportions probably differ from plant to plant through variations in smelting practise. An average figure would be 50% mechanical loss and 50% soluble loss. Two excellent accounts of this problem were published in the early fifties by Ruddle[37] and by Evans,[38] with discussion of the form of copper loss in the slag and the factors affecting copper losses. A recent review has been published by Yannopoulos.[39]

(1) Matte/slag systems

Many investigations into the distribution of copper between a matte and a slag have been reported. With very few exceptions, the conditions under which the investigation was conducted have not been well enough defined to draw more than very general conclusions. The variables most commonly varied have been matte composition and (knowingly or unknowingly) oxygen potential of the system. This work is best summed up by Spira and Themelis,[40] who took the oxygen content of mattes to be a reliable indication of the state of oxidation of the system, and related this to the copper content of the slags at various matte grades. (Fig. 1.6, page 21). The limits of the graph are saturation with pure iron from the work of Yazawa and Kameda,[41] and pSO_2 = 1 atm. from the work of Korakas.[42] The results show that copper slag content increases with increasing copper content of the matte and with increasing oxygen content of the matte. The results are at more or less constant slag composition of silica saturated iron silicate. Bor and Tarassoff[43] have recently suggested that the oxygen contents at iron saturation are in error and mattes contain up to 6 wt% O at FeS composition.

The effect of changing slag composition has also been studied. This affects physical as well as chemical properties of the slags, but only the effect on solubility, and not entrapment, is being considered here. The general view is that minimum Cu solubility is found at silica saturation, and that increasing FeO content gives increased copper losses, e.g. 44,45,46.

FIG.1.6

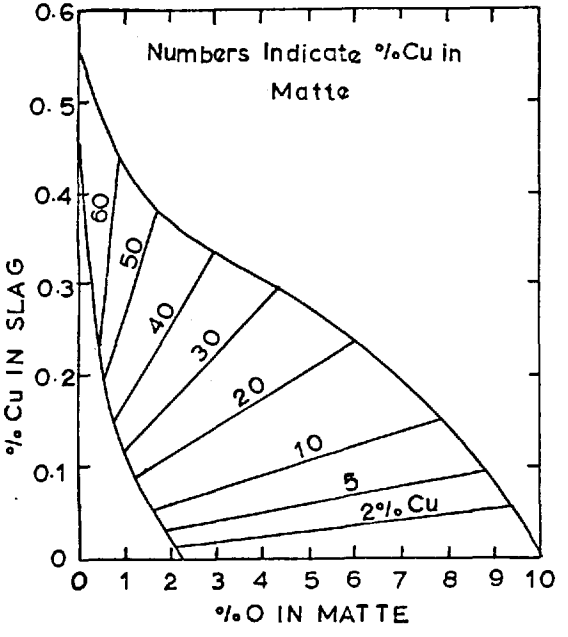

FIG 1.7

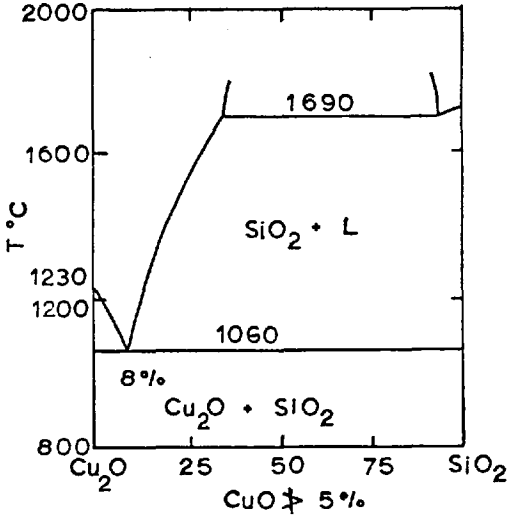

FIG. 1.8

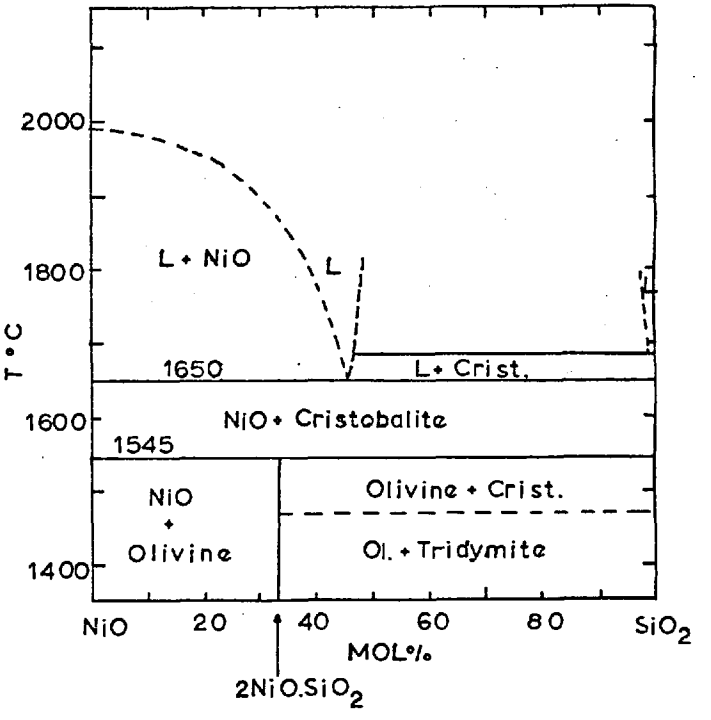

However, these observations say nothing about the effect of slag composition on the activity coefficient of the copper in the slag.

A combination of the two equations

$$FeS + 1\tfrac{1}{2}\, O_2 = FeO + SO_2$$

$$Cu_2S + 1\tfrac{1}{2}\, O_2 = Cu_2O + SO_2$$

gives $$(Cu_2O) + [FeS] = [Cu_2S] + (FeO)$$

hence $$K = \frac{[aCu_2S]\ (aFeO)}{(aCu_2O)\ [aFeS]}$$

Thus for constant matte composition, the activity of FeO in the slag is directly related to the activity of copper oxide in the slag. Addition of silica to give a silica saturated slag will lower the activitiy of FeO to the maximum extent, and hence give the minimum copper loss.

There is general agreement in the literature that addition of CaO decreases the soluble copper content of the slag[44-48] and that MgO acts in a similar way.[46]

Montil'o et al[45] considered replacement of Fe_3O_4 by Al_2O_3 gave lower copper losses and replacement of SiO_2 by Al_2O_3 gave higher copper losses.

Some limited thermodynamic studies of matte/slag/gas systems have been attempted. Korakas[42] studied the formation of magnetite on blowing oxygen into a matte. Bailey et al[49] studied the limits of stability of mattes with respect to oxygen partial pressure. Johansen et al [50] studied matte-metal-magnetite,matte-metal-slag and matte-magnetite-slag three phase equilibria, all under an SO_2pressure of 1 atm. Sehnalek and Imris[51]equilibrated Cu_2S/FeS mattes with silica saturated iron silicate slags and an N_2-S_2-SO_2 gas phase, thus fixing pS_2 and pO_2 for the system. They also equilibrated silica and magnetite saturated slags with a Cu_2S matte and an SO_2 atmosphere. This work is referred to further in the discussion section.

The difficulties of working with such a complex system has led to an approach where individual parts of the system are studied in isolation from the whole, yielding thermodynamic measurements of higher accuracy but which are not necessarily exactly applicable to the more complex system.

(2) Matte systems

The Fe-S system has been studied by Maurer et al,[52] using H_2/H_2S mixtures to define the sulphur potential. Iron activities have also been derived.

Schuhmann and Moles[53] studied the Cu-S system, deriving sulphur and copper activities.

The ternary system Fe-Cu-S was studied by Krivsky and Schuhmann[54] equilibrating the matte with an atmosphere of known sulphur potential. The activities of iron, copper and sulphur were derived. Activities of Cu_2S and FeS for the Cu_2S-FeS pseudobinary were also found and showed almost ideal behaviour, i.e. $aCu_2S \cong N\ Cu_2S$ and $aFeS \cong N\ FeS$. The system was studied in the complete absence of oxygen.

(3) Slag systems

Typical reverbatory slag analyses are given on page 4, Table 1.1. The slags are high silica iron silicates with variable quantities of other oxides, mainly CaO, MgO and Al_2O_3, and some sulphur.

Michal and Schuhmann[55] studied the thermodynamics of iron silicate slags saturated with solid silica at 1250, 1300 and 1350°C. CO/CO_2 gas mixtures were used to define the oxygen potential and activities of FeO were calculated using a Gibbs-Duhem integration.

Schuhmann and Ensio[56] studied the thermodynamics of iron silicate slags saturated with gamma iron by measuring the equilibrium between CO/CO_2 gases and the metal/slag phases. Activities of FeO and SiO_2 were derived.

From the results of these two investigations, and phase diagram data, Schuhmann[57] calculated activities of FeO and SiO_2 in the SiO_2-FeO-Fe_2O_3 system, at 1350°C.

Bodsworth[59] repeated Schuhmann and Ensio's work, using H_2/H_2O rather than CO/CO_2 gas mixtures. The results are in very good agreement. Bodsworth extended his results to the FeO-CaO-SiO_2 system at 1265-1365°C.

Distin et al[59] measured aFeO in FeO-SiO_2 slags equilibrated with molten iron at 1785-1960°C using a levitation technique. The results show that aFeO more nearly approaches Raoultian ideality as the temperature is raised.

Activities of FeO in FeO-(CaO + MgO)-SiO_2 melts have been measured by Chipman and Co-workers,[60,61,62] and the results obtained were revised by Elliott[18] to make them consistent with results for the FeO-SiO_2 system.

Richardson[63] studied the dissolution of sulphur in various slag systems, and described the results in terms of sulphur capacities, where

$$Cs = \frac{wt\%S.pO_2^{\frac{1}{2}}}{pS_2^{\frac{1}{2}}}$$

The phase diagram for Cu_2O-SiO_2 system has been published,[64] Figure 1.7, page 21. It shows no copper silicate compound formation and a wide range of immiscibility.

$Cu_2O.Al_2O_3$ is reported to have a small negative free energy of formation (-4000 ± 1000 cal/mol) at 1000°C.[65,66]

(4) Metal/slag systems

Richardson and Billington[67] equilibrated copper metal at reduced activity with CaO-Al_2O_3-SiO_2 slags and CO/CO_2 gas mixtures at 1500°C. They concluded from their results that small amounts of copper dissolved in the slag as copper metal, small amounts of CuO were formed at high oxygen pressures, but that most of the copper in the slag was as cuprous oxide, Cu_2O. They suggested the copper contents were controlled by the equilibrium

$$2Cu + \tfrac{1}{2}O_2 + (Si\text{-}O\text{-}Si) \rightleftharpoons 2(Cu^+) + 2(Si\text{-}O^-)$$

Ruddle, Bates and Taylor[68] equilibrated pure copper metal with iron silicate slags in silica crucibles, and controlled the oxygen potential with a CO/CO_2 gas stream. The system was quenched for sampling by lowering the crucible from the hot zone of the furnace onto a cold copper block. Runs were conducted at 1300, 1350 and 1400°C over a range of oxygen partial pressures from 10^{-11} to 10^{-6} atm. Activities of Cu_2O were calculated.

Mihalop[69] studied the same system as Ruddle with similar results. Using an industrial slag containing 19% CaO and 17% Al_2O_3, Bailey et al[49] reported significantly lower copper slag contents.

Toguri and Santander[70,71] varied the activity of copper in the metal phase by alloying with gold, giving a range of copper activities from 0.25 to 1.0. The alloys were equilibrated with iron silicate slags containing 34% SiO_2 and ~6% Al_2O_3 from the alumina crucible used to contain the melts. CO/CO_2 gases were used to control the oxygen potential. Activities of Cu_2O were calculated.

Altman and Kellogg[72] equilibrated copper/gold alloys, giving aCu equal to 0.73 and 0.86, with silica saturated slags and a CO_2/CO atmosphere. The slag and metal were sampled directly from the melt at the experimental temperature using a suction technique. The slags were analysed for Fe^{2+}, Fe^{3+}, SiO_2, Cu and Au, and the alloy phase for Cu, Au and Fe. Activities of $CuO_{.5}$ were calculated and aFe, aFeO, aFe_3O_4 and $aSiO_2$ determined following a Gibbs Duhem integration.

(b) Nickel in Slags

There is very little information available in the literature on nickel in iron-silicate slags. Factors affecting nickel losses in a nickel matte/slag system would, however, be expected to be similar to those reported for the copper matte/slag system.

Activities in the Ni-S and Ni-Fe-S systems have recently been determined by Meyer.[73,74]

The equilibrium

$$(NiO) + Fe = (FeO) + Ni$$

was studied by Bardenheuer & Brauns[75] using Fe-Ni alloys and high silica iron silicate slags at 1620°C. The results are referred to in the Discussion.

The phase diagram for the $NiO-SiO_2$ system has been determined by Phillips et al.[76] Figure 1.8, page 21. It shows nickel olivine (Ni_2SiO_4) to be the only nickel silicate compound formed. Ni_2SiO_4 becomes unstable at 1545°C with respect to solid NiO and cristobalite. Ringwood,[77] however, considered Ni_2SiO_4 to be stable up to 1650°C. The NiO liquidus is very tentative above about 1700°C. NiO activities derived from this liquidus are shown in Fig. 4.2, page 132.

The free energy of the reaction

$$2Ni + SiO_2 + O_2 = Ni_2SiO_4$$

has been determined by Lebedev et al[78] (700-1100°C), Burdese et al[79] (700-1250°C) and Cambell and Roeder[80] (1300-1500°C). Agreement between Burdese and Cambell is good. Combination of these results with their own determination of the free energy of the reaction

$$Ni + \tfrac{1}{2} O_2 = NiO$$

allows the free energy for the reaction

$$2NiO + SiO_2 = Ni_2SiO_4$$

to be calculated.

These results are shown in Fig. 1.9, page 26, together with the results of Taylor and Schmalzried[81] who determined free energies of formation of Ni_2SiO_4 from the oxides directly, using galvanic cells at 800-1150°C. The point for the decomposition of Ni_2SiO_4 taken from the phase diagram is also shown. The results suggest a mean heat of formation from 1000-1500°C of about -3.8 Kcals. This can be compared with a value of -3.3 Kcals determined using solution calorimetry at 700°C by Navrotsky.[82] Spenser[83] recommends a value of -3.15 Kcals at 298°C.

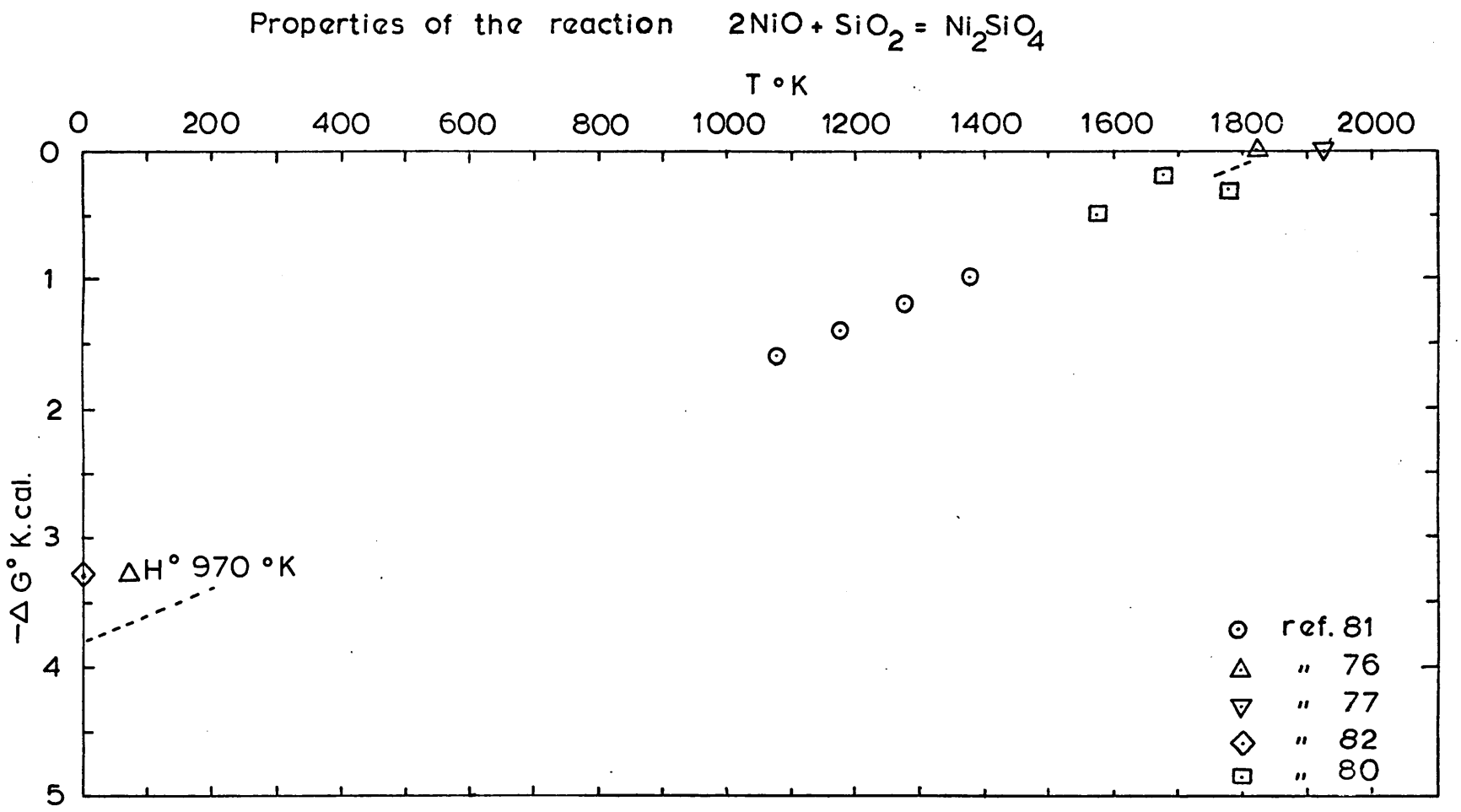
Properties of the reaction 2NiO + SiO2 = Ni2SiO4
T °K
0
200
400
600
800
1000
1200
1400
1600
1800
2000
-ΔG° K.cal.
0
1
2
3
4
5
ΔH° 970 °K
ref. 81
" 76
" 77
" 82
" 80

FIG.1.9

5. AIMS OF THIS WORK

This work was initiated firstly to confirm the results of Ruddle et al.[68], and subsequently Altman and Kellogg,[72] who measured the activity of cuprous oxide in silica saturated iron silicate slags. Secondly, to extend these activity measurements to iron silicate slags which were not saturated with silica, to find the effect of differing iron/silica ratios on the activity coefficient of cuprous oxide.

Data on activities of nickel oxide in iron silicate slags seems almost completely absent from the literature. This is possibly because nickel is somewhat less important commercially than copper, or because the extraction routes have not required the use of slags to the same extent as those of copper. Nevertheless, especially with the inception of oxygen converting of nickel mattes, this represents a considerable gap in our knowledge. The third part of this work, then,was to measure activities of nickel oxide in iron silicate slags over a range of iron to silica ratios.

Molten iron silicate slags are extremely corrosive to refractory materials, and most work on iron silicate slags has been done either at iron or silica saturation, allowing the use of iron or silica crucibles to contain the melts. One alternative approach was that of Chipman[60] who rotated a refractory crucible containing molten iron so that the slag added was held in the cusp of the meniscus, out of contact with the crucible walls. Nevertheless, significant MgO contamination of the slag was reported.

The solution to the problem in this work has been to equilibrate a levitated molten metal drop with slag and gas phases. Although levitation melting has been used frequently over the past ten years or so, it has not before been applied in this way. It is more true to say, then, that the first aim of this work was to test the applicability of the levitation technique by comparison of results for near silica saturated slags with the results of Ruddle, and particularly Altman and Kellogg.

CHAPTER 2.

EXPERIMENTAL

1. EXPERIMENTAL REQUIREMENTS

The experimental approach considered most promising was to equilibrate copper and nickel alloys with iron silicate slags at known oxygen partial pressures, and then to analyse metal and slag samples taken from the system at equilibrium. Copper and nickel oxide activities can be calculated knowing the oxygen partial pressure, and the standard free energies for the reactions:

$$2Cu + \tfrac{1}{2} O_2 = Cu_2O$$

and

$$Ni + \tfrac{1}{2} O_2 = NiO$$

The major problem was thought to be preventing contamination of either the slag or the metal through corrosion of any containing crucible.

2. CHOICE OF TECHNIQUE

Two approaches were considered:

(1) Using single crystal alumina crucibles

These had proved successful in resisting the corrosion of tin-silicate melts under conditions where recrystalized alumina crucibles had shown severe intergranular corrosion.[84] It was hoped the rate of corrosion by copper containing iron silicate slags would be slow enough to cause insignificant slag contamination.

Two crucibles were made, but because of the success of levitation melting, were never used.

(2) Levitation melting

This method overcomes all crucible contamination problems. It consists essentially of levitating a molten alloy in a stream of gas of known CO/CO_2 ratio, adding slag to the alloy and then removing a sample of the slag once equilibrium (or steady state) has been established between the slag, metal and gas phases. The slag is not inductively heated and hangs on the lower half of the metal drop by surface tension, leaving the upper surface free from slag, which allows temperature measurement of the metal using an optical pyrometer. (See photograph, page 31 Fig. 2.1).

FIG. 2.1

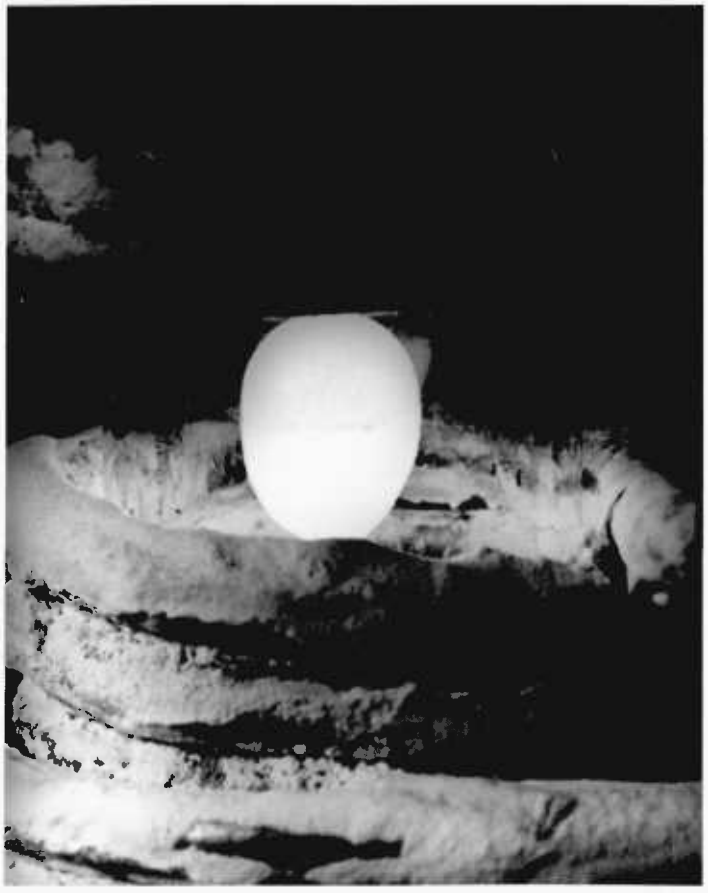

Levitated metal with slag attached

3. LEVITATION MELTING

(a) Introduction

Levitation was first suggested by Muck[85] in 1923, and investigated in detail by Okress et al[86] in the early fifties. Briefly, a high frequency current is passed round a suitably- designed water-cooled coil. If an electronic conductor, such as a metal, is placed within the coil, eddy currents are produced within the metal, and the field from the eddy currents interacts with the coil field sufficiently strongly to support the metal within the coil. The eddy currents also heat the metal, and under suitable conditions the metal is held as a stable molten droplet. Reviews of levitation technique have been published by Jenkins[87] and Peifer.[88]

Temperature control of the molten droplet is perhaps the major problem. Levitation melting characteristically gives too high a temperature and the problem is usually one of keeping the temperature low enough. Temperature can be controlled to some extent by the following means:

(1) By design of the coil. (87,88,89,90)

(2) By the power input to the coil; lowering the power drops the metal lower in the coil where the field is stronger, thus increasing the temperature of the metal

(3) By passing a gas stream over the drop. High gas flow rates and high gas thermal conductivity bring about a cooling of the drop. Helium is frequently used for cooling, being inert and of high thermal conductivity.

An important factor in this present work is that addition of high emissivity slag to a low emissivity metal such as copper brings about a useful reduction of temperature.

(b) Previous Applications

Previous applications of levitation melting have included alloy preparation,[87] metal purification,[91,92] and alloy thermodynamics,[93] vapourization phenomena,[94,95,96] determination of liquid metal density and emissivity,[97,98] studies of supercooling[97] and measurement of surface tension.[99]

Toop,[100] and subsequently Glen[101] and Forster,[102] studied the steady state achieved on passing CO/CO_2 gases over liquid copper and nickel drops. The steady state was found to be equivalent to the isothermal equilibrium state so far as partition of oxygen was concerned. This work is discussed more fully later.

Forster also studied the sulphurization of copper using H_2/H_2S gas mixtures.

Much work has been done on the kinetics of gas/metal reactions, particularly decarburization of iron drops [103,104,105] and rates of oxidation of various metals [101,102,106] where rates of oxygen transfer are thought to be diffusion controlled in the gas phase.

Roberts et al [107] succeeded in levitating various metal sulphides and studied their reaction with oxygen.

Caryll and Ward [108] studied the partition of manganese between two liquid phases; Mn-Fe metal and MnO-FeO slag, under an inert helium atmosphere Equilibrium was calculated to be 99% complete in 0.4 secs. Quenching rates faster than 5.10^5 ^oC/sec. were considered necessary to 'freeze in' the high temperature equilibrium. Samples were dropped from the coil and caught between two copper plates, producing thin metal/slag foils which were analysed by electron probe microanalysis. The Fe-Mn-S-O system was studied using very similar techniques by Booth and Charles.[109]

Knights and Perkins,[110] in studying the partition of elements between a complex slag and steels, collected equilibrated slag specimens by feeding powdered slag onto the levitated metal and allowing the slag to drip off onto a copper plate held below the coil. Once again a helium atmosphere was used.

Distin et al [111] determined the solubility of oxygen in liquid iron by levitating iron metal in contact with FeO in a helium gas stream. Subsequently [59] FeO-SiO_2 slags were equilibrated with the iron, allowing the activity of FeO to be calculated. Metal samples were obtained by a suction technique and slag samples by allowing the slag to run down a molybdenum wire pushed into the slag.

4. APPARATUS AND MATERIALS

(a) Gases

The oxygen potential of the metal/slag system was controlled by passing a mixture of carbon monoxide and carbon dioxide over the levitated drop. For the high nickel alloys it was necessary to mix helium with the CO/CO_2 gas stream to obtain the required temperature range.

The gas flow system employed is shown in Fig. 2.2, page 35. The specifications for the gases used were:

CO_2, 99.8% pure, main impurity water.

CO, 99.8% pure. Impurities: 500 volumes per million N_2, 300 V.P.M. CO_2, 60 V.P.M. hydrocarbons, 25 V.P.M. water, 20 V.P.M. O_2, 20 V.P.M. H_2.

He, 99.995% pure, Impurities: 3-4 V.P.M. N_2, 1-2 V.P.M. H_2O, 1 V.P.M. O_2.

The CO_2 was dried with silica gel and magnesium perchlorate, passed over a Cu/Cu_2O mixture at 450°C to remove oxygen and oxidize any CO to CO_2 and H_2 to H_2O, and then dried again.

The CO was dried, passed over activated copper metal at 450°C to remove oxygen, passed through soda-lime to remove CO_2 and dried again.

The helium was dried and passed over titanium granules at 900°C to remove oxygen.

The flow rates of the CO and CO_2 gases were measured and controlled using orifice flowmeters fitted with dibutyl phthalate-filled blow-off tubes. A suitable range of interchangeable orifices was calibrated for CO and CO_2, using a soap-film meter.[112] It has been shown that these flowmeters are capable of high accuracy in metering gas flows.[113] The CO/CO_2 ratio was not checked analytically, but good agreement was found between the expected oxygen partial pressure and the measured value from the oxygen meter (see below). An accurate helium flowrate was not required and a calibrated rotameter was used to indicate this.

An oxygen meter was also incorporated in the gas line. This was used mainly to monitor the exit gas from the levitation cell and indicate when the cell had been sufficiently flushed out to begin levitation after adding a new sample. The oxygen meter consisted essentially of a lime-stabilized zirconia closed end tube held at 900°C, down one side of which was passed the CO/CO_2 gas stream and down the other, pure oxygen at 1 atm. as the reference gas.

GAS FLOW SYSTEM

FIG. 2.2

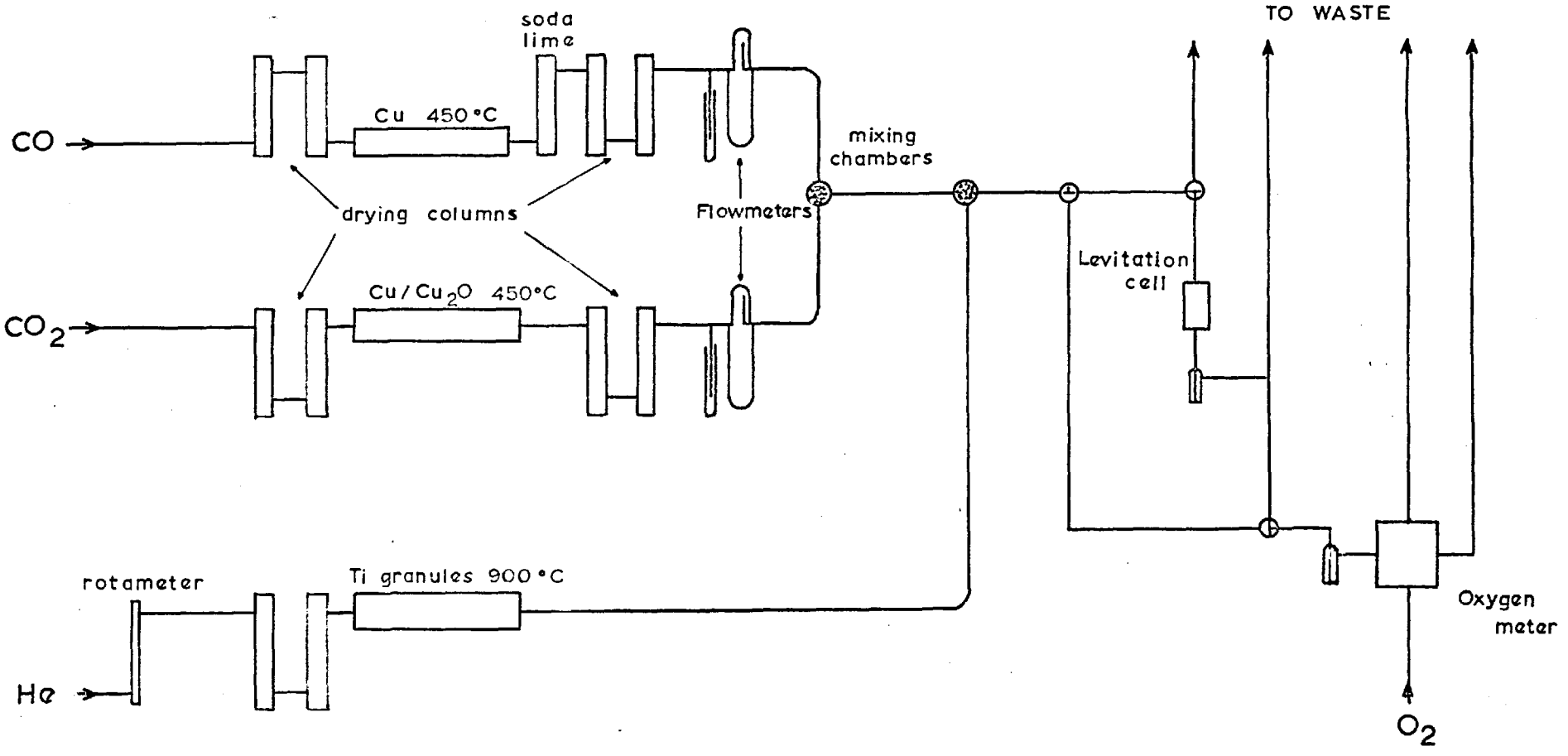

Platinum electrodes attached inside and outside the tube, were connected across a digital voltmeter which measured the E.M.F. between them. The E.M.F. developed is a simple function of the oxygen pressure in the gas stream.

(b) Metals

The metals levitated in this work were copper, gold and nickel as copper/gold and copper/nickel alloys, and were of the Johnson Matthey 'spec-pure' grade. Gold was purchased in the form of gold sponge, the nickel as 5 m.m. dia. rod, and the copper as 5 m.m. and 7 m.m. dia. rods.

None of the metals were prefused into alloys for levitation. Weighed amounts of the pure components were introduced into the coil and allowed to fuse 'in situ' before the slag was added.

For the copper-10 wt% gold alloys, the 5 m.m. copper rod was drilled axially to a depth of 5 m.m. with a size 28 drill. The drilled end of the rod was sawn off to varying lengths to give a range of alloy sample weights. The drilled hole was packed with gold sponge to give a sample with an overall composition of 90 wt% Cu, 10 wt% Au.

Most of the copper-20 wt% nickel alloys were made by drilling the 7 m.m. copper rod with a 5 m.m. drill and ramming a weighed piece of nickel rod into the hole to make up the required composition. The copper-50 wt% nickel alloys were made up in much the same way.

An easier method of alloying was finally used for the copper-35 wt% nickel and copper-10 wt% nickel alloys. For the 35% Ni alloys, the weighed pieces of copper and nickel were put into the coil, at the same time, as separate pieces. For the 10% Ni alloys, the copper piece was melted alone in the coil and the nickel piece quickly pushed into the molten copper.

The weights of the metal alloys were varied to ease the problem of attaining a suitable range of temperatures. Under the same levitation conditions, the drop temperature will be higher the higher the nickel content and the heavier the sample. The table below gives the levitation conditions for all the alloy compositions used. The total CO plus CO_2 flowrate was kept constant at about 600 ml/min. (measured at room temperature).

Alloy Composition	Temp. Range ^{o}C	Weight Range	Helium Flowrate
10 wt% Au	1300 - 1450	1.0 - 1.5 gm	zero ml/min.
10 wt% Ni	1350 - 1500	0.90- 1.4 gm	zero ml/min.
20 wt% Ni	1350 - 1500	0.80- 1.1 gm	500 - 0 ml/min.
35 wt% Ni	1350 - 1500	0 80- 1.05 gm	1200- 300 ml/ min.
50 wt% Ni	1350 - 1500	0.75- 0.95 gm	1700- 400 ml/ min.

Metal weights below about 0.70 gm were difficult to view with the pyrometer and gave very small slag samples.

(c) Slags

Four stock slags, designated B, C, D and E, of differing iron/silica ratio were made up. The materials used were crushed quartz, maximum impurity 40 p.p.m. Fe, analar Fe_2O_3 and electrolytic iron powder, mixed together to give FeO/SiO_2 slags of the composition shown below:

Slag	Expected analysis FeO wt%	Expected analysis SiO_2 wt%	Actual analysis FeO wt%	Actual analysis SiO_2 wt%
B	67.0	33.0	66.5	33.5
C	73.0	27.0	71.4	28.6
D	79.0	21.0	77.2	22.8
E	87.0	13.0	86.7	13.3

On adding a slag to the levitated metal sample, the iron in the slag distributes itself between the metal and the slag phase, the distribution depending on the alloy composition, the oxygen partial pressure and to a small extent, the temperature. Because of the large bulk ratio of metal to slag, this has a significant effect on the slag composition. The effect is minimised by 'doping' the metal with slag as described later, but the table above should be taken only as a rough guide to slag composition.

The slags were pre-fused in iron crucibles using induction heating under an argon atmosphere. The apparatus is shown half scale in Fig. 2.3 page 38.

The crucibles were machined from Swedish iron with the following approximate impurities: 0.03% C, 0.01% Si, 0.12% Mn, 0.005% P, 0.01% S, 0.005% Cr, 0.005% Ni, 0.01% Cu and 0.002% Sn.

Approximately 40 gm of each slag was fused in separate crucibles. The fused slag was drilled from its crucible using a half inch diameter water lubricated diamond trepanning drill. The slags were then crushed using a mortar made from the Swedish iron and using the crucible itself as the pestle. Free iron particles were removed from the slag with a magnet.

(d) Temperature Measurement and Pyrometer Calibration

Because of the tendency for the slag to collect at the bottom of the drop, it is possible to view the top metal surface of the drop without interference from the slag. (Fig. 2.1, page 31).

Accurate temperature measurement of a levitated drop is probably the most difficult aspect of levitation technique. It has proved impossible to probe a levitated drop with a thermocouple, therefore for calibration, it is usually necessary to hold the metal in a crucible and compare pyrometer readings with readings from a thermocouple immersed in the melt.

SLAG FUSION APPARATUS FIG. 2.3

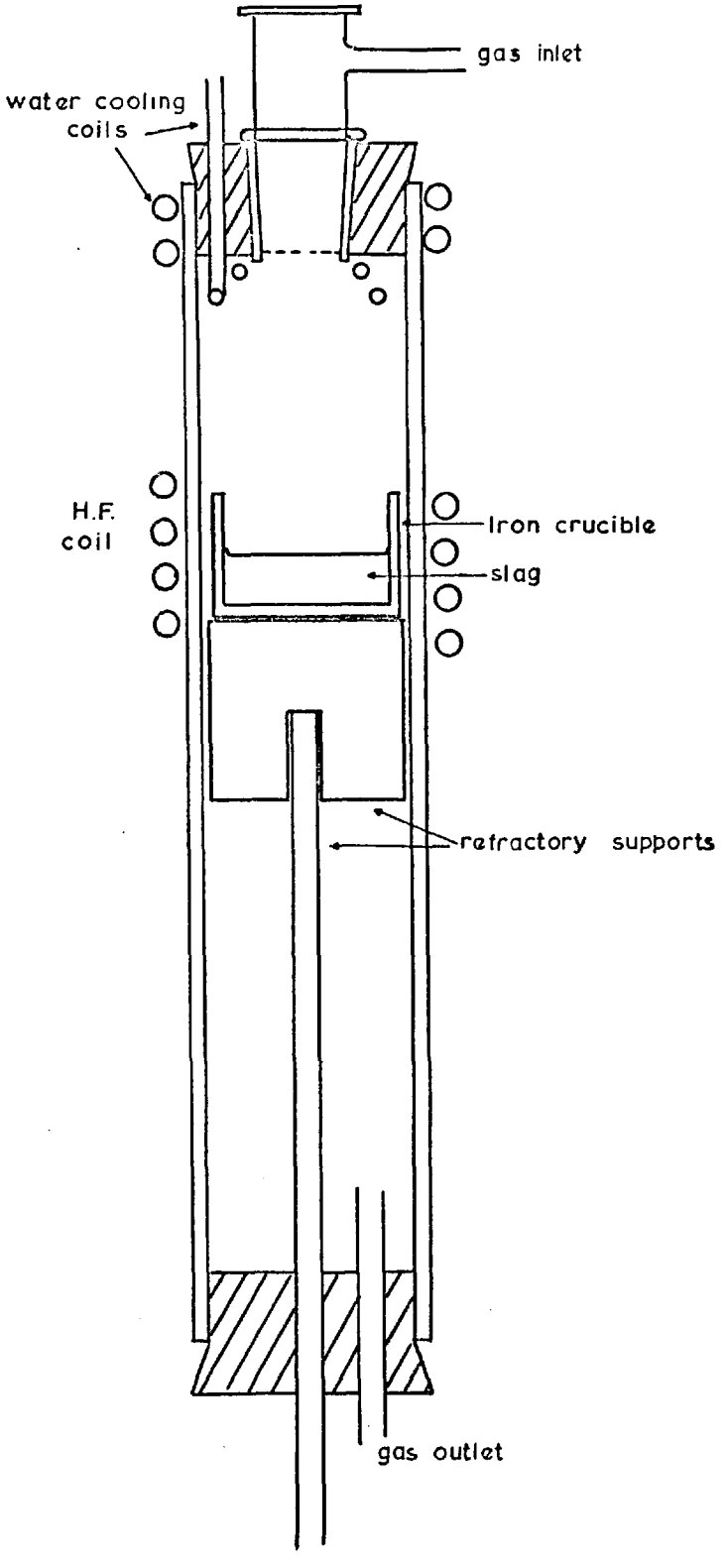

The pyrometer used was an 'Ardocol' two colour radiation pyrometer connected to a 'Kompensograph' continuous line potentiometric recorder with a scale range of 1200-1800°C.

The pyrometer was originally intended for industrial use where large surface areas were viewed at a distance of several yards. It had been adapted with a close-up lens for laboratory work by the manufacturer, but at the recommended target to pyrometer distance of 28 cm, the levitated drops covered only a small part of the total field of view. It was also found that when viewing the drop from above the gas inlet tube, radiation reflected from the sides of the tube lowered the recorded temperature by up to 50°C. In order to view drops of different sizes under similar conditions, and to aid calibration, two radiation shields, with central holes, were introduced between the drop and the pyrometer, giving a collimated beam of light.(Figs. 2.4, 2.6). Viewed through the pyrometer, the droplet completely filled the hole in the lower radiation shield. The upper shield blocked off any light reflected from the sides of the gas entry tube.

The apparatus used for the calibration is shown half scale in Fig. 2.4, page 40. Care was taken that the physical dimensions of the levitation cell light path were accurately reproduced in the calibration apparatus. The area of the top surface of the metal in the crucible was obviously much greater than that of a levitated drop, but the two surfaces appeared similar when viewed through the radiation shields.

Calibration procedure.

Previous workers[100] have reported an increase in the emissivity of copper with increasing oxygen content, up to 1 wt% O. An initial series of calibration runs were performed with pure copper using five CO/CO_2 ratios, giving oxygen partial pressures of 10^{-13} to 10^{-5} atm. at 1300°C, and oxygen contents up to $\sim$0.1 wt% O. the calibration was repeated using forming gas. No significant difference was found over this range of gas compositions. All subsequent calibration was done under a forming gas atmosphere.

The crucibles used in the calibration were of recrystalized alumina with re-entrant thermocouple sheaths, type N 5029, manufactured by Morgan Refractories Ltd. The metals were 'spec pure' gold, copper, and nickel.

Sufficient metal to fill the crucibles was weighed out and fused in

PYROMETER CALIBRATION APPARATUS FIG. 2.4

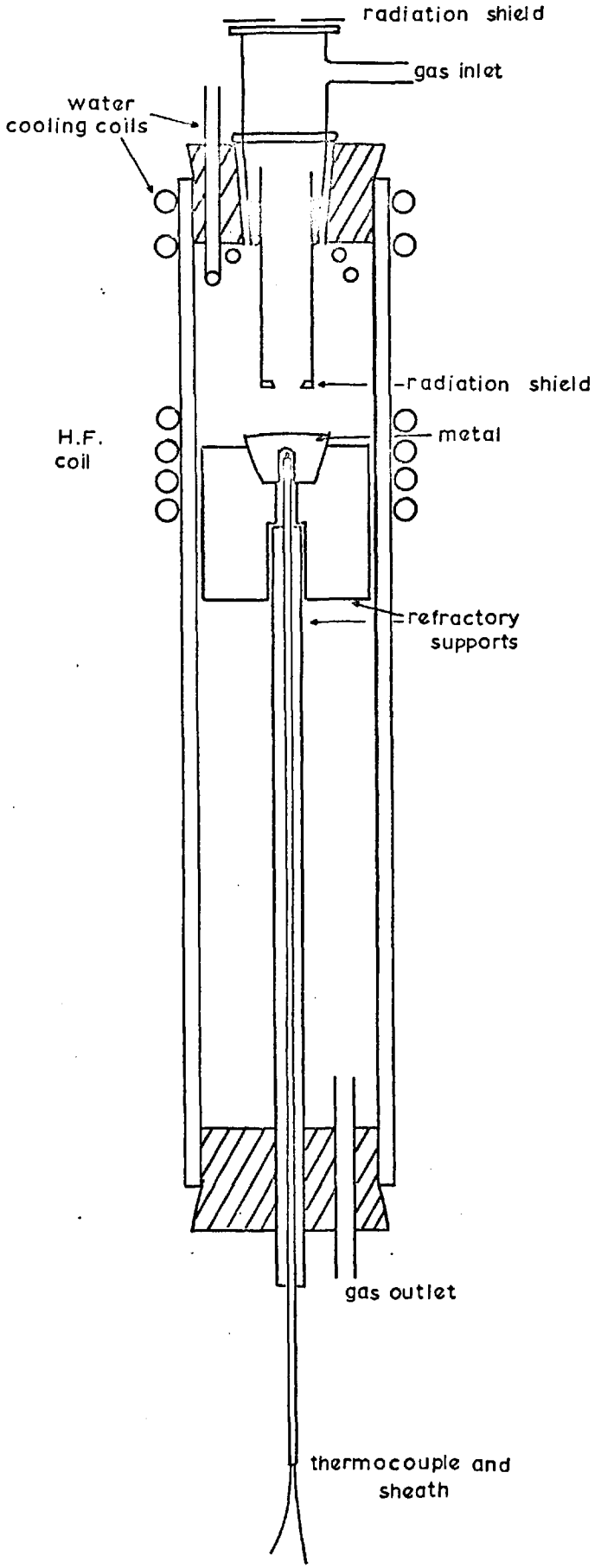

the crucible, usually in two batches, under a forming gas atmosphere. Simultaneous readings of the pyrometer and thermocouple were taken as the metal was heated, in five or six steps, from its melting point to about 1470°C and then cooled, also in stepwise fasion.

The pyrometer was sensitive to emissivity differences between the alloys used, and calibration curves were obtained for 10% Au, 10% Ni, 20% Ni, 35% Ni and 50% Ni alloys, the balance being copper. These are shown in Fig. 2.5, page 42. Samples of the alloys were analysed using atomic absorption spectrophotometry and results are also included in Fig. 2.5.

The 35% Ni and 50% Ni alloys gave similar calibration curves. A partial check on the Cu/Ni calibration was obtained by observing the melting of a pure nickel drop in the levitation apparatus. This point is included in Fig. 2.5 and falls very close to the 35%-50% line. No such check was possible for the copper since the pyrometer read down to 1200°C only.

For the Cu/Ni alloys, a further complication was that the levitated metals also contain small quantities of iron (up to 2 wt%). Previous levitation work has suggested that the emissivities of iron and nickel are fairly similar, and so for calibration purposes, iron in the levitated drops was considered to act as nickel. Curves of (100 - wt% copper in alloy) against pyrometer temperature were drawn from Fig. 2.5 for 1350, 1400, 1450 and 1500°C. Thus the pyrometer temperature corresponding to those true temperatures could be found knowing the composition of the levitated drop. A single average analysis was used for each run. (See tables of metal analyses, pages 80 to 82.)

In the case of the copper/gold alloys, the iron content is much lower than in the copper/nickel alloys, being usually below 0.3 wt%. The effect of the gold on the emissivity of the copper is also much less than the effect of nickel. Thus in determining the true temperature for the copper/gold runs, it was not thought worthwhile to attempt to make any allowance for the difference in composition between the calibration alloy and the levitated specimens.

(e) The Levitation Cell

The levitation cell used in all this work is shown half scale in Fig. 2.6, page 43. The main features of the apparatus have been labelled on the diagram.

Pyrometeter Calibration FIG.2.5

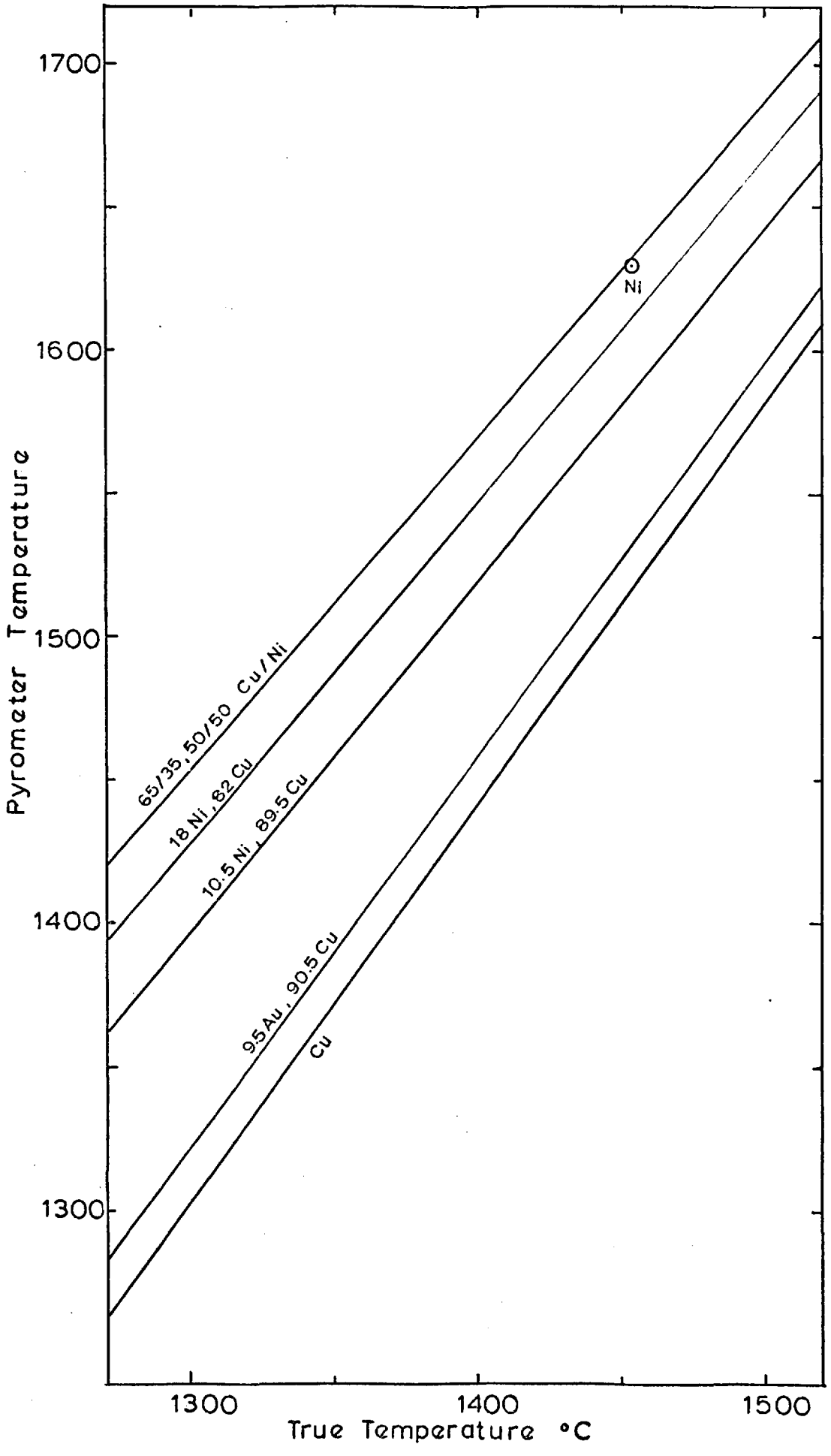

LEVITATION CELL FIG. 2.6

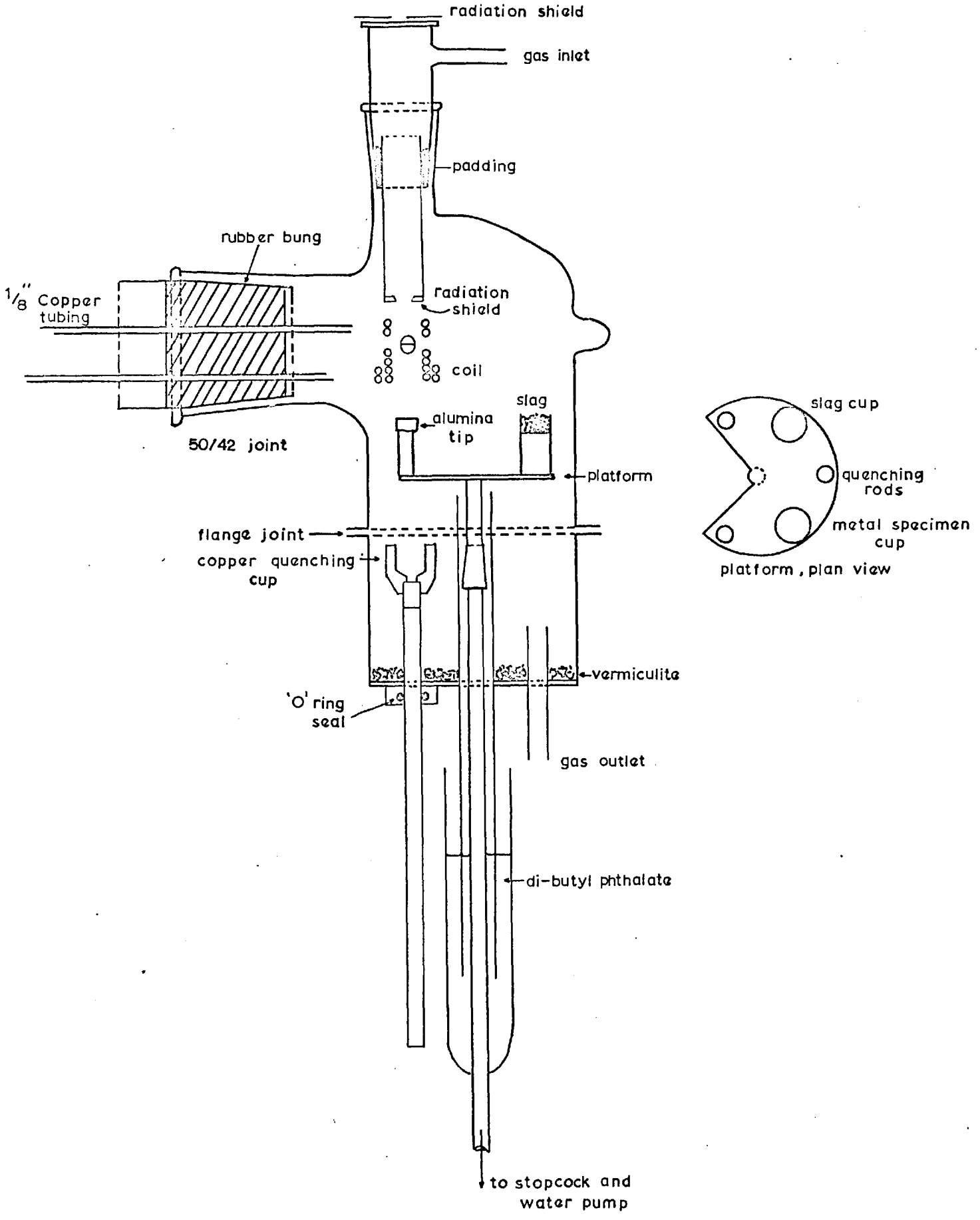

The platform, shown also in plan view, has three 'quenching rods' and two small 'cup holders' attached to it, spaced as shown. One cup holds powdered slag and the other holds the specimen prior to levitation. The quenching rods consist of lengths of Pyrex tubing tipped with solid recrystallized alumina rod. The dibutyl phthalate liquid seal is particularly useful in allowing free and easy movement of the platform during runs. The operation of the cell is described later.

The bottom of the cell, which is of brass, Araldited onto the Pyrex glass sides of the cell, is covered with a layer of Vermiculite. This was introduced to prevent cracking of the glass when metal droplets accidentally fell onto the bottom of the cell.

(f) The Levitation Coil

The two coils used in this work are shown in Fig. 2.8, page 45. Both coils were made from $^{1}/_{8}$" O.D. copper tubing. The design differs from the more usual coil design in that the sides of the lower half of the coil are parallel to the axis of the coil, and not inclined at an angle. The straight-sided coil is easier to wind and seems to give better levitation properties, particularly when a wide diameter in the lower coil is necessary.

The coil used for the copper/gold alloys had an internal diameter of 16 m.m. This was reduced to 14 m.m. for the copper/nickel alloys to produce cooler levitation characteristics. The coils were coated with a mixture of potassium silicate and alumina powder. This mixture sets hard at room temperature without firing, but remains water soluble. The coating gives the coil rigidity and prevents deformation and shorting between the turns.

(g) The High Frequency Generator

This was a phillips type F13/720/1 generator producing a maximum output of 6 K.W. at 250 K. Hertz.

FIG.2.8(a)

Cross section of
coil used for Cu/Au alloys

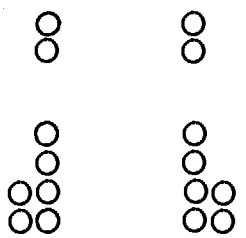

FIG. 2.8(b)

Cross section of
coil used for Cu/Ni alloys

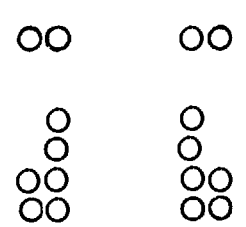

5. EXPERIMENTAL PROCEDURE

The furnaces in the CO, CO_2 and He gas lines were brought up to temperature with a slow flow of gas passing through and out to waste. The platform, loaded with powdered slag and the metal specimen, the lower half of the cell and the liquid seal were assembled and joined to the fixed upper half of the cell at the ground glass flange. The cone and socket joint below the platform was made gas tight by evacuating the tube connecting the platform to the lower stopcock, using a water pump..

The outlet from the cell was connected into the gas line and the CO/CO_2 gas mixture diverted through the cell. The flowmeters were adjusted to give the approximate CO/CO_2 ratio required. The total flowrate of CO + CO_2 was kept at about 600 ml/min. for all runs. Composition of the exit gas from the cell was monitored by the oxygen meter. Levitation was begun when the E.M.F. given by the exit gas was about 99% of the inlet value. The flushing of the cell took about 5 minutes.

The cup containing the metal specimen was raised into the coil, the set switched on, and the cup withdrawn, leaving the metal levitated in the coil. As soon as the drop became molten, the platform was swivelled round and the slag cup pushed into the coil until the slag particles contacted with the bottom of the drop. The cup was withdrawn, leaving solid slag particles clinging to the molten metal surface. The slag melted and formed a homogenous liquid within about half a minute of addition. More slag could be added as required.

As mentioned on page 37, iron from the slag enters the metal phase, thus changing the slag composition. To minimise this effect, a large quantity, about 0.1 to 0.2 gm, of slag was initially added to the droplet and allowed to equilibrate for a few minutes with the metal, thus raising the iron content of the metal. this slag was then removed from the drop and discarded. Fresh slag was added (about 0.04 gm) and allowed to equilibrate with the metal and the gas stream.

Adjustments were made to the CO, CO_2 and He flow rates and the power from the H.F. generator to give the required CO/CO_2 ratio and metal temperature. The temperature was continuously recorded on a chart recorder connected to the pyrometer. Once the conditions were set, the droplet would remain permanently levitated at a steady temperature. Under ideal conditions, the recorded temperature was constant within $\pm$ 2°C over a short term period, say ten minutes, but a slow drift, either upwards or

downwards , could be detected over a long term period of an hour or so. Rapid temperature changes in the order of 10°C at a rate of 1°C per second occasionally occurred. The reason for this was not discovered, but was thought to arise from a variation in output from the set.

After a steady equilibration of about 20 minutes, a slag sample was taken. This was done by raising a quenching rod into the coil and touching the surface of the alumina onto the slag. On touching, the slag stuck lightly to the alumina surface and with immediate withdrawal of the rod, a small bead of slag was detached from the system with remarkable smoothness.

Further slag was immediately added to the metal to prevent the drop becoming too hot. The equilibration process was repeated and a second and often third slag sample was taken. As soon as the last slag sample had been taken, the metal was dropped out of the coil into the copper quenching cup. The gas was turned to waste, the cell opened and the metal and slag samples collected. The slag samples usually could be detached from the quenching rods with ease. A slight smear of graphite on top of the rods helped greatly to prevent sticking. The quenching rods were periodically resurfaced on a diamond wheel.

6. DEFINITION OF A 'RUN'

In a normal day, it was usually possible to complete one run, that is, levitation of five or six metal samples of the same composition, with the same CO/CO_2 gas ratio, using the same stock slag, over a range of temperatures of about 150°C. This yielded 12-15 slag samples of weights varying from 0.005 to 0.03 gm, but usually between 0.01 and 0.02 gm.

Each run has been given a separate code number describing the alloy composition, the slag composition and the oxygen partial pressure range. (See Table 3.1, page 59)

7. ANALYSIS OF SLAG AND METAL

(a) The Atomic Absorption Spectrophotometer

All analysis was done using a Perkin Elmer model 290B atomic absorption spectrophotometer.

In principle, a solution of the material to be analysed is sprayed into a controlled air or nitrous oxide/acetylene flame. A beam of light containing wavelengths characteristic of the element of interest is shone through the flame onto a detector. Absorption of the light by the element in the flame is a function of the amount of that particular element in the flame. The degree of absorption is indicated as a peak height on a chart recorder trace. The concentration of the element in solution is found by comparing the peak height with the peak heights given by standard solutions of known concentrations. The weight of the element in the original sample can be found knowing the weight of the sample in the solution and the initial volume of the solution.

(b) Slag Analysis

(1) Procedure

After weighing, the slag samples were dissolved in 1 ml of 40% hydroflouric acid in volumetrically calibrated screw cap polypropylene bottles. High silica slags usually dissolved overnight, while low silica slags occasionally took over a week to dissolve. Addition of one drop of HNO_3 often speeded up dissolution. There was no visual or analytical evidence that the slags did not eventually dissolve completely in the hydroflouric acid.

Once the dissolution was complete, the bottles were filled to their calibrated marks with water.Three sizes of bottles were used: 35 ml for samples below 0.01 gm, 65 ml for samples between 0.01 and 0.022 gm and 155 ml for larger samples. The calibration mark was in the narrow neck of the bottle and bottles could be refilled to an accuracy of one or two drops of water.

(2) Some general observations on the analysis

(a) Usually the slags from one run would be analysed as a batch of 12-15 solutions. Each element in solution was analysed in duplicate, and occasionally in triplicate, if the concentration was low (e.g. silicon in low silica slags).

(b) Under some conditions, one element in solution will interfere with the analysis of another. A series of solutions were made up, at concentrations similar to those found in the actual slag solutions, to test the following:

The effect of iron and copper on the silicon analysis
The effect of silicon and copper on the iron analysis
The effect of iron and silicon on the copper analysis
The effect of nickel on the iron analysis
The effect of iron on the nickel analysis

No evidence was found that the presence of any element in the solution affected the analysis of any other element under the conditions used.

(c) Standard solutions were made from commercially available 1000 parts per million standard atomic absorption solutions. The copper and nickel standards were in N HNO_3 and the iron in N HCl. The silicon standard was a sodium silicate solution.

(d) All elements except silicon were analysed using a two inch slot burner and an air/acetylene flame.

(e) A 2Å resolution was used for all analyses except for gold, where 7Å was used.

(f) Peak heights were measured relative to a base line given by distilled water.

(3) Copper analysis

The optimum concentration for copper is from 2 to 8 p.p.m. (p.p.m. = parts per million, i.e. grams per million millilitres). The bottle volumes were chosen to bring the copper concentration into this optimum range. In practice, the copper concentration varied from 1 p.p.m. to 40 p.p.m., but was generally below 10 p.p.m.

No particular difficulty was encountered in analysing the copper and duplicated results agreed with $\pm$ 1% of themselves.

(4) Nickel analysis

The most sensitive line for nickel is at 2320 Å. However, Perkin Elmer report possible interference between nickel and iron using this line, so a line at approximately 2308 Å was used instead.

The reproducibility of results was similar to that for copper (within $\pm$ 1%).

(5) Iron analysis

The iron contents of the solutions were in the order of 80-160 p.p.m. The optimum range for iron is about 5-10 p.p.m. No attempt was made to dilute the solutions as dilution errors would probably be as great as the analytical errors encountered. A less sensitive line was used.

It was noticed during analysis of slags from the copper/nickel runs that solutions with very high iron contents gave excessively high analysis results. This was cured by using a corrosion resistant nebulizer for the uptake of the solution into the flame.

Results were not as reproducible as those of copper and nickel, but generally agreed within $\pm$ 2-3%.

(6) Silicon analysis

Silicon was the most difficult element to analyse. This was mainly because the solutions contained from 20-60 p.p.m. Si whilst the optimum concentration was about 100-200 p.p.m.

A nitrous oxide acetylene flame, hotter than the air/acetylene flame, and a high temperature burner are necessary for silicon analysis. It is also necessary to use a very rich flame to detect silicon, and this leads to carbon build-up around the burner slot, which must be removed periodically.

Results were generally reproducible to within $\pm$ 3-5%. In many cases, triplicate analyses were made.

(7) Gold analysis

The gold content of the slags was extremely low, ($\sim$0.005 wt%). Because of this, a special series of slag samples were taken during the early copper/gold runs. The slag samples of about 0.05 gm in weight, were made up into solutions of only 15 mls. Gold concentrations of about 0.2 p.p.m. were achieved. Since the optimum level for analysis is about 15 p.p.m., errors of $\pm$ 50% could be expected in the analysis.

(c) Metal analysis

Drillings of about 0.05 to 0.10 gm. were taken from the metal samples, weighed and dissolved in $\sim$1.5 mls of conc.acid in small beakers. A mixture of conc. HCl and HNO_3 was used for the copper/gold alloys and conc. HNO_3 alone for the copper/nickel alloys. The resulting solution was made up to 100 ml in a graduated flask. 10 ml of this first

solution was made up to 250 ml in a second graduated flask. The first solution was analysed for iron and the second solution for copper and gold or copper and nickel. This gave a total metallic content of the second solution of 30-40 p.p.m. and an iron content of 0.1 to 40 p.p.m. in the first solution.

The metal was not analysed for silicon. Because of the large negative free energy of formation of SiO_2 from Si and O_2, the concentration of Si in the metal was expected to be very small.

All analysis was done using the Perkin Elmer atomic absorption spectrophotometer. Conditions were similar to those reported for the slag analyses, except that the corrosion resistant nebulizer was not used for the iron analyses, and the iron results had better reproducibility.

Copper/gold alloys

Because of the constancy of the copper/gold results, only 20 of these samples were analysed for copper and gold. All samples were analysed for iron.

Copper/nickel alloys

All copper/nickel alloys were analysed for copper, nickel and iron.

8. DISCUSSION OF EXPERIMENTAL TECHNIQUE

(a) Use of Copper/Gold Alloys

Gold was added to the copper for two main reasons. The gold itself is virtually insoluble in the slag (Altman and Kellogg[72] suggest 0.008 wt%), and so any appreciable quantity of gold found in the slag can be attributed to the presence of entrained alloy. Analysis of the gold would allow the amount of entrained copper in the slag to be calculated, and subtraction of this value from the total slag copper would give the true copper solubility.

Richardson and Billington[67] found that equilibration of pure copper with a $CaO-Al_2O_3-SiO_2$ slag gave rise to precipitation of pure metal in the slag due to local supersaturation caused by small temperature fluctuations. Alloying with gold lowers the copper activity and reduces the probability of supersaturation with respect to pure copper. Ideally, a higher gold content would have been used, but alloys with significantly higher gold contents have poor levitation characteristics.

Sixteen slags were analysed for gold as described in the analysis section. The results are plotted against wt% copper in the slag in Figure 2.9, page 54. Two of the slags were too small for successful analysis. The gold contents are very low and there seems no correlation between gold and copper contents. This suggests that entrainment of alloy in the slag was not a significant feature of the experiments. Even if all the gold in the slag was from entrained alloy, then for a slag containing 2 wt% copper, 98 wt% of this copper would be soluble copper, and only 2% would be from entrainment. Therefore, copper (and nickel) in the slags was always considered to be in true solution.

Visual observation of a levitated drop shows that both the metal and the slag phase are well stirred. This should encourage entrainment of the metal in the slag.The lack of entrainment found experimentally suggests that the nature of the levitation forces inhibits movement of metal droplets away from the main levitated drop.

(b) Gas/Metal Equilibrium

Toop and Richardson[100] have investigated the steady state resulting from passing CO/CO_2 gas mixtures over levitated drops of copper and nickel at temperatures from 1200 to 1650°C. The results show that the steady state obtained with cold gas and hot metal is the same as the isothermal equilibrium state so far as partition of oxygen is concerned. Difficulty was found in reaching a steady state at the lower temperatures, and this was further investigated by Glen,[101] and Forster.[102] It was found

Gold contents of slags FIG. 2.9

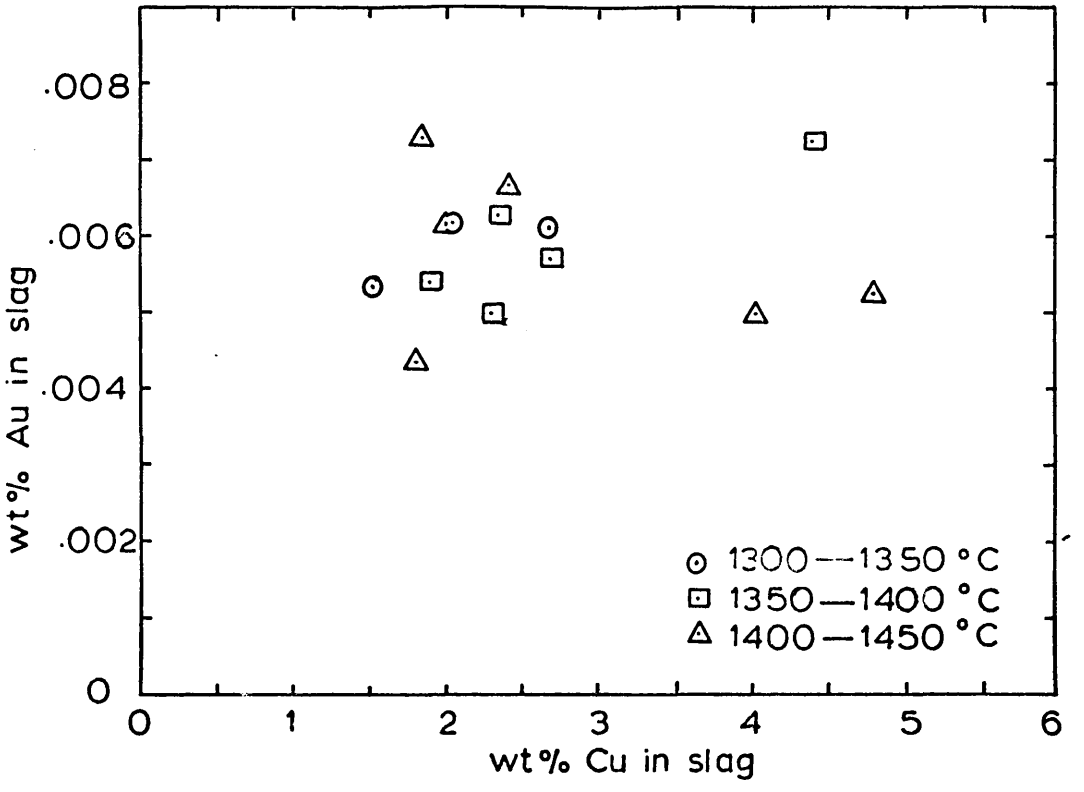

FIG. 2.10

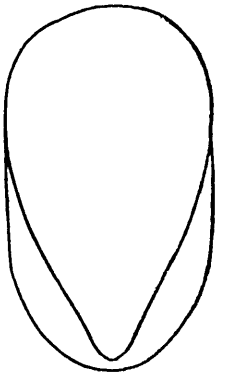

Cross section of levitated metal with slag attached

that very small quantities of silicon in the metal greatly inhibited the transfer of oxygen to the drop, possibly by forming a solid SiO_2 'monolayer skin' around the drop. Removal of the SiO_2 allowed steady state conditions to be rapidly achieved, within 1-2 minutes.

No kinetic problems were expected with a slag metal system where the silica activity is less than unity. Even if oxygen transfer between the gas and metal phase is inhibited, there is a good mechanism of transfer of oxygen between the gas and slag phases through the presence of Fe^{2+} and Fe^{3+} ions.

(c) Slag and Metal Temperatures

Temperature measurements of an inductively heated liquid drop (not levitated) supports the view that the temperature of a levitated drop should be uniform throughout, as heat can be lost only from the surface, and it is in the surface that heat is generated.[100]

The slag phase was less inductively heated, and there must have been a temperature gradient across the slag between the metal and the gas phase. Several factors suggest this temperature gradient was small:

(1) 1 gm copper drops were loaded with about 0.2-0.3 gm of slag and then rapidly solidified with helium whilst still levitated. A typical cross-section of such a drop is shown in Figure 2.10, page 54, and shows that the metal elongates as slag is added, giving a rather thin slag layer at any point. With the weights of slag used in the actual experiments ($\sim$0.04 gm) the slag layer was extremely thin ($\sim$0.15 mm) and visual observations suggested that temperature gradients over the surface of the slag were very small. Temperature gradients could be seen when large quantities of slag were added, which was the main reason that slag weights were kept to a minimum.

(2) Possibly, too, the gas may be significantly preheated by passing over the upper metal phase, although the Reynolds Number for the gas passing over the drop, calculated at room temperature, shows the flow was well into the turbulent region. ($Re_{actual} \cong 85$, and $Re_{critical} \cong 1$).

(d) CO, CO_2 and the He Flowrates

In all experiments the total CO plus CO_2 gas flowrate was kept at about about 600 ml/min. This flowrate was chosen mainly for experimental

convenience. High flowrates would have cooled the copper/gold alloys excessively, and would have diluted the He required for the copper/nickel alloys.

Addition of helium to the gas stream did not seem to affect the equilibrium between the metal and the CO/CO_2 gases. While there may be a thermal segregation effect between the helium and the heavier gases, helium should not affect the ratio of CO to CO_2 and so should not affect the oxygen potential at the drop surface. In the 20% Ni runs, the higher temperature equilibrations did not require the use of helium, and no anomaly was observed when helium was added for the lower temperature equilibrations.

(e) Gas/Metal/Slag Equilibrium

Previous work[101,102,109] has suggested that equilibrium between the three phases is reached within a minute or so. A series of samples were levitated with equilibration times ranging from over an hour down to five minutes, with no significant difference in the results. For practical convenience, equilibration times of about 20 minutes were used.

No direct evidence was obtained that a slag with an initially high copper content would give the same equilibrium copper level as the copper-free slags used, but because of variations in temperature to which a drop was subjected, the experiment would be unworkable if this were not the case.

(f) Slag Sampling Technique

The main aim in choosing the slag sampling technique was to allow the slag to be cooled out of contact with the metal phase. Other workers[108,109] have emphasised the rapidity with which redistribution between phases can occur on cooling. Caryll and Ward[108] overcame the problem by catching the drop between two copper plates. The resultant slag/metal foil is difficult to analyse.

It is not known how much the equilibrium was disturbed using the technique adopted in this work. With increasing nickel content of the alloys, there was an increasing tendency for the drop to stick to the alumina rod and for a bead of metal to be detached along with the slag. This tendency probably accounts for the relatively high scatter of copper and nickel slag contents from the 35% Ni and 50% Ni alloys, and was the reason that alloys of higher nickel contents were not used.

Distin et al[59] recently sampled iron silicate slags on levitated

iron droplets at $\sim$1700-1900^{o}C by allowing the slag to run down a molybdenum wire pushed into the slag. It was impossible to sample slags from copper/gold and low nickel/copper alloys in this way, but some success was achieved in taking samples from slags equilibrated with pure nickel.

(g) Ferrous and Ferric Iron Analyses

No attempt was made to differentiate between iron in the ferrous and ferric state. This was mainly because of the small size of the samples, and partly because of the slow cooling rate of the slag. On cooling with limited access to oxygen, a competitive situation is set up between copper and iron for oxygen. The overall effect is that a reaction such as

$$3FeO + Cu_2O \longrightarrow 2Cu + Fe_3O_4$$

proceeds to the right, precipitating copper, and changing the Fe^{2+}/Fe^{3+} ratio in the slag.

CHAPTER 3.

RESULTS

Guide to Experimental Runs. TABLE 3.1

Alloy	Code	Slag	CO_2/CO	Temp. Range °C
10% Au/Cu	CB(a)	B	2.028	1300-1450
"	CB(b)	B	20.53	"
"	CC(a)	C	1.732	"
"	CC(b)	C	8.471	"
"	CC(c)	C	36.09	"
"	CD(a)	D	1.741	"
"	CD(b)	D	8.447	"
"	CD(c)	D	21.45	"
"	CD(d)	D	25.93	"
"	CE(a)	E	1.736	"
"	CE(b)	E	5.040	"
10% Ni/Cu	N10C(a)	C	2.00	1350-1500
"	N10B(a)	B	5.00	"
"	N10B(b)	B	12.0	"
"	N10E(a)	E	5.00	"
20% Ni/Cu	N20B(a)	B	2.27	1350-1500
"	N20B(b)	B	5.00	"
"	N20C(a)	C	8.36	"
"	N20B(c)	B	16.4	"
"	N20E(a)	E	2.26	"
"	N20E(b)	E	5.00	"
"	N20E(c)	E	8.62	"
35% Ni/Cu	N35C(a)	C	2.00	1350-1500
"	N35B(a)	B	5.00	"
"	N35B(b)	B	12.0	"
"	N35E(a)	E	5.00	"
50% Ni/Cu	N50C(a)	C	8.55	1350-1500
"	N50E(a)	E	8.52	"

This table is reproduced as a fold-out sheet at the end of the thesis.

1. GUIDE TO EXPERIMENTAL RUNS AND RESULTS

Table 3.1, page 59, shows the experimental runs which were carried out. The nominal composition of the slags is given on page 37. In the Cu/Ni alloy runs, the intention was to compare the two slags B and E, of high and low silica content. Slag C was occasionally used in place of slag B to give a more constant slag composition throughout the high silica runs, although its use in runs N20C(a) and N50C(a) was misjudged.

Each run has been given a descriptive code number, as shown in Table 3.1. The first letter distinguishes between Copper/gold runs and copper/Nickel runs.

The slag and metal samples from the runs were analysed as described in the 'Experimental' section. The results of these analyses are given in this chapter, together with the calculated values of $CuO_{.5}$ and NiO activities, and other relevant quantities.

The 'Results' section has been set out in the following order.

(1) Table of thermodynamic data used in the calculations.

(2) Tables of the slag and metal analyses, with graphs of wt% Cu and Ni in the slags against temperature.

(3) Notes on the treatment of these results, followed by tables of quantities calculated from the results, and other relevant information.

(4) Graphical representation of various aspects of the results and calculations, preceded by an index to the graphs.

All analytical results are given in weight percent unless otherwise stated.

Table of Thermodynamic Data Table 3.2

(1)	$2(Cu) + \frac{1}{2}O_2 = 2(CuO_{.5})$	ΔG^o_T =	-29,260 + 10.488 T cal.
(2)	$(Ni) + \frac{1}{2}O_2 = [NiO]$	ΔG^o_T =	-59,187 + 22.124 T "
(3)	ΔS_{fusion} NiO =	6.0 cal/ deg/ mol.	
(4)	$(Ni) + \frac{1}{2}O_2 = (NiO)$	ΔG^o_T =	-45,645 + 16.124 T "
(5)	$CO + \frac{1}{2}O_2 = CO_2$	ΔG^o_T =	-66,950 + 20.20 T "
(6)	$[Fe]_\gamma + \frac{1}{2}O_2 = (FeO)$	ΔG^o_T =	-54,880 + 10.54 T "
(7)	$3[Fe]_\gamma + \frac{1}{2}O_2 = [Fe_3O_4]$	ΔG^o_T =	-261,186 + 71.86 T "
(8)	$2[Fe]_\gamma + 1\frac{1}{2}O_2 = [Fe_2O_3]$	ΔG^o_T =	-193,001 + 58.74 T "
(9)	Activities in Cu/Au alloys, see note (9)		
(10)	Activities in Cu/Ni alloys, see note (10)		

( ) indicates liquid

[ ] indicates solid

2. THERMODYNAMIC DATA USED

A table of thermodynamic data used in the calculations is given on page 61. Some notes on the data are given below.

(1) The equation used by Altman and Kellogg,[72] taking data from Mah et al.[114]

(2) Taken from Kellogg[115] for the reaction

$$Ni_{(s)} + \tfrac{1}{2} O_2 = NiO_{(s)}$$

and extended to higher temperatures for liquid nickel by Worner.[116] This is in good agreement with the equation of Steele[117] for 900-1400°K, and assuming ΔH_{fusion} of nickel is 4.2 Kcal.

(3) The heat of fusion of nickel oxide has not been measured experimentally, but it was thought preferable to estimate a heat and entropy of fusion rather than give nickel oxide activities relative to solid nickel oxide.

The high temperature crystal structure of NiO is of the NaCl type. Ionic compounds of this structure typically have an entropy of fusion of about 6.0 to 6.3 cal/deg/mol., for example, ΔS_f for NaCl = 6.2, for KF = 6.0, for KCl = 6.1 cal/deg/mol. This is somewhat lowered for predominantly covalently bonded compounds (e.g. ΔS_f AgCl = 4.25 cal/deg/mol.). For the first transition group divalent oxides of NaCl-type structure, entropies of fusion are available for TiO, ΔS_f = 6.1; MnO, ΔS_f = 6,2 and FeO, ΔS_f = 4.6 cal/deg/mol.[118] Covalency is not very high in the first transition series, but there is some evidence that covalency tends to increase along the series from Ti^{2+} to Ni^{2+}. The increase appears to be small, however, and the electronic conductivity and paramagnetism of (stoichiometric) NiO suggest an essentially isolated Ni^{2+} ion in an oxide anion lattice.[119] Wells[120] calls the FeO structure a distorted variant of the NaCl structure. Covalency can bring about distortion of the lattice, but the next two oxides in the series, CoO and NiO are not distorted. The low ΔS_f value for FeO is therefore not thought to be due to covalency, but is more probably connected with the non-stoichiometric nature of FeO. TiO, MnO and NiO also show varying degrees of non-stoichiometry, but this is not accompanied by significant distortion. Therefore ΔS_{fusion} for NiO has been estimated as 6.0 cal/deg/mol, a value in line with TiO and MnO rather than FeO.

(4) This is derived from (2) and (3), taking the melting point of NiO as 1984°C [118] and ignoring specific heat differences between solid and liquid NiO, so:

$$NiO_{(s)} = NiO_{(l)} \quad \Delta G^{o}_{T} = 13,542 - 6.0\ T$$

(5) Recommended by Schwerdtfeger and Turkdogan[112] from JANAF tables.[121]

(6) Derived from the equations used by Schuhmann and co-workers[55,56] in their studies on iron silicate melts. Standard states were chosen as aFeO = 1 for pure Fe-O melts (0% SiO_2) in equilibrium with γiron, and aFe = 1 for solid γFe.

(7) and (8) are the best straight line equations for the data for those reactions in the JANAF tables.[121]

(9) Activities for copper in the copper/gold alloys were derived from the data of Edwards and Brodsky,[122] and are given below. The variation of aCu with temperature over the range 1300-1450°C is negligible at high copper contents.

N Cu	aCu
0.80	0.803
0.85	0.858
0.90	0.906
0.95	0.952

(10) Values of aNi and aCu in the Cu/Ni alloys were derived from the data recommended by Elford et al,[123] and are plotted in Fig. 3.1, page 64.

activities in Cu/Ni alloys FIG. 3.1

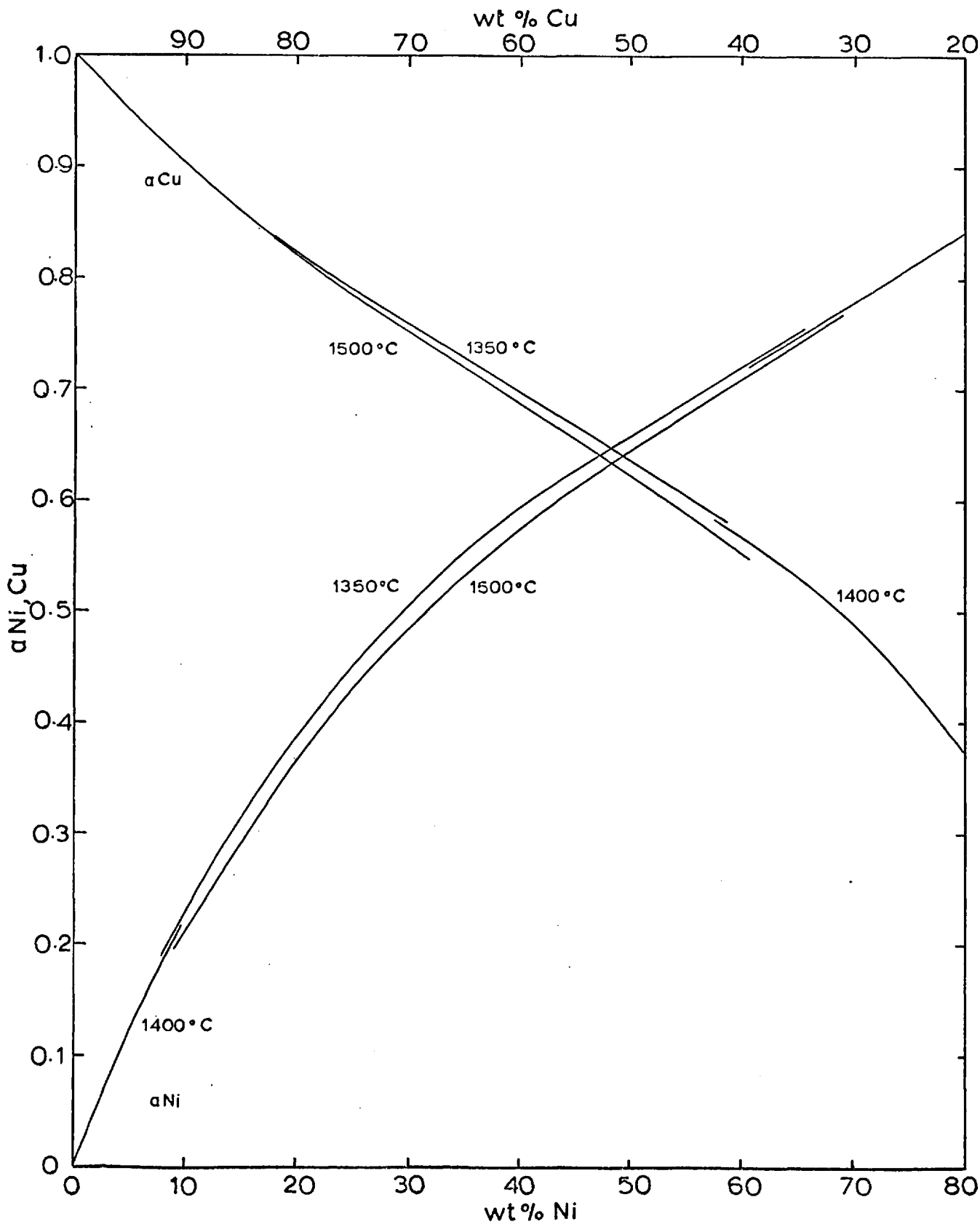

3. RESULTS OF ANALYSES

(a) Copper/Gold Runs - Slag Analyses Results

The slag analyses for the copper/gold runs are given between pages 66 and 69. The 'Total' given is the sum of Cu_2O + SiO_2 + FeO. Also included are the iron analyses of the metal drops with which the slags were equilibrated. The iron analysis is placed alongside the analysis of the slag sample taken immediately before the metal was quenched. For the gold content of the slags, see Chapter 2, section 8(a), page 53.

(b) Copper/Nickel Runs - Slag Analyses Results

The slag analyses for the copper/nickel runs are given between pages 70 and 78. The 'Total' given is the sum of Cu_2O + NiO + SiO_2 + FeO. The asterisk alongside some of the slag temperatures is used to indicate the slag sample taken immediately before the metal drop was quenched. Brackets around the figure in the 'Total' column, i.e. (100), indicates that the iron analysis was unsatisfactory (see Chapter 2, section 7(b)(5), page 51) and the value given is an estimated one.

(c) Copper/Gold Runs - Metal Analyses Results

Twenty copper/gold alloys were analysed for copper and gold. Typical results are given in the table on page 79. The average analysis for all copper/gold alloys was taken to be 89.8 wt% Cu, 10.1 wt% Au, and 0.1 wt% Fe for calculation of copper activities.

All the copper/gold alloys were analysed for iron. The results are given in the tables of analyses for the Cu/Au runs, pages 66 to 69. The iron analysis is placed alongside the analysis of the slag sample taken immediately before the metal was quenched.

(d) Copper/Nickel Runs - Metal Analyses Results

All the copper/nickel alloys were analysed for copper, nickel and iron. The totalled weight percents were usually within $\pm$ 2 wt% of 100% and the results given here have been adjusted to a 100 wt% total. The results are given on pages 80 to 82.

As in the case of the copper/gold alloys, the temperature refers to the temperature of the slag sample taken immediately before the metal was quenched. An average analysis of copper and nickel is given at the foot of each section. This analysis was used for the calculation of activities of copper and nickel in the metal.

Cu/Au Runs, Analyses in Wt.%

Run	Cu	Cu_2O	FeO	SiO_2	Total	T°C	Fe in metal
CB(a)	1.17	1.31	60.1	34.3	95.7	1302	0.302
	1.26	1.42	60.6	35.4	97.4	1303	
	1.28	1.44	57.3	-	-	1327	
	1.33	1.49	62.0	-	-	1328	0.335
	1.55	1.75	58.9	-	-	1357	
	1.59	1.78	59.3	36.9	98.0	1357	0.249
	1.75	1.96	60.8	38.1	100.9	1396	
	1.66	1.86	63.3	36.4	101.6	1396	0.352
	2.03	2.27	59.2	37.9	99.3	1429	0.291
	2.13	2.40	58.9	-	-	1444	0.289
	1.98	2.22	58.9	-	-	1449	0.318
	2.21	2.47	58.4	40.0	100.8	1465	0.368
CB(b)	4.19	4.72	63.9	-	-	1288	0.030
	4.20	4.72	58.6	33.2	96.5	1289	
	3.80	4.28	56.3	-	-	1291	
	4.88	5.47	60.1	34.4	99.9	1324	
	4.86	5.45	60.2	33.7	99.4	1324	0.045
	5.44	6.10	62.2	33.4	101.7	1355	
	5.52	6.19	59.5	32.4	98.1	1356	0.045
	6.58	7.38	58.1	32.8	98.3	1397	0.139
	7.72	8.66	57.4	33.0	99.0	1431	0.043
CC(a)	1.28	1.44	67.5	34.7	103.6	1337	0.377
	1.41	1.59	67.4	33.2	102.2	1349	
	1.27	1.42	68.2	30.3	99.9	1351	0.566
	1.37	1.54	66.6	34.4	102.5	1355	
	1.58	1.78	65.5	36.3	103.6	1373	0.429
	1.58	1.78	66.6	32.9	101.3	1378	
	1.52	1.72	65.2	33.1	100.0	1386	
	1.67	1.88	64.4	35.9	102.2	1401	
	1.68	1.89	64.4	34.9	101.2	1413	0.490
	1.87	2.10	62.7	31.2	96.0	1438	0.576

Cu/Au Runs, Analyses in Wt.%

Run	Cu	Cu_2O	FeO	SiO_2	Total	T°C	Fe in metal
CC(b)	2.52	2.83	68.1	32.1	103.0	1297	
	2.33	2.62	69.0	29.9	101.5	1297	0.137
	3.09	3.48	68.7	31.5	103.6	1345	
	2.75	3.10	68.9	31.0	102.9	1346	0.101
	3.43	3.86	66.8	29.5	100.2	1378	
	3.48	3.92	67.3	29.0	100.2	1389	0.104
	3.74	4.21	66.1	29.6	99.9	1400	
	4.41	4.96	67.8	29.8	102.6	1437	
	4.41	4.96	67.8	28.5	101.2	1438	0.138
	4.62	5.20	66.5	30.2	101.9	1445	0.112
	4.79	5.39	66.1	29.6	101.1	1449	
CC(c)	6.61	7.44	64.7	28.6	100.7	1302	
	7.80	8.78	62.7	25.0	96.5	1343	
	7.67	8.64	60.1	25.0	93.7	1345	
	8.36	9.41	61.8	26.9	98.1	1373	0.182
	8.69	9.78	62.3	26.7	98.8	1378	
	9.96	11.21	60.3	25.7	97.2	1397	
	11.00	12.38	60.7	26.0	99.1	1410	0.098
	11.64	13.11	58.7	24.2	96.3	1430	
	13.20	14.90	58.9	25.9	99.7	1448	0.050
	14.75	16.61	58.9	26.0	101.5	1459	
CD(a)	1.26	1.41	73.1	25.5	100.0	1332	0.616
	1.34	1.51	66.8	29.0	97.3	1357	
	1.35	1.52	69.2	27.8	98.5	1359	0.540
	1.52	1.71	72.0	26.9	100.6	1371	
	1.51	1.69	73.9	24.4	100.0	1385	
	1.54	1.73	73.8	24.6	100.1	1389	0.644
	1.56	1.74	69.7	29.1	100.5	1395	
	1.69	1.90	69.9	28.1	99.9	1410	
	1.81	2.04	69.2	27.8	99.0	1418	
	1.84	2.07	72.7	25.1	99.9	1425	0.706
	1.99	2.24	67.4	28.2	97.8	1441	
	2.00	2.25	73.6	24.5	100.3	1448	

Cu/Au Runs, Analyses in Wt.%

Run	Cu	Cu_2O	FeO	SiO_2	Total	T°C	Fe in metal
CD(b)	2.40	2.71	73.5	22.5	98.7	1315	0.194
	2.56	2.88	72.9	24.1	99.9	1326	
	2.48	2.79	73.3	23.4	99.5	1336	
	3.12	3.51	74.7	24.2	102.4	1354	
	3.32	3.74	73.3	23.1	100.1	1360	0.259
	3.42	3.85	72.2	22.5	98.6	1374	
	3.22	3.63	71.5	22.9	98.0	1375	0.177
	4.02	4.53	73.1	22.9	100.5	1404	
	3.95	4.45	72.6	23.6	100.6	1407	0.084
	4.02	4.53	71.0	23.4	98.9	1427	
	4.26	4.79	72.8	21.6	99.2	1437	
	4.61	5.18	70.5	22.5	98.2	1447	
CD(c)	4.15	4.67	71.5	22.3	98.5	1291	
	4.59	5.17	71.5	22.1	98.8	1309	0.110
	4.44	5.00	71.0	21.9	97.9	1319	
	4.81	5.42	69.6	20.1	95.1	1335	
	5.36	6.03	70.7	21.4	98.1	1345	
	5.21	5.87	70.0	20.3	96.2	1350	0.105
	5.95	6.70	71.3	21.3	99.3	1373	
	6.26	7.05	70.7	21.9	99.6	1386	0.057
	7.14	8.04	68.7	20.4	97.1	1397	0.055
	7.36	8.29	70.0	20.1	98.4	1407	
	7.20	8.11	69.2	20.3	97.6	1416	0.058
	7.85	8.84	68.4	20.8	98.0	1430	0.062
CD(d)	6.09	6.86	69.1	21.3	97.3	1349	
	6.60	7.43	68.8	20.2	96.4	1357	
	6.75	7.60	68.7	20.8	97.1	1374	

Cu/Au Runs, Analyses in Wt.%

Run	Cu	Cu_2O	FeO	SiO_2	Total	T°C	Fe in metal
CE(a)	1.47	1.66	84.7	13.5	99.9	1344	0.788
	1.51	1.70	82.6	14.4	98.7	1363	
	1.59	1.79	84.4	13.7	99.9	1380	
	1.57	1.77	83.6	13.2	98.6	1385	0.764
	1.52	1.71	81.3	15.8	98.8	1386	
	1.56	1.76	83.8	14.2	99.8	1393	
	1.61	1.81	78.7	16.9	97.4	1405	
	1.70	1.91	80.9	17.4	100.2	1419	
	1.88	2.11	81.8	14.4	98.3	1429	
	1.95	2.19	83.9	13.8	99.9	1439	0.749
	2.01	2.27	82.6	14.6	99.5	1441	
	1.96	2.21	82.8	14.9	99.9	1454	0.738
	1.97	2.22	81.6	15.8	99.6	1464	
CE(b)	2.27	2.56	82.1	13.0	97.7	1351	
	2.38	2.69	81.0	13.5	97.2	1353	
	2.16	2.43	84.1	13.1	99.6	1354	
	2.37	2.67	83.6	13.0	99.4	1364	0.354
	2.33	2.62	82.3	13.0	97.9	1373	
	2.68	3.02	83.6	13.7	100.3	1385	
	2.58	2.91	84.3	12.6	99.8	1389	
	2.74	3.08	84.1	13.2	100.4	1400	0.262
	2.65	2.98	83.2	14.3	100.5	1402	0.364
	2.97	3.34	82.3	13.9	99.5	1412	
	3.24	3.65	82.5	13.4	99.6	1416	
	3.07	3.46	83.4	13.4	100.3	1422	
	3.53	3.97	78.5	13.8	96.3	1436	
	3.79	4.27	79.1	13.6	97.0	1452	0.260

Cu/Ni Runs, Slag Analyses in Wt.%

Run	Cu	Cu_2O	Ni	NiO	FeO	SiO_2	Total	T°C
N10C(a)	1.45	1.63	0.348	0.443	63.4	33.6	99.1	1332
	1.70	1.91	0.435	0.554	55.4	38.8	96.7	1342
	1.51	1.70	0.355	0.452	62.8	33.6	98.6	1355*
	1.53	1.72	0.350	0.445	64.6	31.4	98.2	1378*
	1.79	2.02	0.435	0.554	54.5	41.1	98.2	1379
	1.63	1.84	0.385	0.490	60.7	33.3	96.3	1379
	1.76	1.99	0.413	0.526	58.4	36.8	97.7	1386
	1.63	1.84	0.404	0.514	63.3	32.1	97.8	1398*
	1.83	2.06	0.422	0.537	60.2	34.4	97.2	1402
	2.06	2.31	0.486	0.618	58.1	35.4	96.4	1438
	1.92	2.16	0.451	0.574	61.4	33.6	97.7	1442
	1.89	2.12	0.468	0.596	63.3	31.0	97.0	1449*
	2.10	2.36	0.508	0.646	56.6	38.5	98.1	1455
	2.02	2.27	0.502	0.639	57.9	37.2	98.0	1459
	2.18	2.45	0.503	0.640	58.4	37.8	99.3	1463
	1.94	2.18	0.512	0.652	59.4	37.4	99.6	1481*
N10B(a)	2.04	2.29	0.680	0.870	62.3	33.4	98.9	1324*
	2.19	2.47	0.830	1.06	62.7	34.3	100.5	1329
	2.40	2.70	0.899	1.14	61.0	35.5	100.3	1334
	2.43	2.73	0.850	1.08	62.8	33.4	(100)	1343
	2.48	2.79	0.884	1.12	62.6	33.9	100.4	1349
	2.51	2.82	0.905	1.15	63.3	32.7	(100)	1357*
	2.46	2.77	0.866	1.10	62.6	33.7	(100)	1370
	2.52	2.84	0.930	1.18	62.1	33.2	99.3	1381*
	2.80	3.15	0.990	1.26	62.5	35.4	102.3	1383
	2.95	3.32	1.03	1.31	62.5	32.9	(100)	1410*
	3.10	3.49	1.07	1.36	62.3	35.1	102.2	1411
	2.83	3.18	1.08	1.37	61.5	33.4	99.4	1414
	3.45	3.88	1.19	1.52	-	32.9	-	1451*
	3.56	4.01	1.27	1.62	59.6	33.2	98.4	1453
	3.80	4.28	1.34	1.71	61.1	33.4	100.5	1469

Cu/Ni Runs, Slag Analyses in Wt.%

Run	Cu	Cu_2O	Ni	NiO	FeO	SiO_2	Total	T°C
N10B(b)	3.32	3.74	1.59	2.02	58.4	33.3	97.5	1321
	3.16	3.56	1.54	1.97	59.9	32.6	98.0	1324*
	3.39	3.82	1.83	2.32	59.3	33.4	98.8	1334
	3.42	3.85	1.63	2.07	60.6	31.8	98.3	1350
	3.83	4.33	1.93	2.45	58.9	31.7	97.4	1362*
	4.07	3.61	2.00	2.55	60.2	31.7	98.1	1376
	4.21	4.74	1.99	2.53	57.9	32.1	97.3	1386
	4.37	4.92	2.14	2.72	58.1	31.8	97.5	1389
	4.29	4.82	2.12	2.70	58.4	31.9	97.8	1393*
	4.82	5.43	2.34	2.98	56.9	31.2	96.5	1426*
	4.84	5.45	2.42	3.08	57.1	30.6	96.2	1434
	5.40	6.08	2.55	3.24	56.1	30.6	96.0	1435
	5.11	5.75	2.36	3.00	56.1	31.4	96.2	1450
	6.15	6.92	2.96	3.77	56.7	31.2	98.6	1474
	6.11	6.88	3.17	4.03	56.3	30.2	97.4	1486*
N10E(a)	2.17	2.44	0.813	1.03	80.5	12.5	96.5	1341
	2.29	2.58	0.870	1.11	80.4	13.4	97.5	1349
	2.52	2.84	0.913	1.16	80.5	13.4	97.9	1356
	2.34	2.63	0.873	1.11	80.1	11.7	95.5	1365*
	2.71	3.05	1.02	1.30	80.4	13.2	97.9	1384
	2.52	2.84	1.00	1.27	79.9	12.8	96.8	1387*
	2.69	3.03	1.05	1.34	80.4	13.0	97.8	1397
	2.86	3.22	1.08	1.37	78.6	13.2	96.4	1400
	3.22	3.63	1.21	1.55	81.2	13.2	99.6	1420
	3.18	3.59	1.21	1.54	79.8	12.8	97.7	1430*
	3.48	3.92	1.33	1.69	79.1	12.3	97.0	1448
	3.62	4.08	1.35	1.72	78.0	12.9	96.7	1457
	3.78	4.26	1.45	1.85	78.9	12.8	98.2	1471

Cu/Ni Runs, Slag Analyses in Wt.%

Run	Cu	Cu_2O	Ni	NiO	FeO	SiO_2	Total	T°C
N20B(a)	1.41	1.59	0.602	0.766	63.6	34.5	100.5	1330*
	1.82	2.05	0.892	1.13	58.6	36.9	98.7	1362
	1.74	1.96	0.728	0.926	62.9	35.1	100.9	1363
	1.87	2.11	0.776	0.987	61.6	35.3	(100)	1398*
	2.06	2.32	0.860	1.09	56.5	39.8	99.7	1404
	1.99	2.24	0.888	1.13	55.0	36.5	98.5	1413
	1.93	2.17	0.816	1.04	62.7	34.1	(100)	1418*
	2.06	2.31	0.846	1.08	54.6	39.0	97.0	1420
	2.09	2.35	0.921	1.17	60.0	36.7	(100)	1444
	2.24	2.52	0.966	1.23	63.4	32.7	(100)	1451*
	2.13	2.40	0.888	1.13	59.8	35.6	98.9	1453*
	2.03	2.29	0.830	1.06	53.3	40.7	97.4	1459
	2.58	2.90	1.09	1.38	53.8	38.6	96.7	1478
	2.50	2.81	1.07	1.36	57.2	38.3	99.7	1485
	2.52	2.83	1.09	1.38	60.9	34.3	99.4	1491*
N20B(b)	2.28	2.57	1.32	1.68	58.5	35.9	98.6	1340
	2.14	2.41	1.32	1.68	58.9	36.2	99.2	1345*
	2.28	2.57	1.57	2.00	56.7	35.9	97.2	1365
	2.97	3.34	1.95	2.48	53.4	38.7	97.9	1395
	2.67	3.01	1.63	2.07	56.3	36.4	97.8	1400
	2.81	3.16	1.62	2.06	56.3	35.7	97.2	1405*
	3.07	3.46	1.84	2.34	55.4	37.1	98.3	1421
	2.69	3.03	1.75	2.23	58.1	36.4	99.8	1427
	3.07	3.46	1.88	2.39	57.4	34.2	97.5	1447*
	3.24	3.65	2.00	2.55	54.8	35.3	96.3	1456
	2.98	3.36	2.00	2.55	56.0	36.6	98.5	1468
	2.86	3.22	2.08	2.65	58.1	34.4	98.4	1481*
	3.98	4.48	2.40	3.05	55.6	35.5	98.6	1484
	2.76	3.11	2.19	2.79	56.7	34.9	97.4	1493
	3.81	4.29	2.44	3.10	57.6	33.6	98.6	1498*

Cu/Ni Runs, Slag Analyses in Wt.%

Run	Cu	Cu_2O	Ni	NiO	FeO	SiO_2	Total	T°C
N20C(a)	2.49	2.80	2.08	2.65	65.4	26.6	97.4	1348*
	2.80	3.15	2.34	2.98	66.2	27.6	(100)	1358
	2.90	3.26	2.36	3.00	63.7	27.4	97.4	1368
	3.16	3.56	2.64	3.36	64.3	27.3	98.5	1386*
	3.03	3.41	2.64	3.35	67.1	26.1	100	1386
	3.52	3.96	2.85	3.62	63.8	26.5	97.8	1412*
	3.65	4.11	3.11	3.96	64.2	26.7	99.0	1415
	3.89	4.38	3.26	4.14	62.3	27.1	97.9	1425
	4.13	4.65	3.54	4.50	63.9	26.5	99.6	1440*
	4.36	4.91	3.78	4.81	62.9	25.9	98.5	1452
	5.42	6.10	4.48	5.70	61.4	24.8	98.0	1487
	5.77	6.50	4.57	5.82	61.5	25.3	99.1	1489
	5.03	5.66	4.70	5.98	62.2	26.2	(100)	1492*
N20H(c)	4.53	5.10	4.24	5.40	58.8	30.7	(100)	1360
	4.96	5.58	4.90	6.24	55.5	29.5	96.8	1365*
	4.80	5.40	5.09	6.48	59.8	28.7	100.4	1381
	4.75	5.35	4.52	5.75	58.7	30.2	(100)	1390*
	4.87	5.48	4.61	5.87	57.9	29.7	99.0	1401
	5.40	6.08	5.07	6.45	56.9	30.2	99.6	1426
	5.58	6.28	5.25	6.68	57.1	30.0	100.1	1429
	6.06	6.82	6.26	7.94	58.8	27.4	101.0	1430
	6.26	7.05	6.25	7.95	56.6	29.1	100.7	1446*
	7.06	7.95	7.15	9.10	52.7	27.7	97.5	1458*
	7.24	8.15	7.34	9.34	54.4	27.0	98.9	1459
	7.96	8.96	7.64	9.72	54.8	26.5	(100)	1503
	8.73	9.83	8.37	10.65	51.8	27.4	99.8	1511
	8.85	9.96	8.94	11.38	52.2	26.4	(100)	1516*

Cu/Ni Runs, Slag Analyses in Wt.%

Run	Cu	Cu_2O	Ni	NiO	FeO	SiO_2	Total	T°C
N20E(a)	1.19	1.32	0.502	0.639	78.5	19.6	(100)	1346
	1.23	1.38	0.564	0.718	81.0	16.9	(100)	1361*
	1.35	1.52	0.630	0.802	77.5	19.8	99.6	1390
	1.20	1.35	0.588	0.748	76.6	21.3	(100)	1402
	1.69	1.90	0.818	1.04	82.5	15.0	100.4	1403*
	1.83	2.05	0.844	1.07	78.1	18.1	99.3	1428
	1.67	1.88	0.787	1.00	78.8	18.3	(100)	1437
	1.72	1.94	0.763	0.971	67.4	29.4	99.7	1437*
	1.86	2.09	0.888	1.13	81.5	15.3	(100)	1469
	2.17	2.45	1.06	1.35	80.4	14.9	99.1	1474
	2.32	2.61	1.08	1.37	76.1	19.9	(100)	1478
	2.08	2.34	1.05	1.34	80.8	17.9	102.4	1479
	2.25	2.53	1.10	1.40	79.4	16.6	(100)	1482*
	2.42	2.72	1.16	1.47	76.2	18.3	98.6	1494
	2.39	2.69	1.11	1.42	69.6	21.9	95.6	1496
	2.65	2.98	1.23	1.57	77.2	18.3	(100)	1502*
N20E(b)	2.28	2.57	1.44	1.84	78.0	15.6	98.0	1375
	2.29	2.57	1.44	1.83	73.1	13.9	91.4	1381
	2.51	2.83	1.64	2.11	78.6	13.9	97.4	1396
	2.42	2.72	1.59	2.02	76.7	15.5	96.9	1398*
	2.51	2.83	1.66	2.14	77.3	14.2	98.4	1404
	2.76	3.10	1.78	2.27	76.2	14.9	96.5	1414
	2.70	3.04	1.85	2.35	79.1	12.9	97.4	1428
	2.89	3.25	2.05	2.60	77.8	12.1	95.7	1440
	3.16	3.56	2.01	2.56	80.8	13.3	100.2	1461*
	3.32	3.74	2.20	2.80	75.8	15.2	97.5	1467
	3.36	3.78	2.24	2.86	71.1	12.7	90.4	1476
	3.40	3.83	2.41	3.06	77.3	14.2	98.4	1489*
	3.56	4.01	2.50	3.17	75.4	16.4	99.0	1505
	3.84	4.32	2.75	3.50	-	-	-	1513

Cu/Ni Runs, Slag Analyses in Wt.%

Run	Cu	Cu_2O	Ni	NiO	FeO	SiO_2	Total	T°C
N20E(c)	3.25	3.66	2.65	3.37	79.7	13.3	(100)	1364
	3.52	3.96	3.10	3.94	79.4	12.7	(100)	1383
	3.61	4.06	3.00	3.82	80.1	12.0	(100)	1389
	3.59	4.04	2.96	3.77	79.8	12.4	(100)	1390
	3.52	3.96	3.25	4.14	80.3	11.6	(100)	1399 *
	3.95	4.45	3.60	4.58	78.8	12.2	(100)	1430
	4.35	4.90	3.74	4.76	78.1	12.3	(100)	1431
	4.22	4.75	3.94	5.01	78.7	11.5	(100)	1447 *
	5.05	5.69	4.41	5.61	76.4	12.3	(100)	1477
	4.97	5.60	4.25	5.41	76.9	12.0	(100)	1481
	5.17	5.82	4.67	5.94	76.8	11.5	(100)	1502 *
N35C(a)	2.10	2.36	1.71	2.18	58.5	35.6	98.6	1375
	1.79	2.02	1.39	1.78	53.8	37.0	94.6	1383
	1.71	1.92	1.32	1.68	56.6	38.1	98.3	1383
	1.78	2.00	1.27	1.61	61.0	33.5	98.1	1395 *
	2.16	2.44	1.78	2.27	54.0	37.2	95.9	1401
	2.06	2.32	1.49	1.90	58.5	35.9	98.6	1415
	1.90	2.14	1.34	1.71	58.1	35.1	97.1	1425 *
	2.21	2.49	1.61	2.05	50.6	39.1	94.2	1440
	2.08	2.34	1.39	1.77	53.8	39.6	97.5	1446
	1.89	2.13	1.30	1.65	54.5	40.5	98.8	1455 *
	2.17	2.44	1.38	1.76	52.5	41.7	98.4	1472
	1.98	2.22	1.21	1.54	54.9	38.5	97.2	1479 *
	2.14	2.41	1.33	1.69	55.6	35.9	95.6	1485
	2.23	2.51	1.47	1.86	56.0	37.9	98.3	1501
	2.21	2.49	1.54	1.96	56.3	35.7	96.5	1509
	2.36	2.66	1.51	1.92	57.6	37.9	100.1	1524 *

Cu/Ni Runs, Slag Analyses in Wt.%

Run	Cu	Cu_2O	Ni	NiO	FeO	SiO_2	Total	T°C
N35B(a)	2.39	2.68	2.41	3.06	55.3	37.1	98.1	1374
	2.38	2.68	2.31	2.93	56.3	36.6	98.5	1383
	2.36	2.66	2.22	2.83	56.7	36.8	99.0	1394*
	2.82	3.18	2.84	3.61	55.1	37.5	99.4	1400
	2.64	2.97	2.53	3.22	56.0	37.2	99.4	1407
	2.61	2.93	2.41	3.06	56.3	37.6	99.9	1432
	3.12	3.51	3.02	3.85	53.5	39.1	100.0	1446
	2.87	3.23	2.64	3.36	52.4	38.8	97.8	1447*
	2.96	3.33	2.78	3.53	52.1	39.5	98.5	1448
	3.10	3.49	2.78	3.54	54.0	39.8	100.8	1461
	3.57	4.02	3.31	4.21	53.8	47.4	109.4	1464*
	3.00	3.38	2.82	3.59	53.4	41.7	102.0	1464
	3.64	4.10	3.43	4.36	52.9	35.7	97.1	1506
	3.40	3.83	3.27	4.17	53.0	37.0	98.0	1518
	3.45	3.88	3.52	4.47	54.7	35.3	98.3	1519*
N35B(b)	2.92	3.29	3.73	4.75	58.5	35.1	101.6	1373
	3.00	3.38	3.70	4.71	56.1	35.7	99.9	1378
	2.82	3.18	3.51	4.47	58.4	33.2	99.2	1390*
	3.83	4.31	4.63	5.89	53.3	32.3	95.8	1436
	3.77	4.24	5.08	6.46	58.0	31.2	99.9	1443*
	3.82	4.30	4.50	5.73	57.2	32.3	99.5	1444
	4.16	4.68	6.20	7.89	54.9	32.1	99.6	1478
	4.48	5.04	6.20	7.89	53.5	31.4	97.8	1482*
	4.29	4.83	6.00	7.64	55.6	31.0	99.1	1482
	4.50	5.07	6.30	8.02	55.3	30.2	98.6	1500
	4.81	5.42	6.90	8.78	54.4	29.2	97.8	1519
	5.23	5.89	7.28	9.26	55.1	29.1	99.3	1521*

Cu/Ni Runs, Slag Analyses in Wt.%

Run	Cu	Cu_2O	Ni	NiO	FeO	SiO_2	Total	T°C
N35E(a)	2.19	2.47	2.37	3.02	78.4	14.0	97.9	1381
	2.10	2.36	2.17	2.76	75.9	17.3	98.3	1383
	2.19	2.47	2.34	2.98	78.6	14.4	98.4	1384*
	2.77	3.12	2.64	3.36	77.8	15.5	99.8	1428
	2.55	2.87	2.79	3.55	77.6	14.4	98.5	1431
	2.53	2.85	2.61	3.32	78.2	15.1	99.4	1434*
	2.84	3.20	3.02	3.84	78.9	13.9	99.8	1464
	2.71	3.05	2.89	3.68	79.0	14.4	100.1	1467*
	2.84	3.20	3.07	3.91	76.3	15.5	98.9	1478
	3.22	3.63	3.70	4.71	78.5	12.8	99.6	1519
	4.00	4.50	4.10	5.22	74.8	14.7	99.3	1522
	3.65	4.11	4.20	5.34	77.1	13.1	99.5	1523*
N50C(a)	2.01	2.26	3.11	3.96	65.2	28.2	99.7	1353*
	3.07	3.46	4.88	6.21	62.6	29.1	101.4	1361
	2.80	3.15	4.54	5.78	62.0	27.8	98.8	1391
	2.98	3.36	5.15	6.55	59.7	27.9	97.5	1398
	2.64	2.97	4.98	6.34	61.4	28.9	99.6	1404
	2.87	3.23	5.14	6.54	59.4	31.2	100.4	1408
	2.50	2.81	4.16	5.29	61.2	27.4	96.7	1414*
	3.41	3.84	5.93	7.55	57.8	32.1	101.2	1448
	3.71	4.18	5.86	7.46	57.6	30.8	100.1	1449
	3.50	3.94	5.38	6.85	57.9	31.1	99.8	1451*
	3.35	3.77	5.88	7.48	58.0	30.5	99.7	1455
	4.20	4.73	6.79	8.64	53.0	31.4	97.8	1477
	3.52	3.96	6.13	7.80	57.8	30.5	100.0	1487*
	4.06	4.57	5.73	7.29	59.2	29.9	101.0	1490
	3.66	4.12	5.94	7.56	59.4	29.0	100.1	1496*
	3.96	4.46	6.56	8.35	57.0	31.0	100.8	1511*

Cu/Ni Runs, Slag Analyses in Wt.%

Run	Cu	Cu_2O	Ni	NiO	FeO	SiO_2	Total	T°C
N50E(a)	3.30	3.72	5.45	6.93	77.1	16.8	104.5	1370*
	2.84	3.20	4.72	6.01	76.9	16.6	102.7	1387
	3.14	3.54	5.56	7.07	-	-	-	1400
	3.40	3.83	5.96	7.58	74.9	14.6	100.9	1401*
	2.71	3.05	4.88	6.21	75.2	14.0	98.5	1405
	3.53	3.97	6.00	7.64	-	-	-	1413
	3.51	3.95	6.22	7.92	72.2	15.0	99.1	1444
	3.15	3.55	5.40	6.87	70.9	14.6	95.9	1447
	3.24	3.65	5.94	7.56	75.6	14.8	101.6	1450*
	3.39	3.82	6.35	8.08	72.2	15.4	99.5	1485
	3.74	4.21	6.78	8.63	72.8	15.1	99.7	1487
	4.30	4.84	7.51	9.56	71.9	14.1	100.4	1511*

Cu/Au Runs, Metal Analyses in Wt.%

		Analysed Wt.%				Adjusted to 100% Total		
Run	T°C	Cu	Au	Fe	Total	Cu	Au	Fe
CC(b)	1297	91.3	9.89	0.137	101.3	90.1	9.76	0.135
CC(b)	-	89.2	9.97	0.259	99.4	89.7	10.03	0.260
CC(b)	1389	89.6	10.0	0.104	99.7	89.9	10.03	0.104
CC(b)	1438	88.6	9.88	0.138	98.6	89.8	10.02	0.140
CC(c)	1373	89.0	10.19	0.182	99.4	89.6	10.25	0.183
CC(c)	1410	89.1	10.02	0.098	99.2	89.8	10.10	0.100
CC(c)	1448	88.3	10.35	0.050	98.7	89.5	10.50	0.051

Cu/Ni Runs, Metal Analyses in Wt.%

	T°C	Cu	Ni	Fe
Run	1355	89.0	10.0	0.978
N10C(a)	1378	88.6	10.3	1.02
CO_2/CO	1398	88.8	10.2	0.994
2.00	1449	88.8	10.1	1.06
	1481	89.0	10.2	0.842
Average		88.4	10.16	

	T°C	Cu	Ni	Fe
Run	1365	89.3	10.1	0.546
N10E(a)	1387	89.2	10.2	0.533
CO_2/CO	1410	89.3	10.1	0.560
5.00	1430	89.3	10.2	0.485
	1515	89.2	10.4	0.400
Average		89.24	10.2	

Run	1324	89.5	10.1	0.351
N10B(a)	1357	89.4	10.2	0.312
CO_2/CO	1381	89.5	10.1	0.384
5.00	1410	89.6	10.2	0.283
	1451	89.5	10.3	0.285
Average		89.5	10.2	

Run	1330	78.1	20.4	1.57
N20B(a)	1398	78.6	19.9	1.47
CO_2/CO	1418	78.1	20.2	1.64
2.27	1451	78.2	20.3	1.56
	1453	78.2	20.3	1.48
	1491	78.0	20.3	1.64
Average		78.2	20.23	

Run	1324	89.7	10.2	0.140
N10B(b)	1362	90.0	9.92	0.070
CO_2/CO	1393	89.8	10.1	0.055
12.00	1426	89.8	10.1	0.032
	1486	90.1	9.91	0.026
Average		89.9	10.05	

Run	1345	79.6	19.8	0.567
N20B(b)	1405	79.7	19.7	0.522
CO_2/CO	1447	79.7	19.8	0.483
5.00	1481	79.6	19.9	0.464
	1498	79.2	20.4	0.430
Average		79.6	19.9	

Cu/Ni Runs, Metal Analyses in Wt.%

	T°C	Cu	Ni	Fe
Run	1348	79.4	20.1	0.479
N20C(a)	1386	79.7	19.9	0.409
CO_2/CO	1412	79.6	20.0	0.359
8.36	1440	79.2	20.6	0.247
	1492	79.4	20.3	0.348
Average		79.5	20.2	

	T°C	Cu	Ni	Fe
Run	1398	78.6	20.4	0.978
N20E(b)	1412	78.8	20.2	0.967
CO_2/CO	1461	78.8	20.2	0.895
5.00	1489	78.8	20.4	0.801
	1525	79.3	20.0	0.672
Average		78.8	20.2	

Run	1365	80.2	19.7	0.078
N20E(c)	1390	80.0	19.9	0.105
CO_2/CO	1420	80.3	19.7	0.074
16.42	1446	80.6	19.4	0.055
	1458	80.5	19.4	0.097
	1516	80.4	19.5	0.109
Average		80.3	19.6	

Run	1368	79.5	20.0	0.491
N20E(c)	1399	79.0	20.6	0.373
CO_2/CO	1447	80.1	19.7	0.247
8.62	1502	79.2	20.4	0.417
Average		79.4	20.2	

Run	1361	77.5	19.8	2.72
N20E(a)	1403	77.3	19.9	2.78
CO_2/CO	1437	77.3	20.1	2.63
2.26	1482	77.7	20.0	2.30
	1502	77.7	19.9	2.41
Average		77.55	19.9	

Run	1395	62.7	33.5	3.81
N35C(a)	1425	63.3	34.5	2.23
CO_2/CO	1455	63.2	34.4	2.37
2.00	1479	63.1	34.3	2.61
	1524	62.6	34.7	2.71
Average		63.0	34.3	

Cu/Ni Runs, Metal Analyses in Wt.%

	T°C	Cu	Ni	Fe
Run	1394	64.3	34.7	1.07
N35B(a)	1432	64.2	34.8	1.03
CO_2/CO	1447	64.3	34.8	0.892
5.00	1464	63.6	35.4	0.935
	1519	62.0	37.2	0.861
Average		64.1	34.9	

	T°C	Cu	Ni	Fe
Run	1353	49.2	49.1	1.79
N50C(a)	1381	49.7	48.9	1.39
CO_2/CO	1414	49.1	49.5	1.49
8.55	1451	48.7	49.8	1.55
	1487	49.3	49.6	1.19
	1496	48.7	50.3	1.06
	1511	48.9	50.2	0.932
Average		49.1	49.6	

Run	1390	65.0	34.4	0.630
N35B(b)	1398	64.9	34.5	0.662
CO_2/CO	1443	64.4	35.2	0.410
12.00	1482	64.4	35.3	0.300
	1521	64.7	35.1	0.211
Average		64.6	34.9	

Run	1365	47.5	50.7	1.76
N50E(a)	1370	47.9	50.6	1.45
CO_2/CO	1401	47.6	50.8	1.53
8.52	1424	48.0	50.6	1.46
	1450	47.6	50.8	1.61
	1511	47.3	51.6	1.10
Average		47.7	50.8	

Run	1384	63.3	34.7	2.01
N35E(a)	1434	63.2	34.9	1.91
CO_2/CO	1467	62.6	35.5	1.84
5.00	1523	62.0	36.3	1.77
Average		62.8	35.3	

Using the slag analyses results given on the previous pages, graphs of wt% Cu in the slag and wt% Ni in the slag against temperature were drawn for all runs (Figs. 3.2 to 3.17, pages 84 to 99).

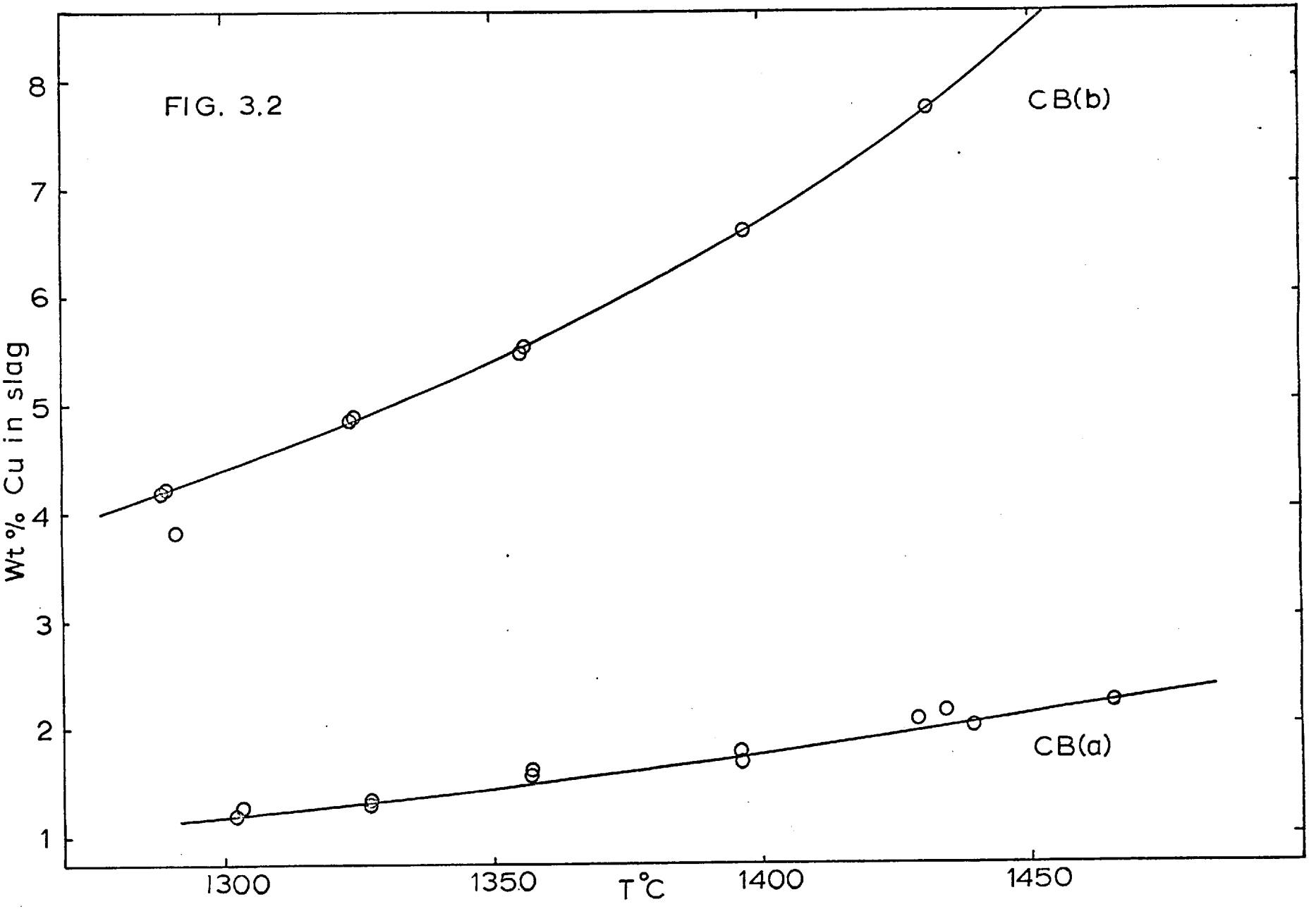
FIG. 3.2
CB(b)
CB(a)
Wt % Cu in slag
T°C
1
2
3
4
5
6
7
8
1300
1350
1400
1450

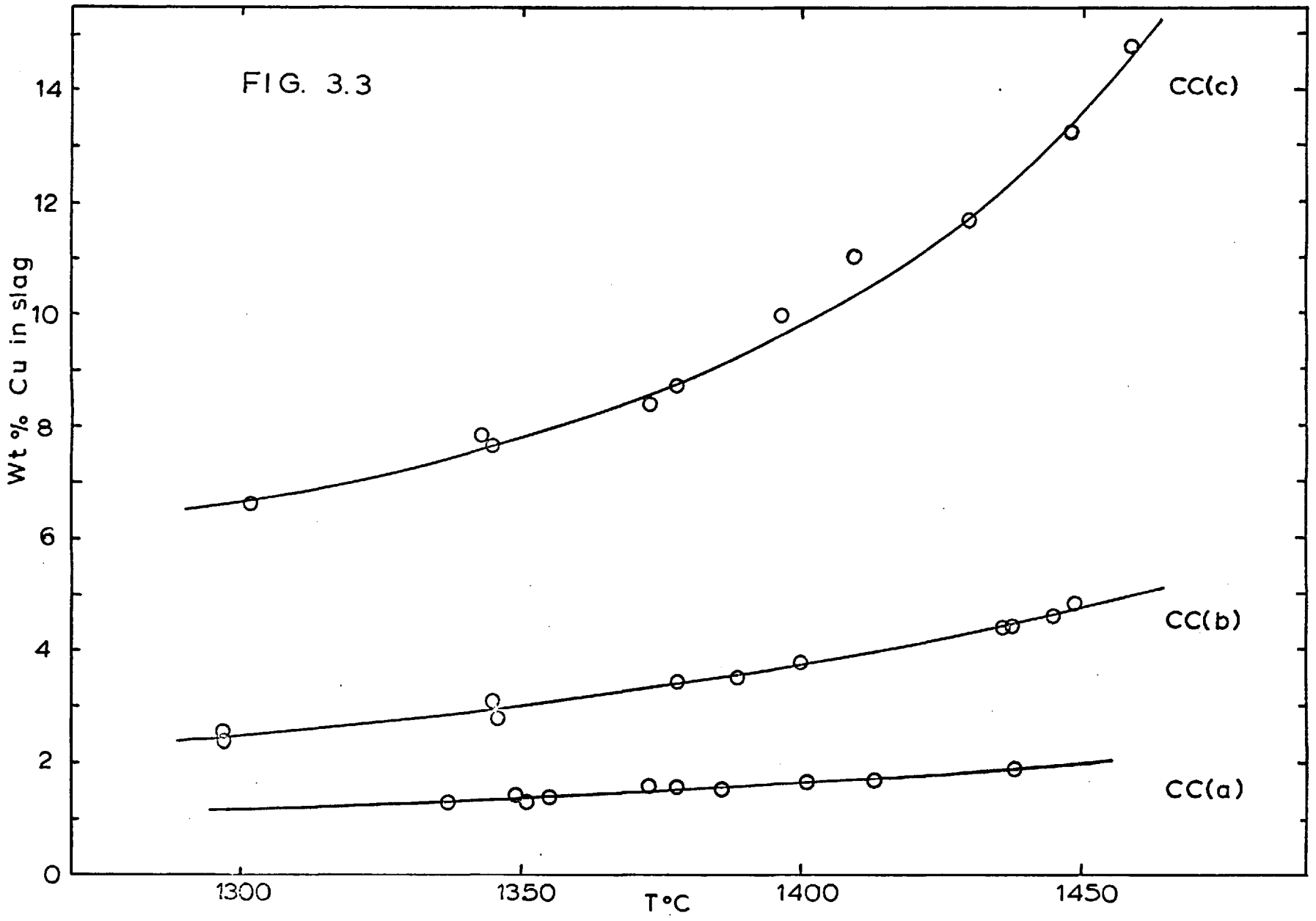
FIG. 3.3
Wt % Cu in slag
0
2
4
6
8
10
12
14
1300
1350
1400
1450
T°C
CC(c)
CC(b)
CC(a)

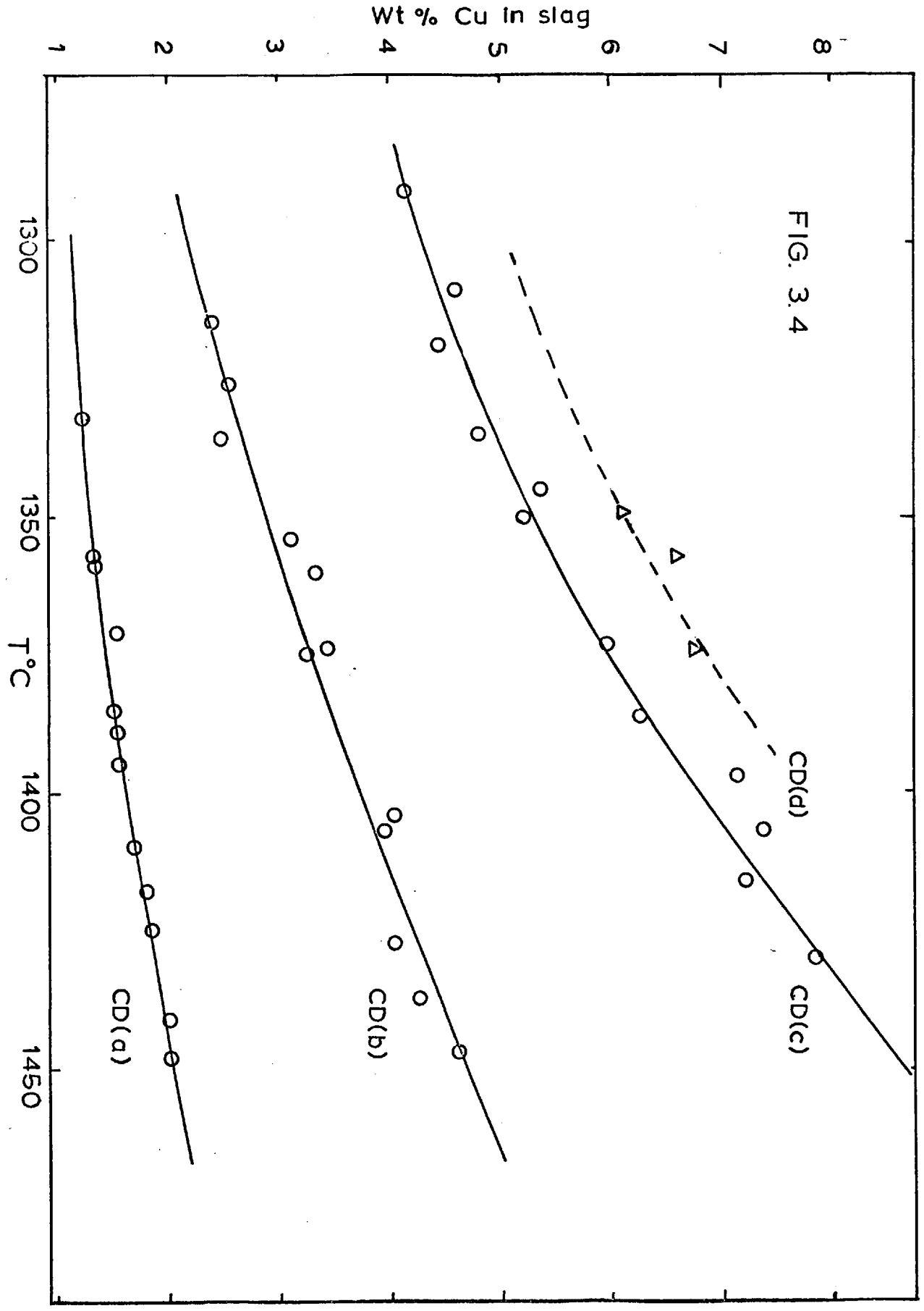

FIG. 3.4

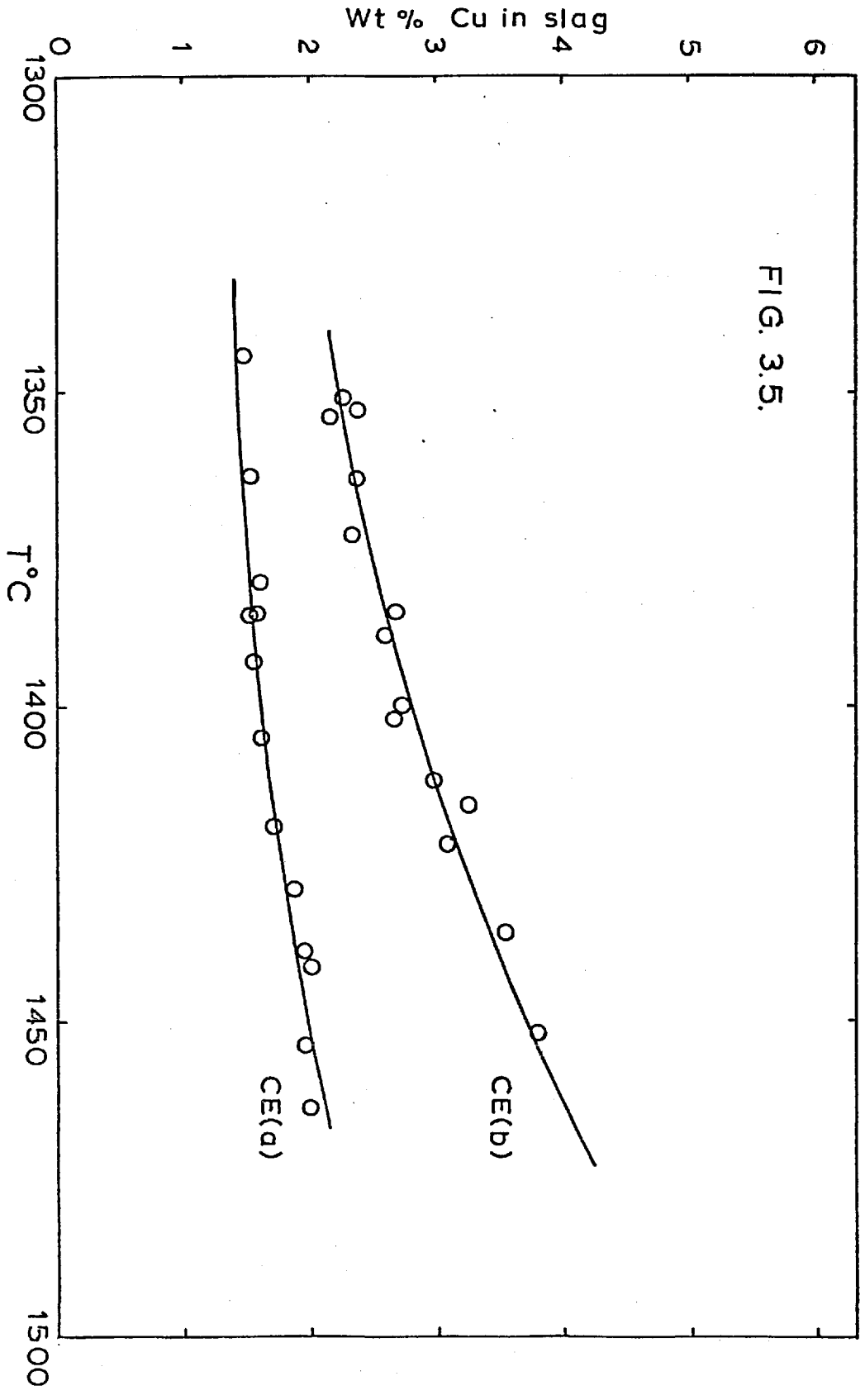

FIG. 3.5.

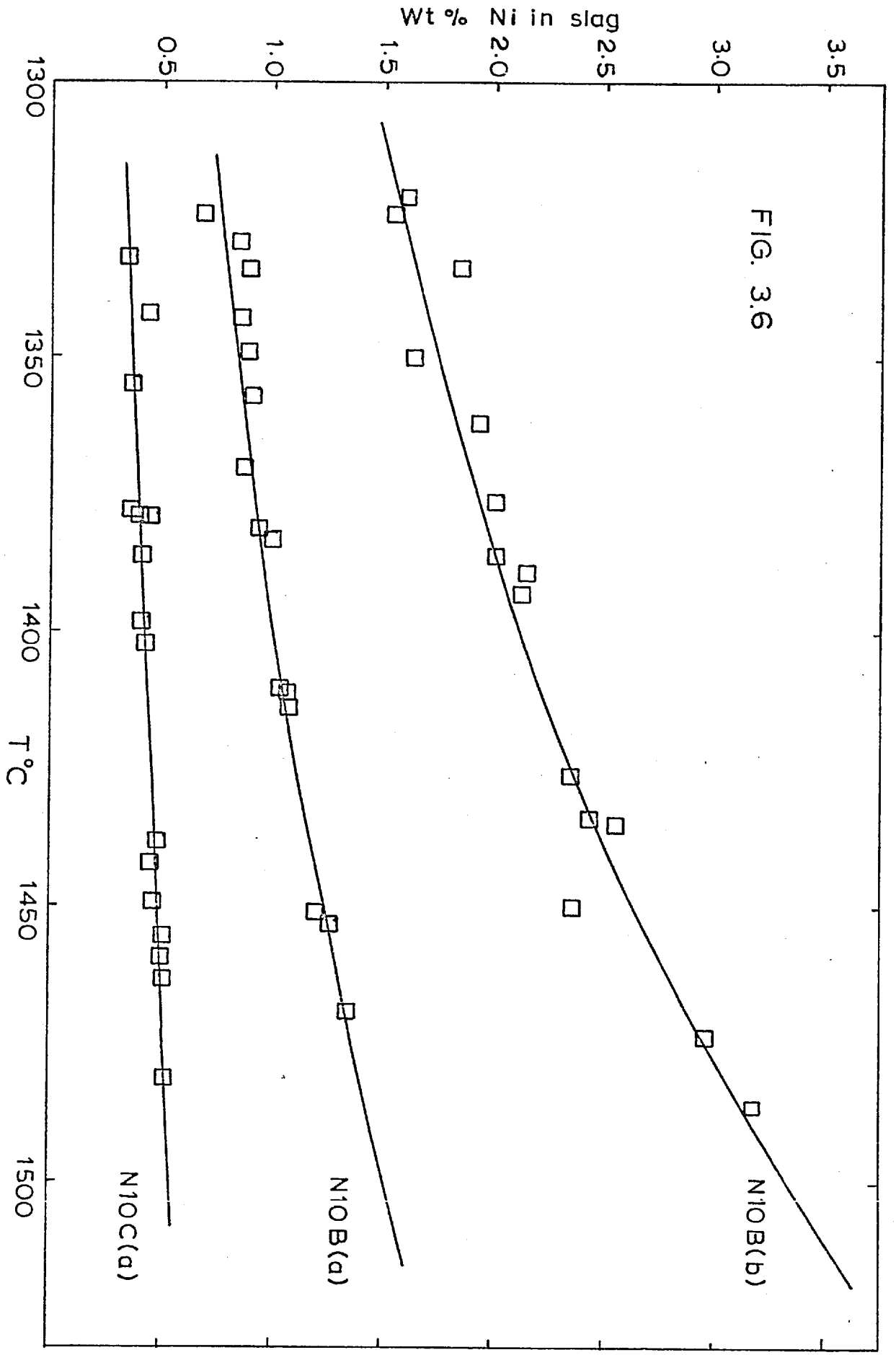
Wt % Ni in slag
0.5
1.0
1.5
2.0
2.5
3.0
3.5
1300
1350
1400
1450
1500
T°C
N10C(a)
N10B(a)
N10B(b)

FIG. 3.6

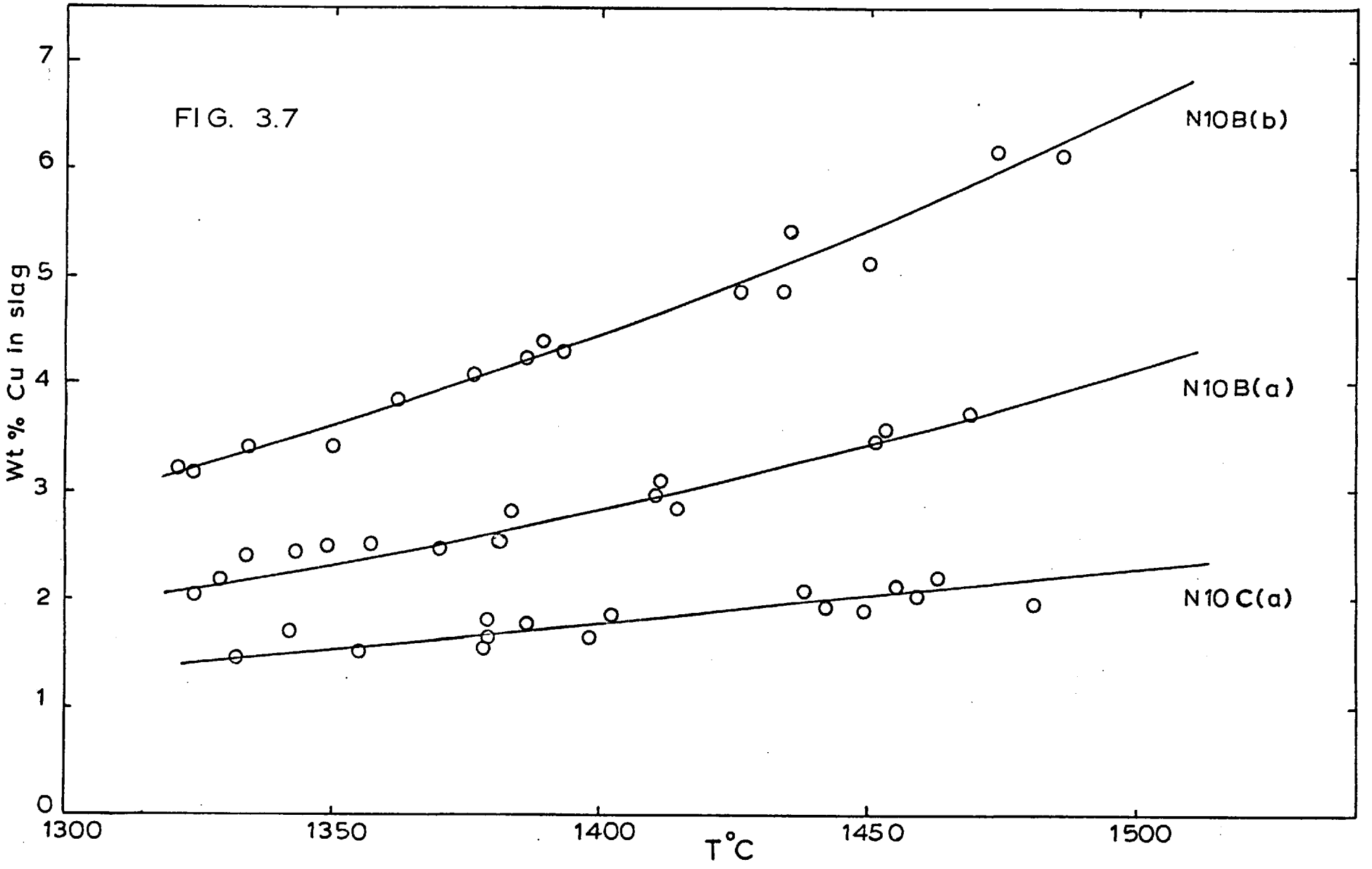
FIG. 3.7
Wt % Cu in slag
T°C
N10B(b)
N10B(a)
N10C(a)
0
1
2
3
4
5
6
7
1300
1350
1400
1450
1500

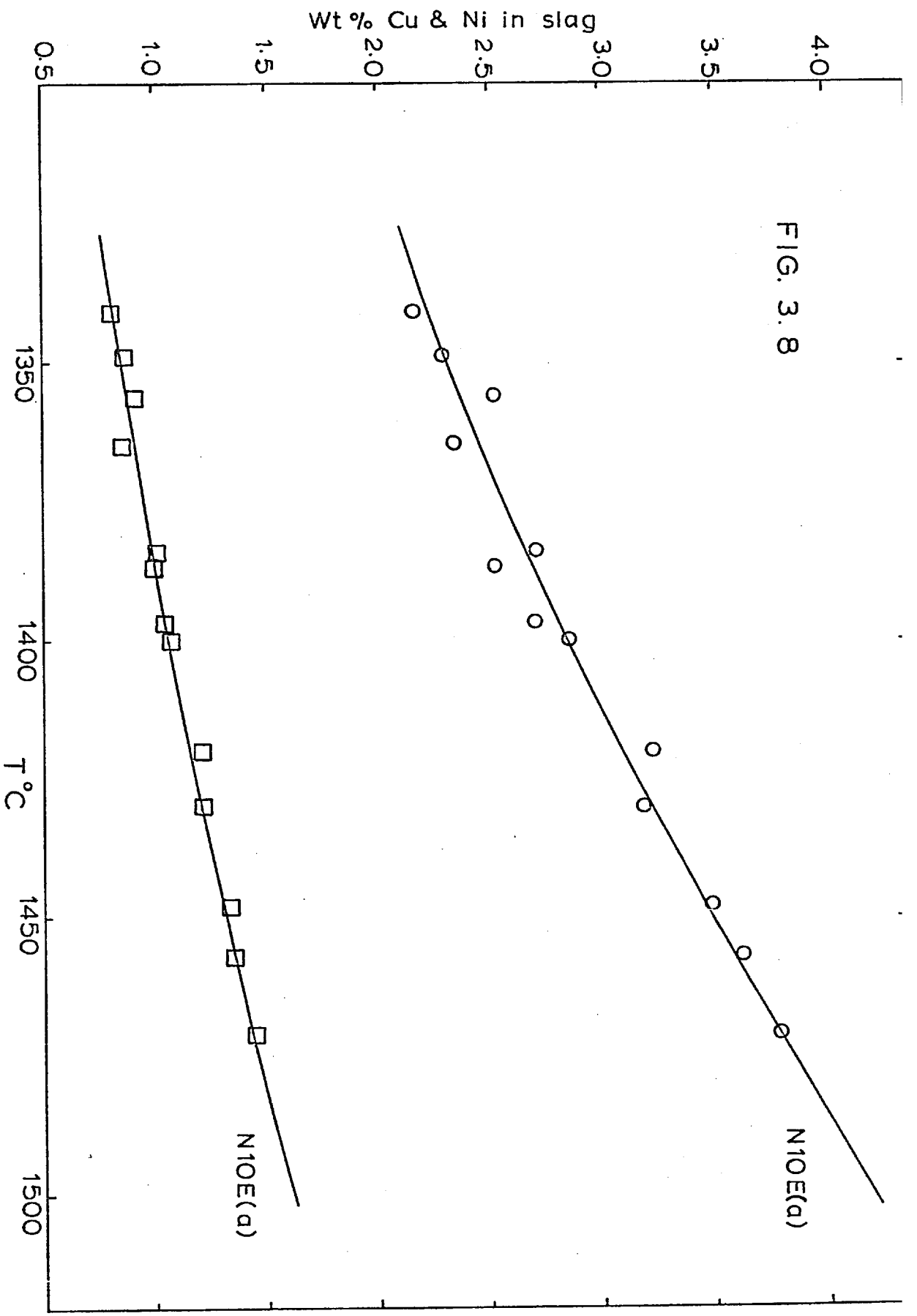
Wt % Cu & Ni in slag
0.5
1.0
1.5
2.0
2.5
3.0
3.5
4.0
1350
1400
1450
1500
T °C
N10E(a)
N10E(a)

FIG. 3.8

FIG. 3.9

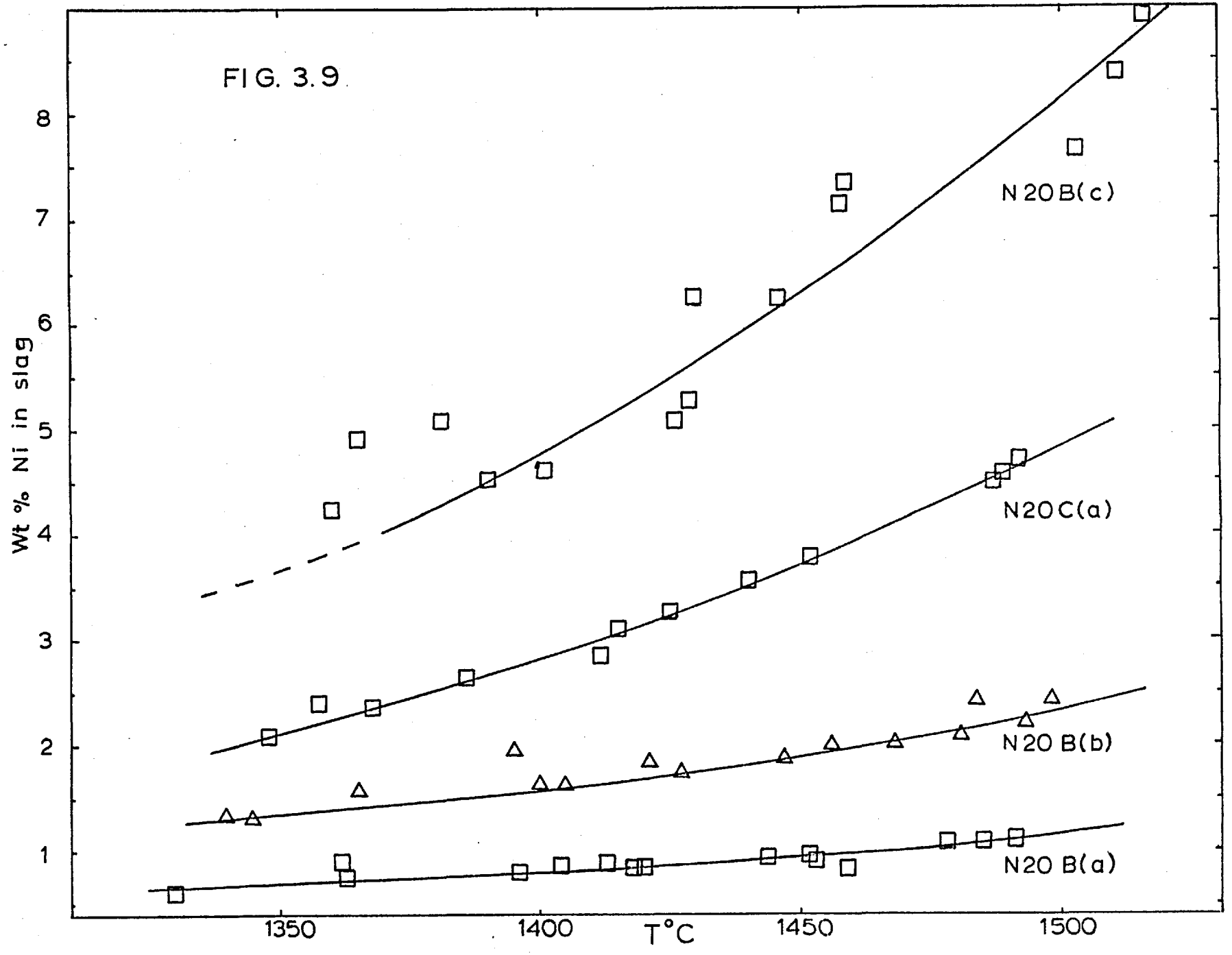
Wt % Ni in slag
1
2
3
4
5
6
7
8
1350
1400
1450
1500
T°C
N 20 B(c)
N20 C(a)
N20 B(b)
N20 B(a)

FIG. 3.10

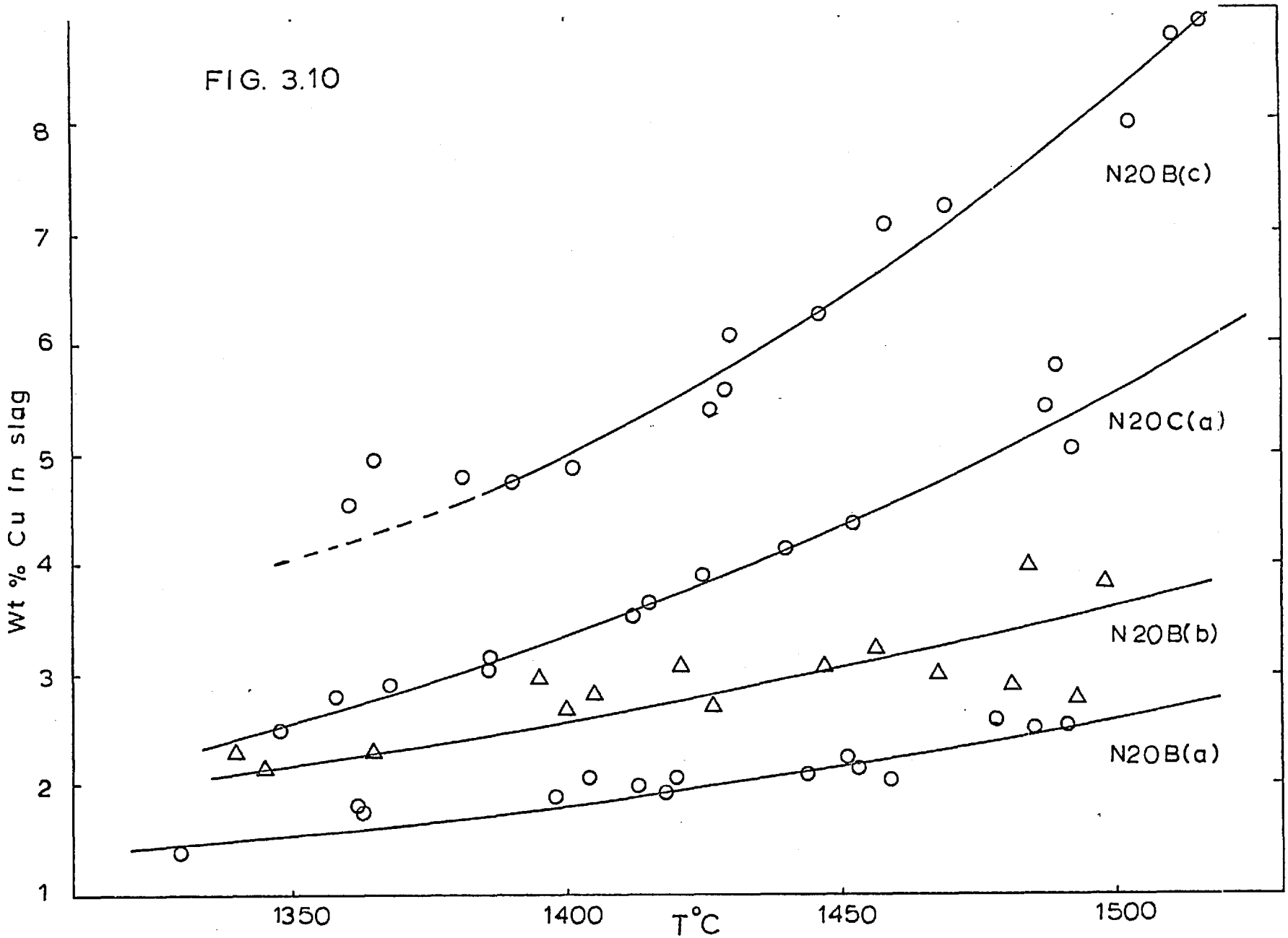
Wt % Cu in slag
8
7
6
5
4
3
2
1
1350
1400
T°C
1450
1500
N20 B(c)
N20 C(a)
N20 B(b)
N20 B(a)

FIG. 3.11

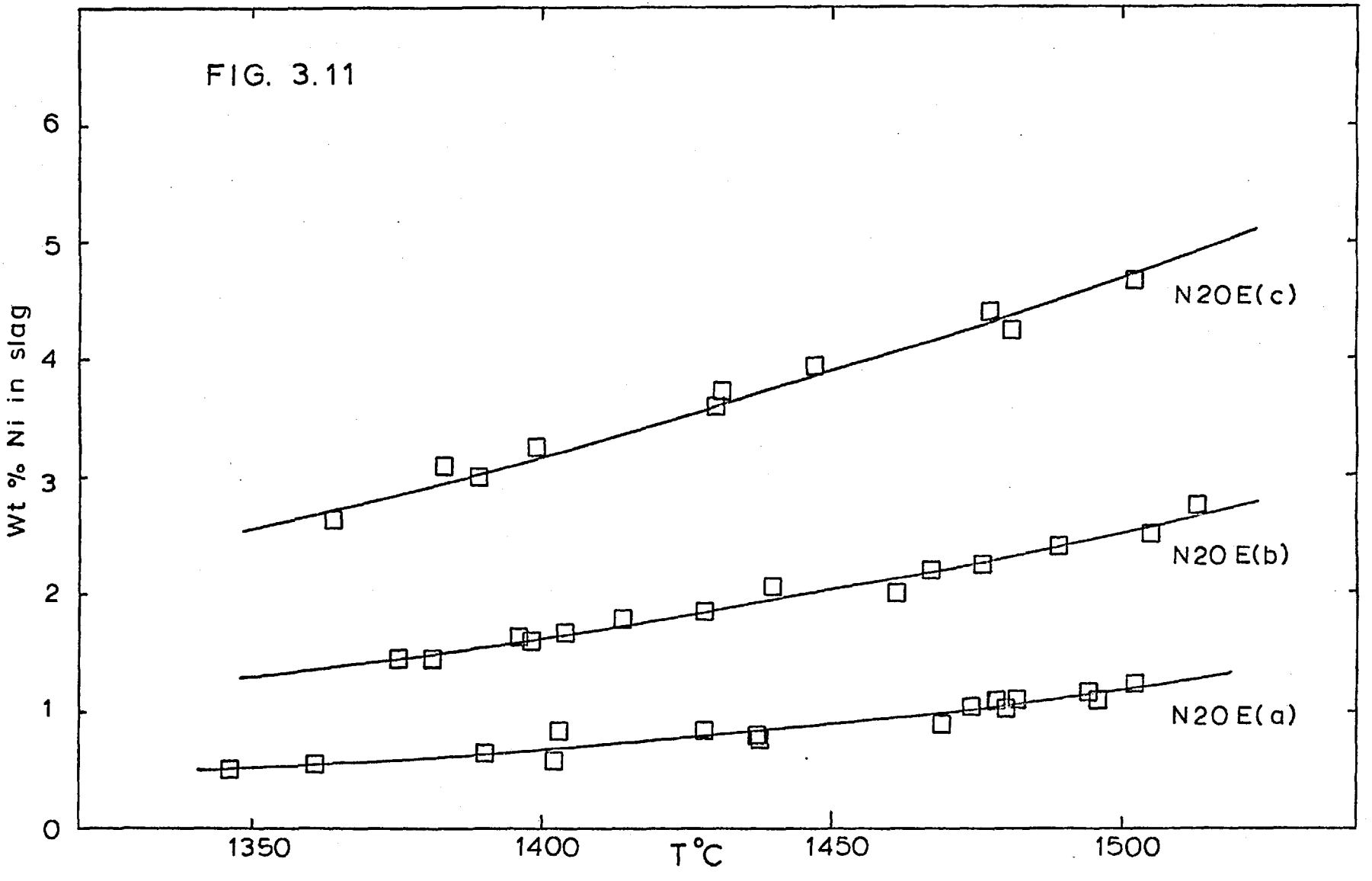
Wt % Ni in slag
0
1
2
3
4
5
6
1350
1400
1450
1500
T °C
N20E(c)
N20E(b)
N20E(a)

FIG. 3.12

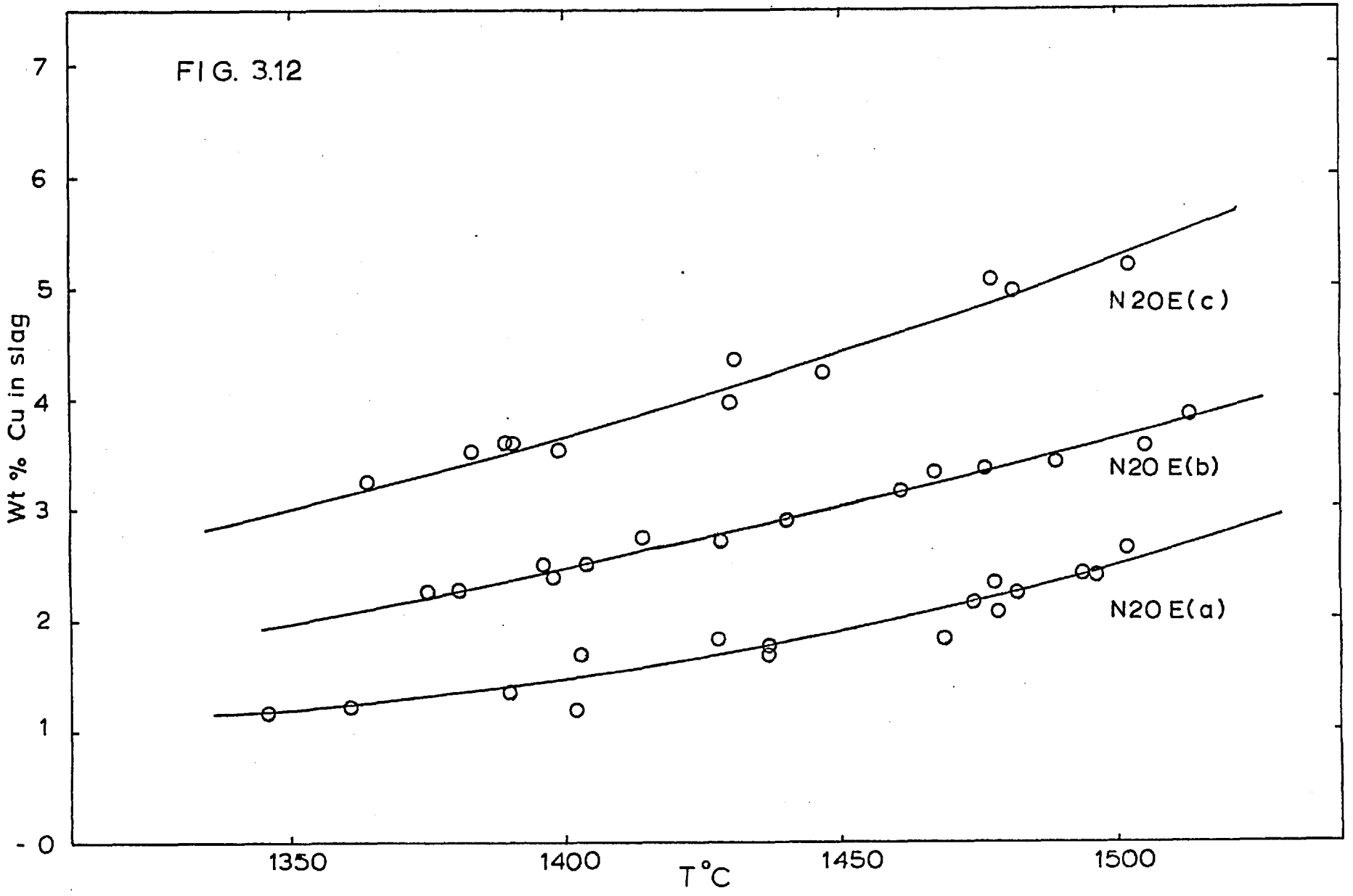
Wt % Cu in slag
0
1
2
3
4
5
6
7
1350
1400
1450
1500
T °C
N20E(c)
N20 E(b)
N20 E(a)

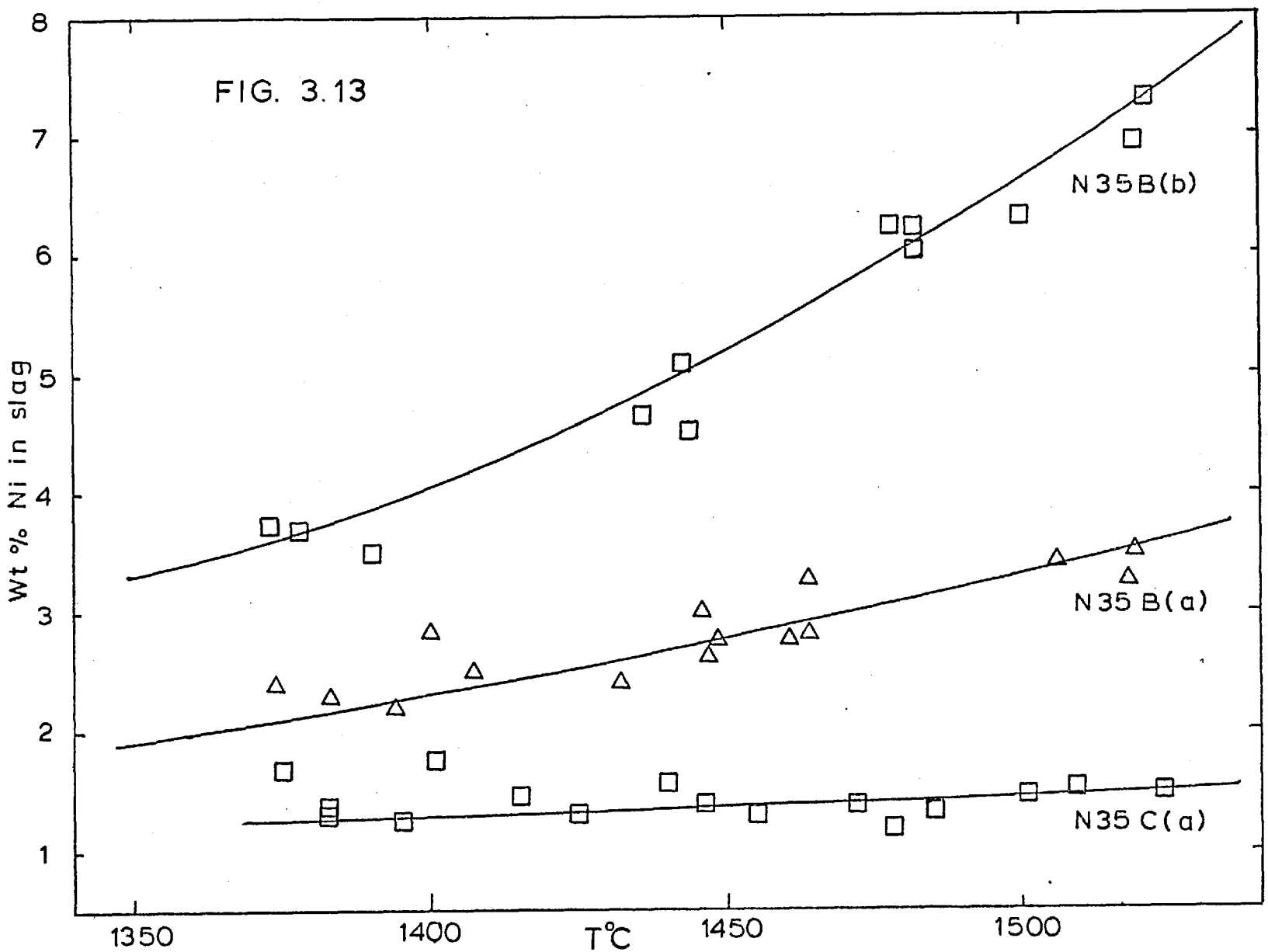
FIG. 3.13
Wt % Ni in slag
8
7
6
5
4
3
2
1
1350
1400
T°C
1450
1500
N35B(b)
N35 B(a)
N35 C(a)

FIG. 3.14

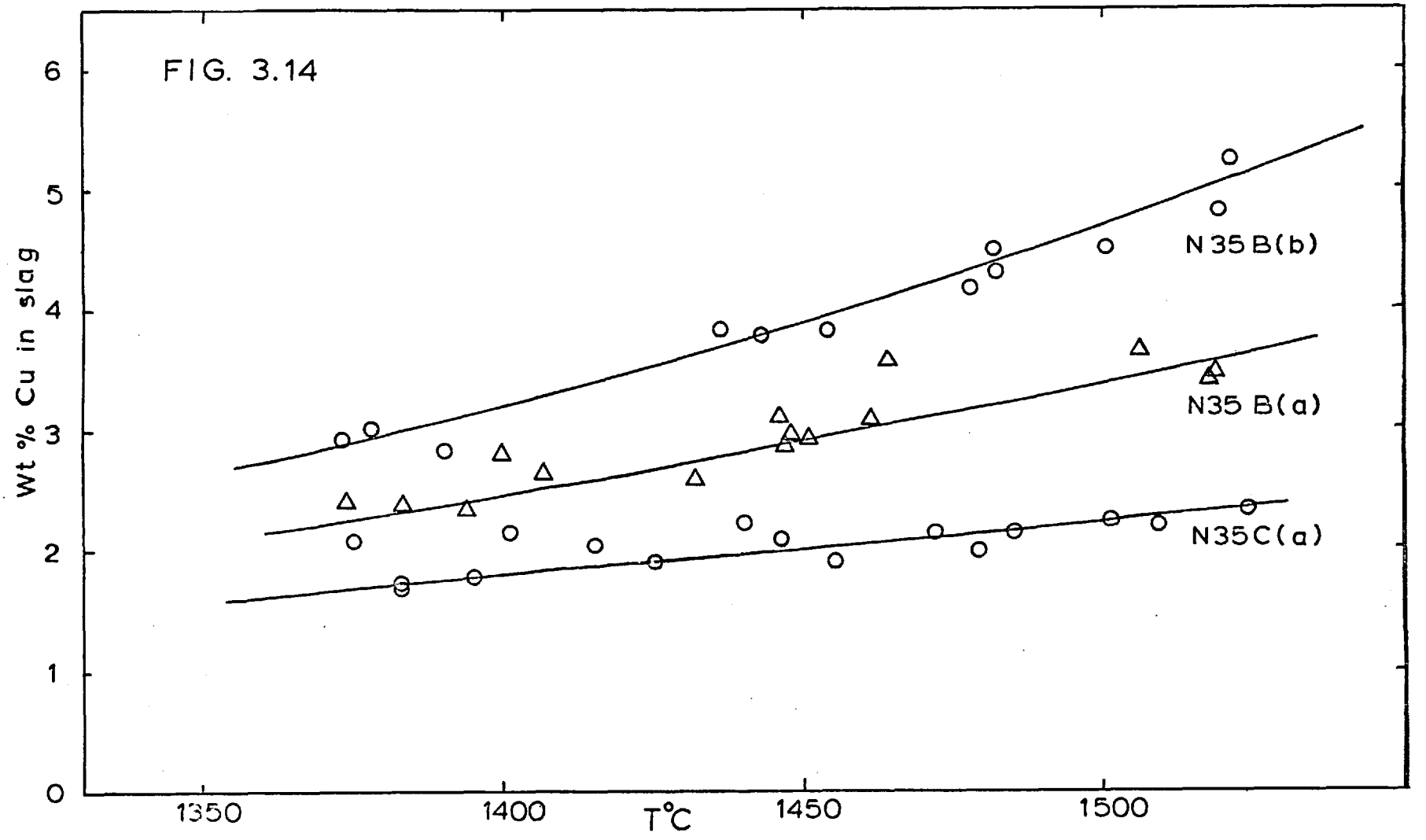
Wt % Cu in slag
0
1
2
3
4
5
6
1350
1400
T°C
1450
1500
N35 B(b)
N35 B(a)
N35C(a)

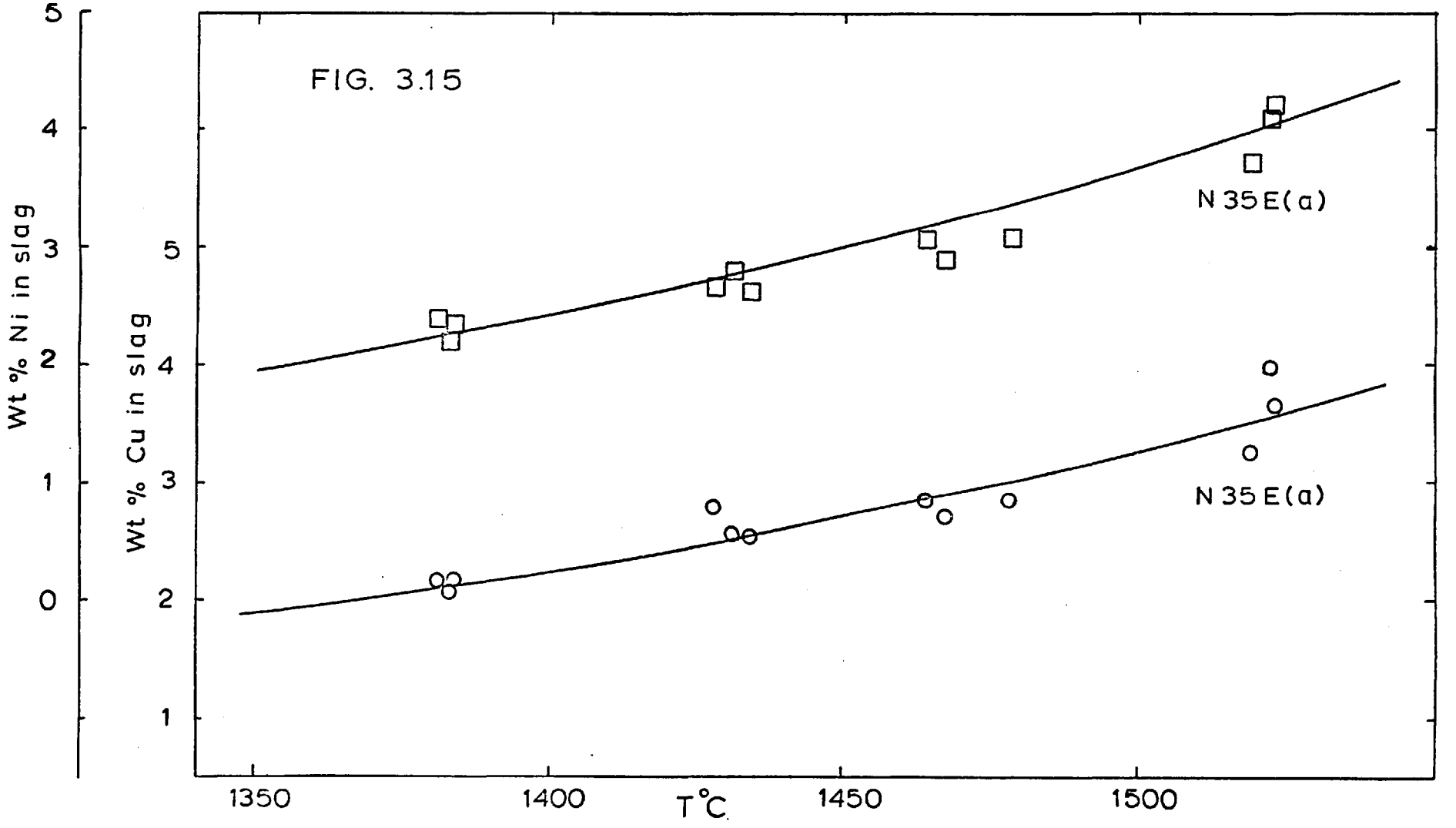
FIG. 3.15
Wt % Ni in slag
Wt % Cu in slag
T°C
1350
1400
1450
1500
N 35 E (a)
N 35 E (a)

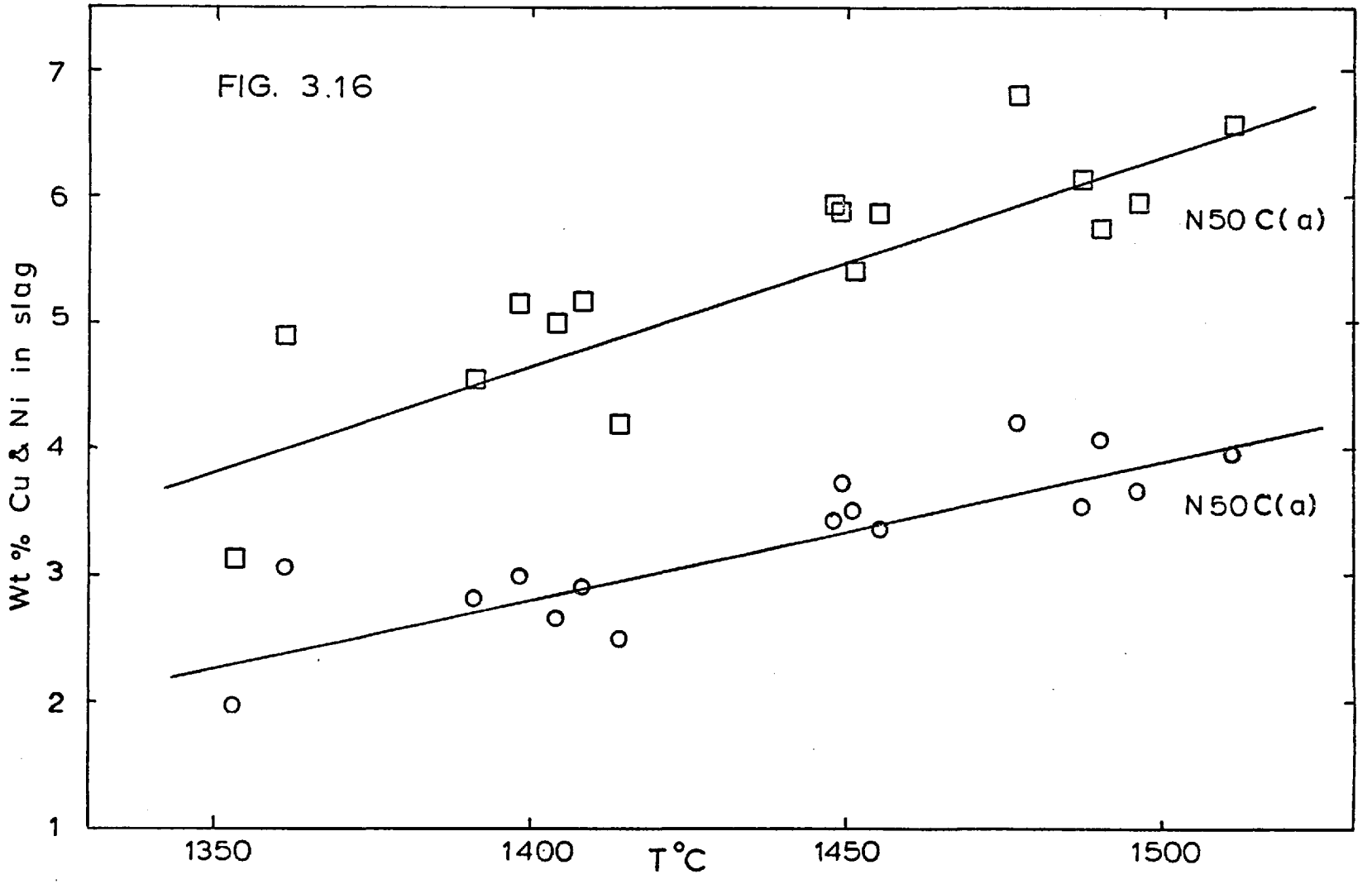
FIG. 3.16
Wt % Cu & Ni in slag
7
6
5
4
3
2
1
1350
1400
T °C
1450
1500
N50 C(a)
N50C(a)

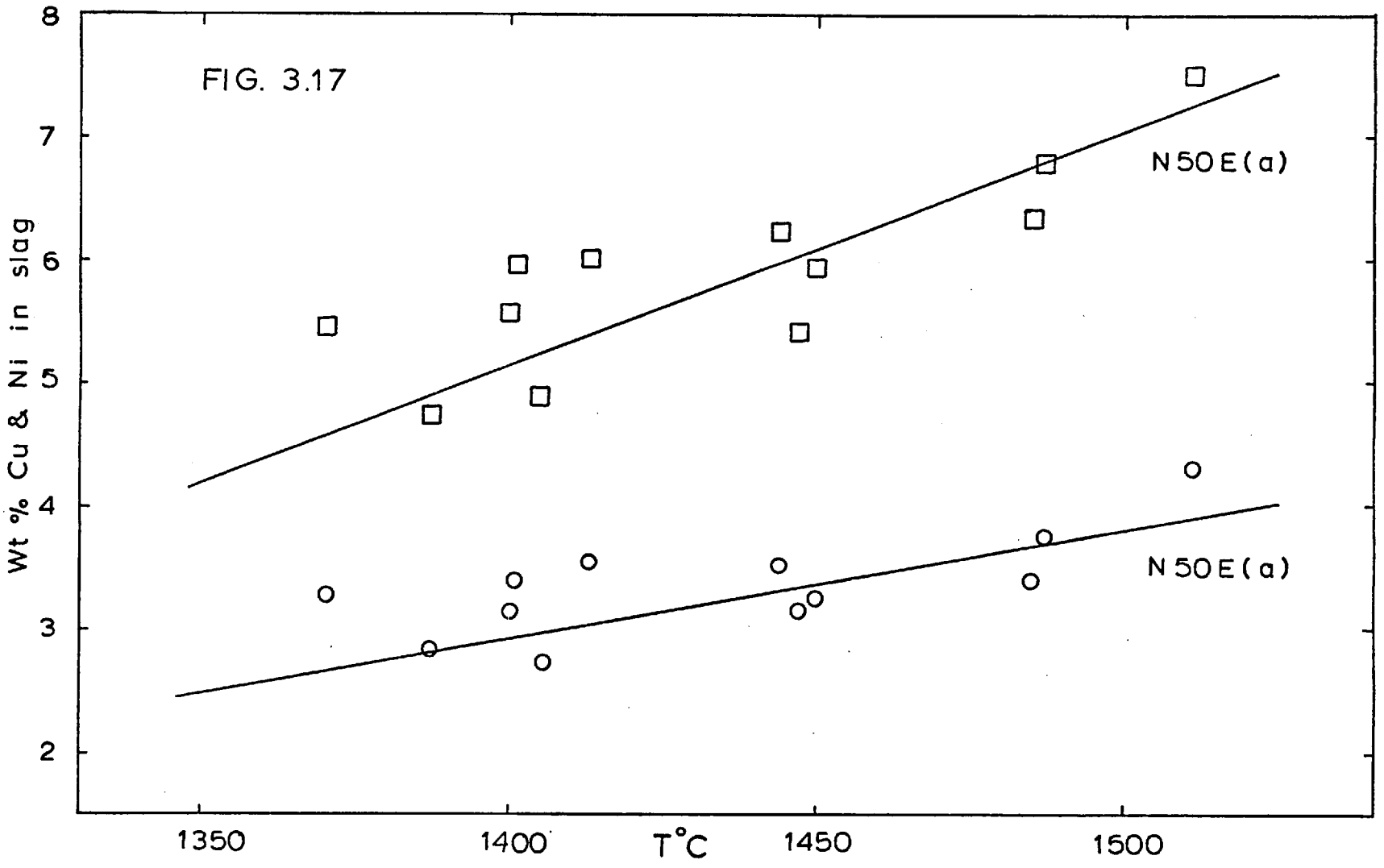
FIG. 3.17
Wt % Cu & Ni in slag
8
7
6
5
4
3
2
N50E(a)
N50E(a)
1350
1400
T°C
1450
1500

4. TREATMENT OF RESULTS

From the graphs of wt% Cu and wt% Ni in the slag against temperature (Figs. 3.2 - 3.17, pages 84 to 99), values of wt% Cu were taken at 1300, 1350, 1400 and 1450°C for the copper/gold runs, and wt% Cu and wt% Ni at 1350, 1400, 1450 and 1500°C for the copper/nickel runs.

Activities of $CuO._5$ and NiO were calculated at these temperatures for each run using the equations given in Table 3.2, page 61, and knowing the experimental CO/CO_2 ratio and the activities of copper and nickel.

Values of wt% FeO and SiO_2, and mol fractions of $CuO._5$, NiO, SiO_2 and FeO, which represent the composition of the slag for each run at four temperatures, were calculated.

All the above quantities are given in the tables between pages 103 and 110, and notes on their derivation are given below.

(a) Activities of Copper in Copper/Gold Alloys

It was assumed that all the copper/gold alloys could be represented by the composition:

89.8 wt% Cu, 10.1 wt% Au, 0.10 wt% Fe (see Chap. 3, sect. 3(c), p 65)

Using the results of Edwards and Brodsky, aCu was taken to be 0.965 for all copper/gold runs. No special allowance was made for the effect on aCu of the difference in interaction between Fe and Cu, and Au and Cu. The Cu activities in the Cu/Fe system[124] show more positive deviations than in the Cu/Au system (at N Cu = 0.9, aCu = 0.906 in the Cu/Au system, and 0.929 in the Cu/Fe system) but at the Fe levels encountered in this work the effect of Fe should be very small.

The effect of temperature on the activity of copper was negligible over the temperature range studied.

(b) Activities of Copper and Nickel in Copper/Nickel Alloys

Activities of copper and nickel were calculated using the data recommended by Elford et al for the Cu/Ni system. No special allowance was made for the effect on aCu of the difference in interaction between Fe and Cu, and Ni and Cu, or for the effect on aNi of the difference in interaction between Fe and Ni, and Cu and Ni. At N Cu = 0.9, aCu = 0.902 in the Cu/Ni system and 0.929 in the Cu/Fe[124] system, and at N Ni = 0.9, aNi = 0.907 in the Ni/Cu system and 0.89 in the Ni/Fe[124] system. With the iron contents of the alloys usually below 1 wt%, the effect of Fe should be small.

The variation of activities with temperature was small, and has been been allowed for.

The analyses of the copper/nickel alloys are given in the tables between pages 80 and 82. The alloy analyses within a run are fairly constant and the average analysis used in the calculation of metal activities is given at the end of the table for each run.

(c) Calculation of Mol. Fraction of Slag Species

The slag species were taken to be NiO, $CuO._5$, FeO and SiO_2. This approach neglects the presence of some oxygen associated with Fe^{3+} ions, but iron was analysed only as total iron and not as ferric and ferrous iron.

If half the iron in the slag were present as Fe^{3+} ions and half as Fe^{2+} ions, then a true analysis of 28.75 wt% Fe_2O_3, 25.85% FeO, 40.3% SiO_2 and 5% Cu_2O would be reported here as 53.5 wt% FeO, 41.5% SiO_2 and 5% Cu_2O. Cuprous oxide is considered to act as $CuO._5$ in the slag for reasons given in the 'Discussion' section, page 126. To remain consistent with this, following the approach of Lumsden,[32] the ferric oxide species is better described as $FeO_{1.5}$ rather than Fe_2O_3. Calculating the mol fraction of $CuO._5$ for the two analyses given above, taking the species as $CuO._5$, FeO, $FeO_{1.5}$ and SiO_2 in the first case and $CuO._5$, FeO and SiO_2 in the second, gives N $CuO._5$ as 0.0478 and 0.0465 respectively, a difference of about 3%.

Altman and Kellogg found a maximum Fe^{3+}/Fe^{2+} ratio of 0.40 in their slags at the lower temperature of 1286°C, so the error involved in ignoring the presence of Fe^{3+} ions is unlikely to make a difference of more than about 2% to the value of N $CuO._5$ under the most unfavourable circumstances.

The slag analyses given in the tables pages 103 to 109, from which the mol fractions were calculated, were derived from the tables of complete slag analyses as follows:

It was considered that the copper and nickel analyses were significantly more accurate than the iron and silica analyses, and were left untouched.

The ratio $FeO/_{SiO_2}$ (designated 'R') was calculated from the tables of complete slag analyses for each slag, and plotted against temperature. The best straight line was drawn through the points for each run and values of R taken at 1300, 1350, 1400 and 1450°C for the copper/gold runs and at 1350, 1400, 1450 and 1500°C for the copper/nickel runs. R was kept constant and new values of FeO and SiO_2 were calculated using the relationships:

$$100 - (\text{wt\% } Cu_2O + \text{wt\% NiO}) = FeO + SiO_2$$

and

$$\frac{FeO}{SiO_2} = R$$

This gave a representative slag analysis totalling 100 wt%, for each run at four temperatures.

Mol. fractions were then calculated using these values of FeO and the analysed values of Cu_2O and NiO.

Cu/Au Runs

	T°C	log pO_2	Cu	$aCuO_{.5}$	FeO	SiO_2	N $CuO_{.5}$	N FeO	N SiO_2	Fe in metal
Run	1300	-9.159	1.21	0.0381	62.24	36.40	0.0127	0.5810	0.4063	0.325
CB(a)	1350	-8.586	1.45	0.0458	61.39	36.98	0.0153	0.5724	0.4123	0.318
CO_2/CO	1400	-8.047	1.76	0.0546	60.32	37.70	0.0185	0.5617	0.4200	0.312
2.028	1450	-7.540	2.12	0.0644	59.18	38.43	0.0225	0.5504	0.4273	0.305
Run	1300	-7.148	4.42	0.1212	60.96	34.06	0.0469	0.5714	0.3817	0.045
CB(b)	1350	-6.575	5.38	0.1460	60.03	33.91	0.0571	0.5628	0.3801	0.044
CO_2/CO	1400	-6.036	6.66	0.1738	58.99	33.51	0.0707	0.5534	0.3759	0.041
20.53	1450	-5.529	8.52	0.2049	57.47	32.94	0.0904	0.5397	0.3699	0.040
Run	1300	-9.296	1.14	0.0352	65.37	33.34	0.0122	0.6137	0.3742	0.496
CC(a)	1350	-8.723	1.34	0.0424	65.23	33.26	0.0142	0.6124	0.3734	0.488
CO_2/CO	1400	-8.184	1.62	0.0505	65.02	33.16	0.0172	0.6109	0.3723	0.480
1.732	1450	-7.677	1.95	0.0595	64.77	33.03	0.0207	0.6083	0.3710	0.473
Run	1300	-7.917	2.49	0.0779	67.28	29.92	0.0266	0.6355	0.3379	0.133
CC(b)	1350	-7.344	3.02	0.0938	66.87	29.73	0.0323	0.6318	0.3359	0.130
CO_2/CO	1400	-6.805	3.71	0.1117	66.40	29.52	0.0396	0.6270	0.3334	0.127
8.471	1450	-6.298	4.76	0.1316	65.51	29.13	0.0509	0.6196	0.3295	0.125

Cu/Au Runs

	$T^{\circ}C$	log pO_2	Cu	$aCuO_{.5}$	FeO	SiO_2	N $CuO_{.5}$	N FeO	N SiO_2	Fe in metal
Run	1300	-6.658	6.62	0.1607	65.08	27.47	0.0710	0.6175	0.3116	0.074
CC(c)	1350	-6.085	7.77	0.1935	63.92	27.33	0.0834	0.6066	0.3101	0.074
CO_2/CO	1400	-5.546	9.73	0.2305	62.13	26.91	0.1045	0.5900	0.3055	0.074
36.09	1450	-5.039	13.6	0.2717	58.79	25.86	0.1467	0.5591	0.2941	0.074
Run	1300	-9.291	1.17	0.0353	70.50	28.18	0.0126	0.6681	0.3193	0.626
CD(a)	1350	-8.718	1.31	0.0425	70.39	28.14	0.0140	0.6671	0.3189	0.621
CO_2/CO	1400	-8.179	1.62	0.0506	70.14	28.04	0.0174	0.6671	0.3188	0.616
1.741	1450	-7.672	2.04	0.0596	69.80	27.90	0.0219	0.6618	0.3163	0.612
Run	1300	-7.920	2.18	0.0778	73.98	23.57	0.0235	0.7072	0.2694	0.200
CD(b)	1350	-7.347	2.90	0.0936	73.29	23.44	0.0314	0.7007	0.2679	0.175
CO_2/CO	1400	-6.808	3.72	0.1115	72.56	23.25	0.0402	0.6939	0.2658	0.150
8.447	1450	-6.301	4.70	0.1314	71.66	23.05	0.0508	0.6855	0.2637	0.124
Run	1300	-7.110	4.30	0.1239	73.19	21.97	0.0466	0.7016	0.2518	0.115
CD(c)	1350	-6.537	5.28	0.1492	72.34	21.72	0.0572	0.6937	0.2491	0.086
CO_2/CO	1400	-5.998	6.87	0.1777	70.96	21.31	0.0745	0.6810	0.2445	0.059
21.45	1450	-5.491	8.66	0.2095	69.41	20.84	0.0940	0.6666	0.2393	0.031

Cu/Au Runs

	$T^{o}C$	log pO_2	Cu	$aCuO_{.5}$	FeO	SiO_2	N $CuO_{.5}$	N FeO	N SiO_2	Fe in metal
Run	1300	-6.945	5.08	0.1362	72.51	21.77	0.0551	0.6953	0.2496	-
CD(d)	1350	-6.372	6.14	0.1640	71.60	21.49	0.0666	0.6869	0.2465	-
CO_2/CO	1400	-5.833	7.74	0.1954	70.21	21.08	0.0840	0.6740	0.2420	-
25.93	1450	-5.326	-	0.2303	-	-	-	-	-	-
Run	1300	-9.294	-	0.0353	-	-	-	-	-	0.802
CE(a)	1350	-8.721	1.46	0.0425	83.94	14.42	0.0160	0.8163	0.1677	0.781
CO_2/CO	1400	-8.182	1.61	0.0506	83.54	14.65	0.0177	0.8121	0.1703	0.759
1.736	1450	-7.675	2.01	0.0596	82.89	14.85	0.0221	0.8055	0.1725	0.738
Run	1300	-8.368	-	0.0601	-	-	-	-	-	0.388
CE(b)	1350	-7.795	2.25	0.0723	84.15	13.32	0.0248	0.8201	0.1553	0.352
CO_2/CO	1400	-7.256	2.80	0.0861	83.34	13.51	0.0308	0.8118	0.1573	0.316
5.04	1450	-6.749	3.68	0.1015	82.22	13.64	0.0405	0.8006	0.1588	0.281

Cu/Ni Runs

	aCu	aNi	T°C	log pO_2	Cu	$aCuO_{.5}$	Ni	aNiO	FeO	SiO_2	N $CuO_{.5}$	N NiO	N FeO	N SiO_2
Run	0.893	0.230	1350	-8.598	1.53	0.0422	0.364	0.00483	63.74	34.08	0.0162	0.00418	0.5975	0.3821
N10C(a)	0.893	0.225	1400	-8.059	1.77	0.0502	0.425	0.00577	62.15	35.31	0.0188	0.00487	0.5814	0.3950
CO_2/CO	0.893	0.219	1450	-7.550	2.04	0.0592	0.486	0.00676	60.31	36.77	0.0215	0.00555	0.5627	0.4102
2.00	0.893	0.215	1500	-7.055	2.27	0.0691	0.550	0.00791	58.66	38.09	0.0239	0.00627	0.5459	0.4239
Run	0.899	0.231	1350	-7.802	2.30	0.0671	0.820	0.0121	62.67	33.70	0.0244	0.00942	0.5881	0.3781
N10B(a)	0.899	0.226	1400	-7.263	2.82	0.0799	1.01	0.0145	62.02	33.52	0.0299	0.0116	0.5823	0.3763
CO_2/CO	0.899	0.220	1450	-6.756	3.44	0.0942	1.24	0.0170	61.14	33.41	0.0365	0.0142	0.5741	0.3751
5.00	0.899	0.215	1500	-6.259	4.14	0.1100	1.51	0.0198	60.29	33.13	0.0440	0.0174	0.5665	0.3722
Run	0.903	0.228	1350	-7.042	3.64	0.1044	1.74	0.0287	60.71	32.99	0.0386	0.0200	0.5705	0.3708
N10B(b)	0.903	0.223	1400	-6.503	4.46	0.1244	2.11	0.0343	59.79	32.50	0.0475	0.0243	0.5626	0.3657
CO_2/CO	0.903	0.218	1450	-6.000	5.45	0.1466	2.63	0.0404	58.64	31.87	0.0581	0.0303	0.5525	0.3591
12.00	0.903	0.214	1500	-5.499	6.58	0.1712	3.33	0.0472	57.24	31.11	0.0702	0.0385	0.5402	0.3511
Run	0.897	0.231	1350	-7.802	2.32	0.0669	0.858	0.0119	82.79	13.51	0.0256	0.0102	0.8068	0.1574
N10E(a)	0.897	0.226	1400	-7.263	2.85	0.0797	1.06	0.0145	82.04	13.38	0.0314	0.0127	0.8000	0.1560
CO_2/CO	0.897	0.220	1450	-6.756	3.49	0.0940	1.32	0.0174	81.15	13.24	0.0385	0.0157	0.7914	0.1544
5.00	0.897	0.215	1500	-6.259	4.20	0.1098	1.62	0.0208	80.20	13.08	0.0463	0.0193	0.7819	0.1525

Cu/Ni Runs

	aCu	aNi	T°C	log pO_2	Cu	$aCuO_{.5}$	Ni	aNiO	FeO	SiO_2	N $CuO_{.5}$	N NiO	N FeO	N SiO_2
Run	0.808	0.389	1350	-8.490	1.54	0.0406	0.693	0.00928	60.64	36.75	0.0163	0.00791	0.5658	0.4100
N20B(a)	0.807	0.382	1400	-7.949	1.84	0.0483	0.789	0.0111	60.35	36.58	0.0194	0.00901	0.5633	0.4083
CO_2/CO	0.806	0.375	1450	-7.442	2.19	0.0570	0.912	0.0131	60.01	36.37	0.0231	0.0104	0.5603	0.4061
2.27	0.806	0.370	1500	-6.945	2.60	0.0665	1.12	0.0154	59.55	36.09	0.0275	0.0129	0.5564	0.4032
Run	0.819	0.384	1350	-7.802	2.16	0.0611	1.34	0.0202	58.70	37.16	0.0228	0.0153	0.5475	0.4144
N20B(b)	0.818	0.377	1400	-7.263	2.56	0.0727	1.58	0.0242	58.25	36.86	0.0270	0.0180	0.5436	0.4113
CO_2/CO	0.817	0.371	1450	-6.756	3.05	0.0856	1.90	0.0286	57.66	36.49	0.0322	0.0217	0.5385	0.4075
5.00	0.816	0.365	1500	-6.259	3.62	0.0999	2.34	0.0336	56.92	36.02	0.0383	0.0268	0.5322	0.4027
Run	0.818	0.388	1350	-7.356	2.56	0.0789	2.11	0.0341	66.66	27.77	0.0264	0.0236	0.6328	0.3152
N20C(a)	0.817	0.381	1400	-6.817	3.38	0.0939	2.84	0.0408	65.34	27.23	0.0363	0.0331	0.6211	0.3095
CO_2/CO	0.816	0.374	1450	-6.310	4.33	0.1100	3.71	0.0483	63.82	26.59	0.0466	0.0432	0.6075	0.3027
8.36	0.816	0.370	1500	-5.813	5.59	0.1290	4.84	0.0569	61.80	25.75	0.0603	0.0565	0.5895	0.2937
Run	0.824	0.379	1350	-6.769	4.07	0.1114	3.66	0.0654	59.99	30.77	0.0435	0.0423	0.5667	0.3475
N20B(c)	0.823	0.374	1400	-6.230	4.98	0.1326	4.74	0.0787	58.41	29.95	0.0533	0.0549	0.5528	0.3390
CO_2/CO	0.822	0.366	1450	-5.723	6.38	0.1562	6.30	0.0928	56.05	28.75	0.0685	0.0732	0.5321	0.3263
16.42	0.822	0.360	1500	-5.226	8.22	0.1823	8.12	0.1088	53.16	27.26	0.0885	0.0946	0.5064	0.3105

Cu/Ni Runs

	aCu	aNi	T°C	log pO_2	Cu	$aCuO_{.5}$	Ni	aNiO	FeO	SiO_2	N $CuO_{.5}$	N NiO	N FeO	N SiO_2
Run	0.805	0.384	1350	-8.490	1.20	0.0404	0.520	0.00912	80.17	17.82	0.0131	0.00615	0.7748	0.2059
N20E(a)	0.804	0.377	1400	-7.953	1.47	0.0480	0.678	0.0109	79.76	17.73	0.0160	0.00802	0.7710	0.2049
CO_2/CO	0.803	0.371	1450	-7.446	1.88	0.0565	0.892	0.0129	79.15	17.59	0.0206	0.0106	0.7655	0.2034
2.26	0.803	0.365	1500	-6.984	2.50	0.0661	1.21	0.0152	78.26	17.39	0.0273	0.0143	0.7571	0.2012
Run	0.814	0.389	1350	-7.802	1.98	0.0608	1.31	0.0204	81.54	14.56	0.0218	0.0156	0.7932	0.1694
N20E(b)	0.813	0.382	1400	-7.263	2.47	0.0723	1.62	0.0245	80.74	14.42	0.0272	0.0193	0.7857	0.1678
CO_2/CO	0.812	0.375	1450	-6.756	3.01	0.0851	2.02	0.0289	79.79	14.25	0.0331	0.0241	0.7769	0.1659
5.00	0.811	0.370	1500	-6.259	3.63	0.0993	2.54	0.0340	78.64	14.04	0.0400	0.0303	0.7662	0.1635
Run	0.818	0.389	1350	-7.329	3.00	0.0802	2.56	0.0352	80.85	12.51	0.0332	0.0306	0.7901	0.1462
N20E(c)	0.817	0.382	1400	-6.790	3.64	0.0954	3.17	0.0422	79.55	12.32	0.0402	0.0379	0.7778	0.1440
CO_2/CO	0.816	0.375	1450	-6.283	4.38	0.1123	3.90	0.0499	78.03	12.08	0.0485	0.0467	0.7635	0.1413
8.62	0.816	0.370	1500	-5.786	5.24	0.1311	4.71	0.0587	76.16	11.79	0.0582	0.0566	0.7474	0.1379

Cu/Ni Runs

	aCu	aNi	T°C	log pO_2	Cu	$aCuO_{.5}$	Ni	aNiO	FeO	SiO_2	N $CuO_{.5}$	N NiO	N FeO	N SiO_2
Run	0.714	0.548	1350	-8.598	1.58	0.0337	1.18	0.0116	59.51	37.20	0.0167	0.0135	0.5550	0.4148
N35C(a)	0.712	0.540	1400	-8.059	1.80	0.0401	1.27	0.0138	58.42	37.94	0.0189	0.0145	0.5441	0.4225
CO_2/CO	0.708	0.533	1450	-7.550	2.01	0.0469	1.36	0.0165	57.45	38.56	0.0211	0.0155	0.5344	0.4289
2.00	0.704	0.528	1500	-7.055	2.22	0.0545	1.46	0.0194	56.29	39.36	0.0233	0.0165	0.5229	0.4372
Run	0.721	0.553	1350	-7.802	2.06	0.0538	1.92	0.0290	56.21	39.03	0.0228	0.0218	0.5220	0.4334
N35B(a)	0.719	0.545	1400	-7.263	2.47	0.0639	2.28	0.0349	55.66	38.66	0.0260	0.0260	0.5179	0.4301
CO_2/CO	0.716	0.538	1450	-6.756	2.89	0.0750	2.75	0.0415	55.03	38.22	0.0304	0.0313	0.5126	0.4256
5.00	0.713	0.534	1500	-6.259	3.31	0.0873	3.29	0.0491	54.34	37.74	0.0349	0.0376	0.5067	0.4208
Run	0.725	0.553	1350	-7.042	2.65	0.0838	3.35	0.0698	58.78	33.98	0.0281	0.0385	0.5519	0.3815
N35B(b)	0.722	0.545	1400	-6.503	3.22	0.0994	4.02	0.0838	57.83	33.42	0.0342	0.0463	0.5437	0.3758
CO_2/CO	0.718	0.538	1450	-6.000	3.88	0.1166	5.20	0.0996	56.41	32.60	0.0413	0.0600	0.5314	0.3672
12.00	0.716	0.533	1500	-5.499	4.72	0.1358	6.66	0.1176	54.63	31.58	0.0504	0.0770	0.5160	0.3566
Run	0.714	0.556	1350	-7.802	1.87	0.0533	1.94	0.0292	80.69	14.73	0.0206	0.0231	0.7850	0.1713
N35E(a)	0.712	0.548	1400	-7.263	2.24	0.0633	2.40	0.0351	79.86	14.57	0.0246	0.0285	0.7756	0.1713
CO_2/CO	0.708	0.542	1450	-6.756	2.70	0.0742	2.98	0.0418	78.79	14.38	0.0297	0.0355	0.7673	0.1674
5.00	0.704	0.538	1500	-6.259	3.25	0.0861	3.67	0.0495	77.52	14.15	0.0358	0.0438	0.7555	0.1649

Cu/Ni Runs

	aCu	aNi	T°C	log pO_2	Cu	$aCuO_{.5}$	Ni	aNiO	FeO	SiO_2	N $CuO_{.5}$	N NiO	N FeO	N SiO_2
Run	0.630	0.656	1350	-7.336	2.27	0.0615	3.80	0.0590	64.02	28.58	0.0243	0.0441	0.6072	0.3243
N50C(a)	0.625	0.652	1400	-6.797	2.80	0.0726	4.63	0.0714	61.81	29.15	0.0300	0.0537	0.5858	0.3305
CO_2/CO	0.618	0.647	1450	-6.290	3.32	0.0847	5.48	0.0854	59.43	29.86	0.0356	0.0635	0.5628	0.3381
8.55	0.614	0.643	1500	-5.793	3.89	0.0982	6.31	0.1011	56.96	30.63	0.0416	0.0730	0.5388	0.3466
Run	0.621	0.664	1350	-7.339	2.50	0.0605	4.20	0.0595	76.45	15.76	0.0274	0.0498	0.7403	0.1825
N50E(a)	0.616	0.660	1400	-6.880	2.94	0.0715	5.14	0.0721	74.93	15.45	0.0323	0.0608	0.7275	0.1794
CO_2/CO	0.611	0.656	1450	-6.293	3.37	0.0836	6.10	0.0863	73.38	15.13	0.0371	0.0727	0.7142	0.1761
8.52	0.605	0.652	1500	-5.796	3.82	0.0966	7.04	0.1022	71.85	14.82	0.0421	0.0841	0.7010	0.1724

From the preceding tables, graphs have been drawn of:

Cu/Au Runs, slags B,C,D,E FIG. 3.18

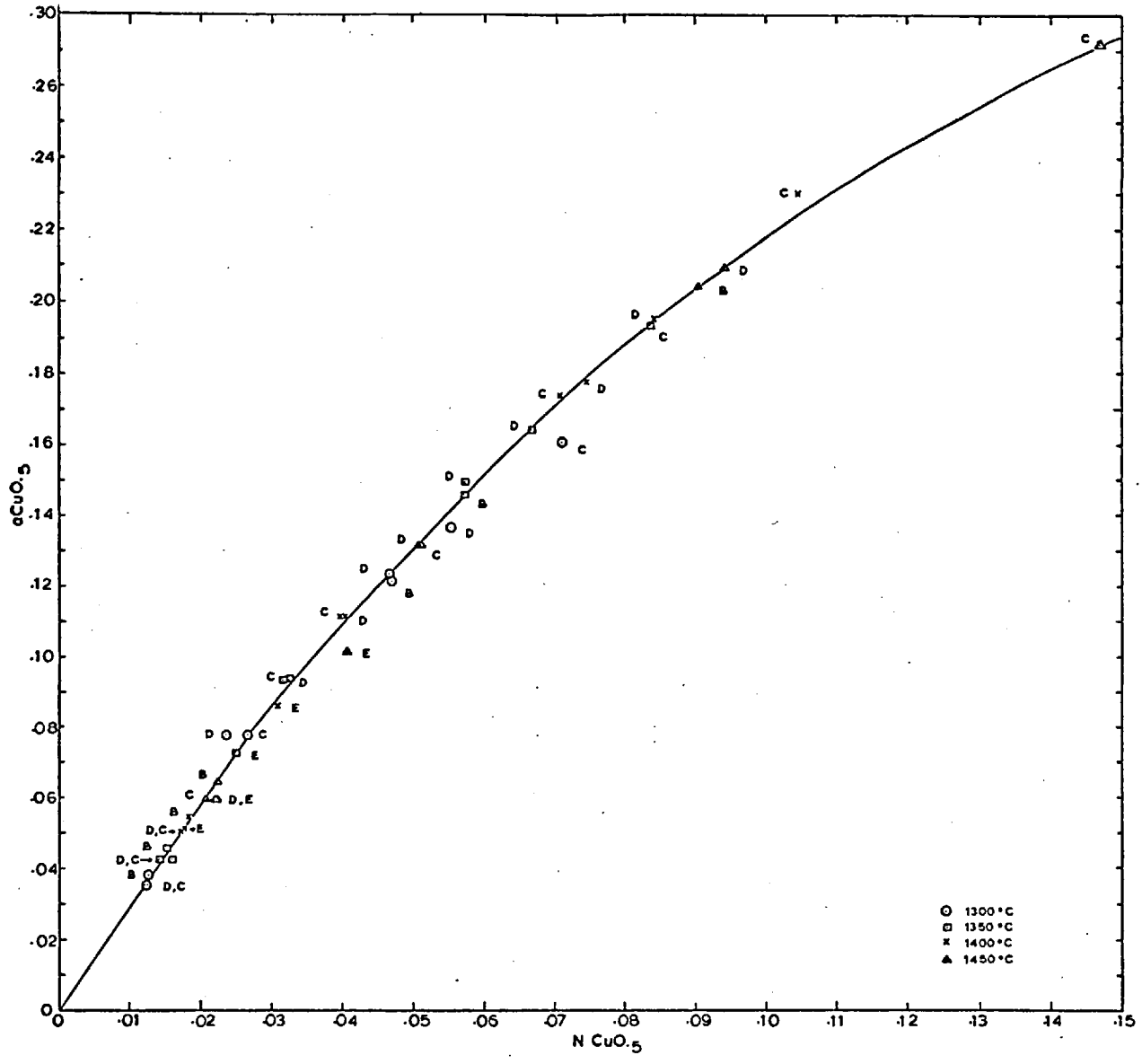

Cu/Au Runs, slags B,C,D and E FIG. 3.18(a)

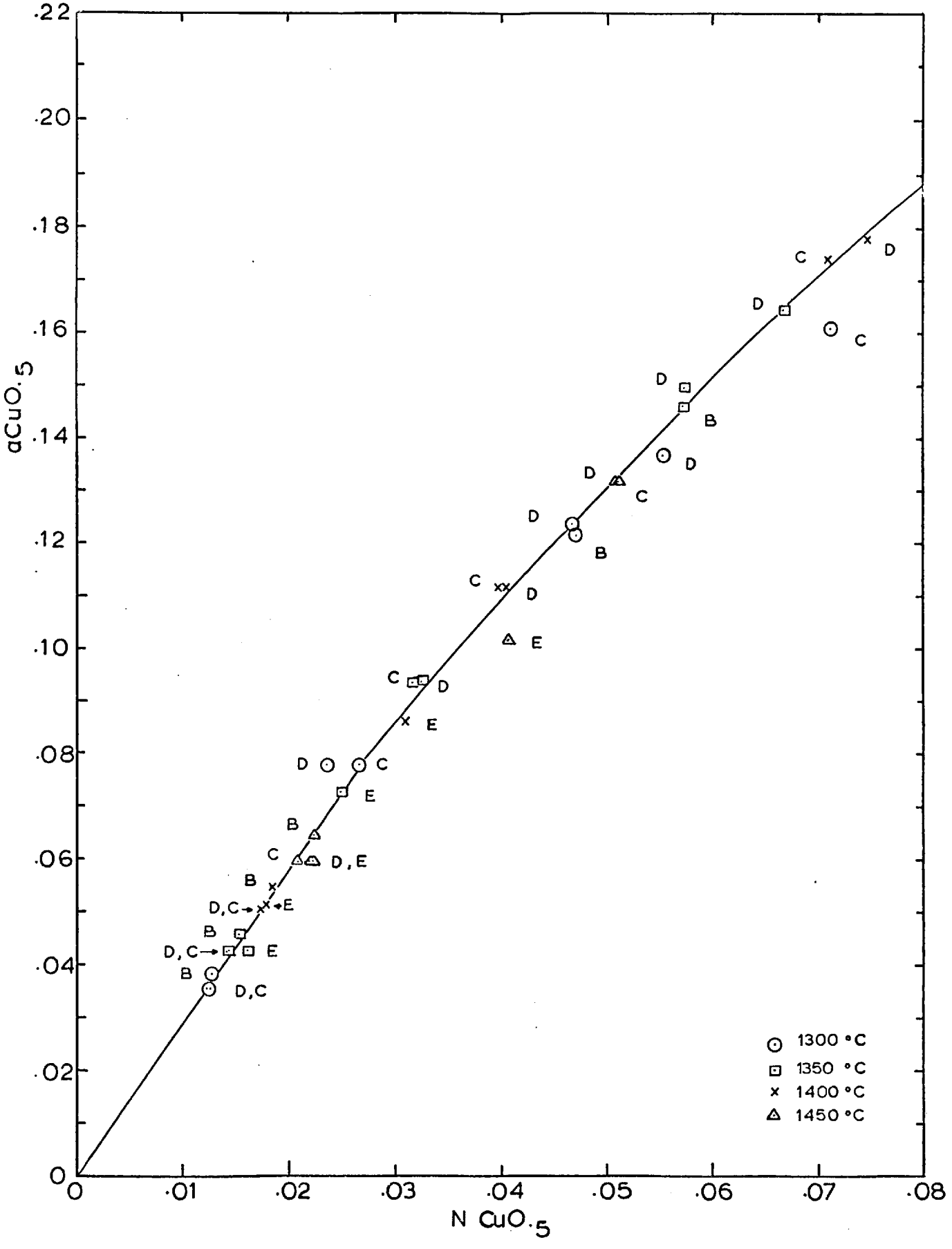

FIG. 3.19

Cu/Ni Runs, slag B

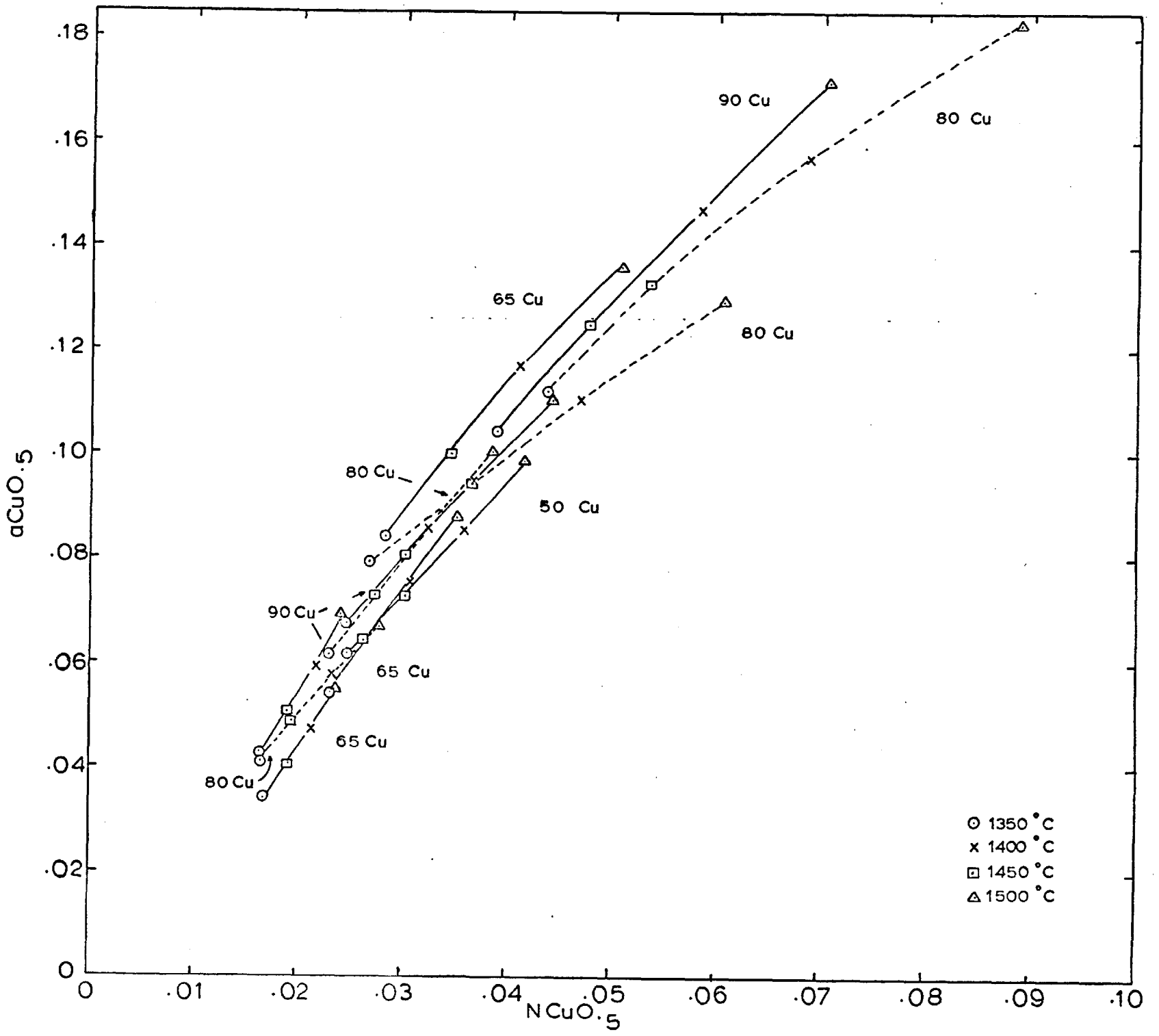

Cu/Ni Runs, slag E FIG. 3.20

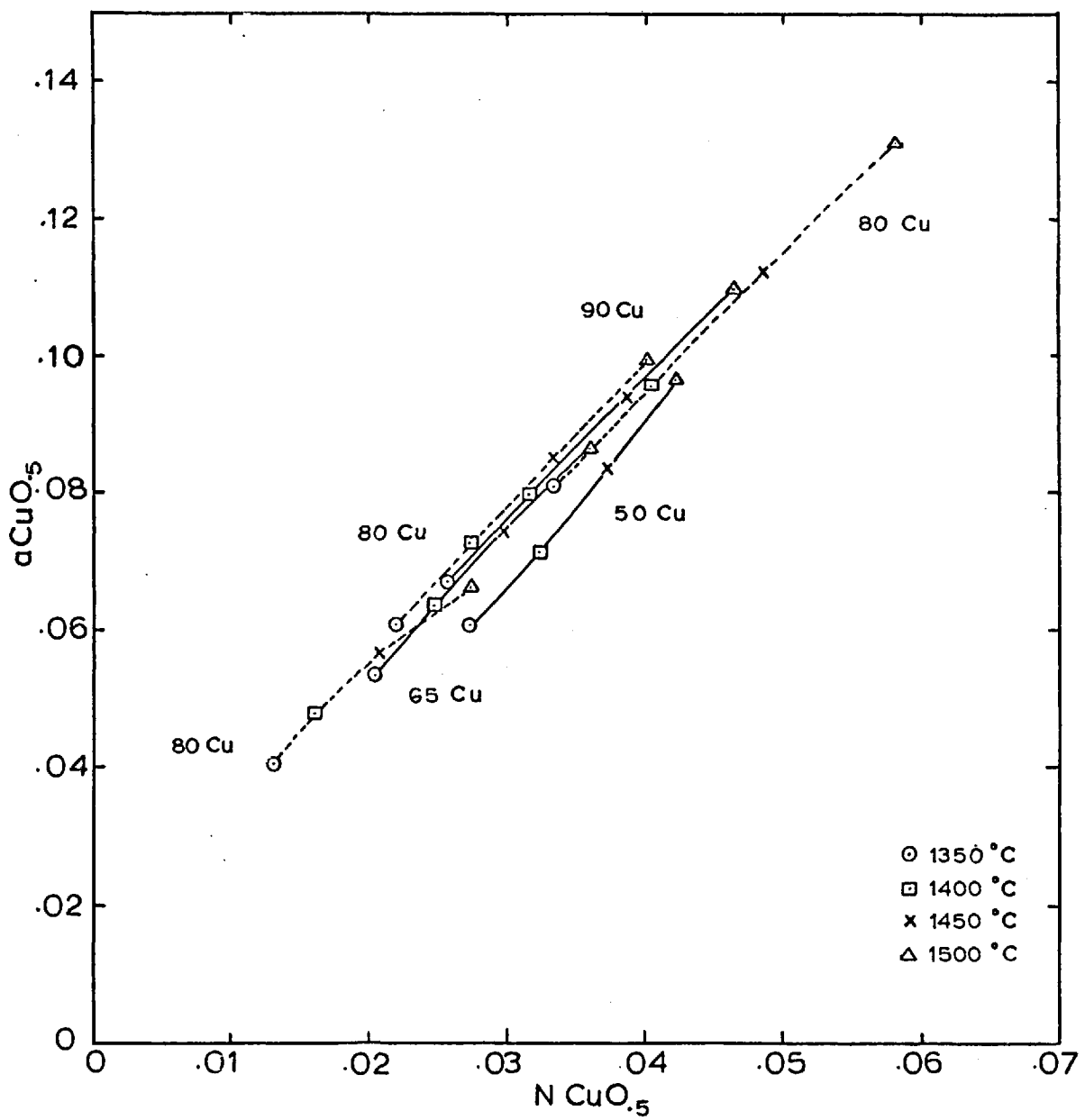

FIG. 3.21

Cu/Ni Runs, slag B

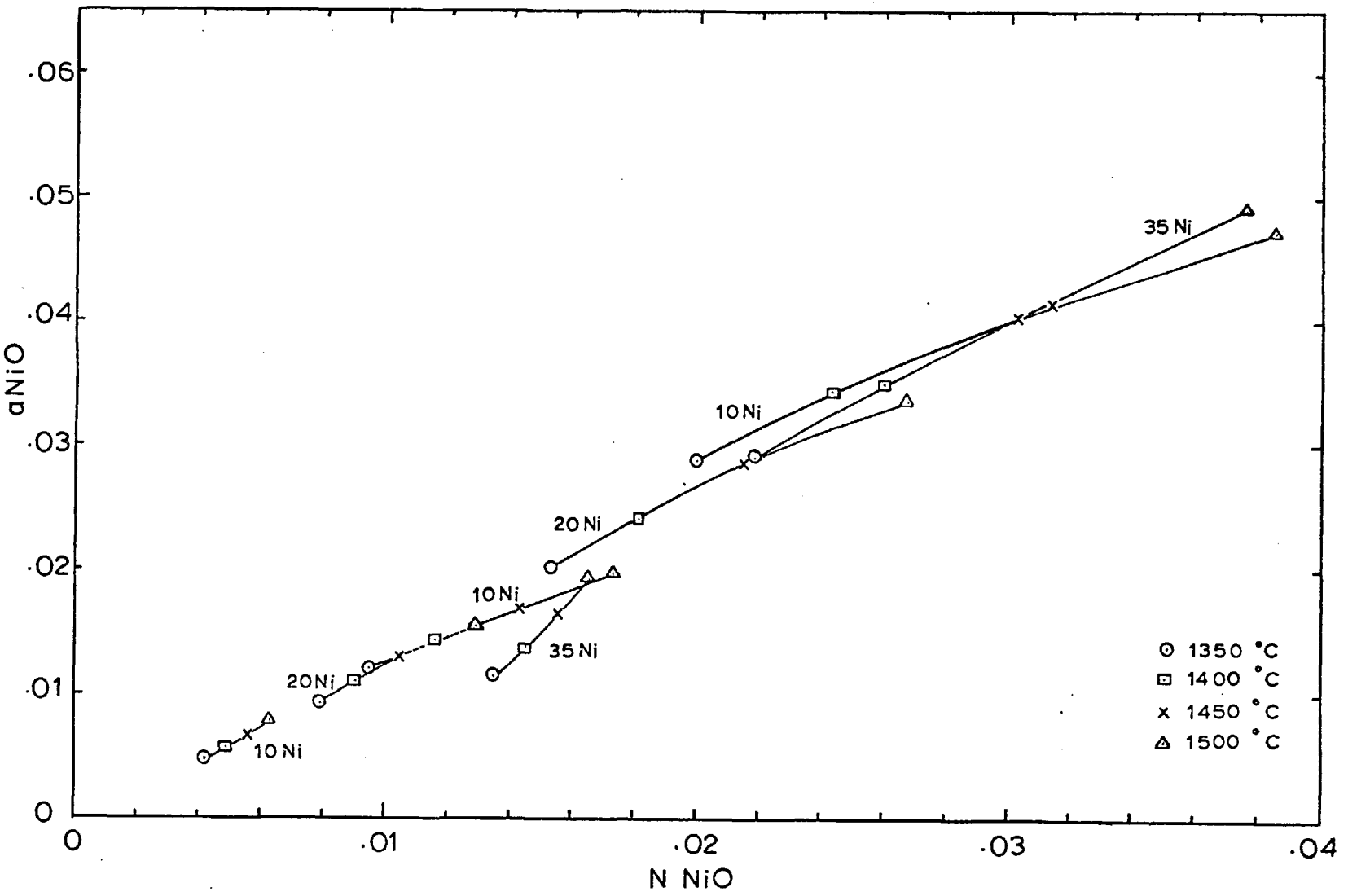

FIG. 3.22

Cu/Ni Runs, slag B

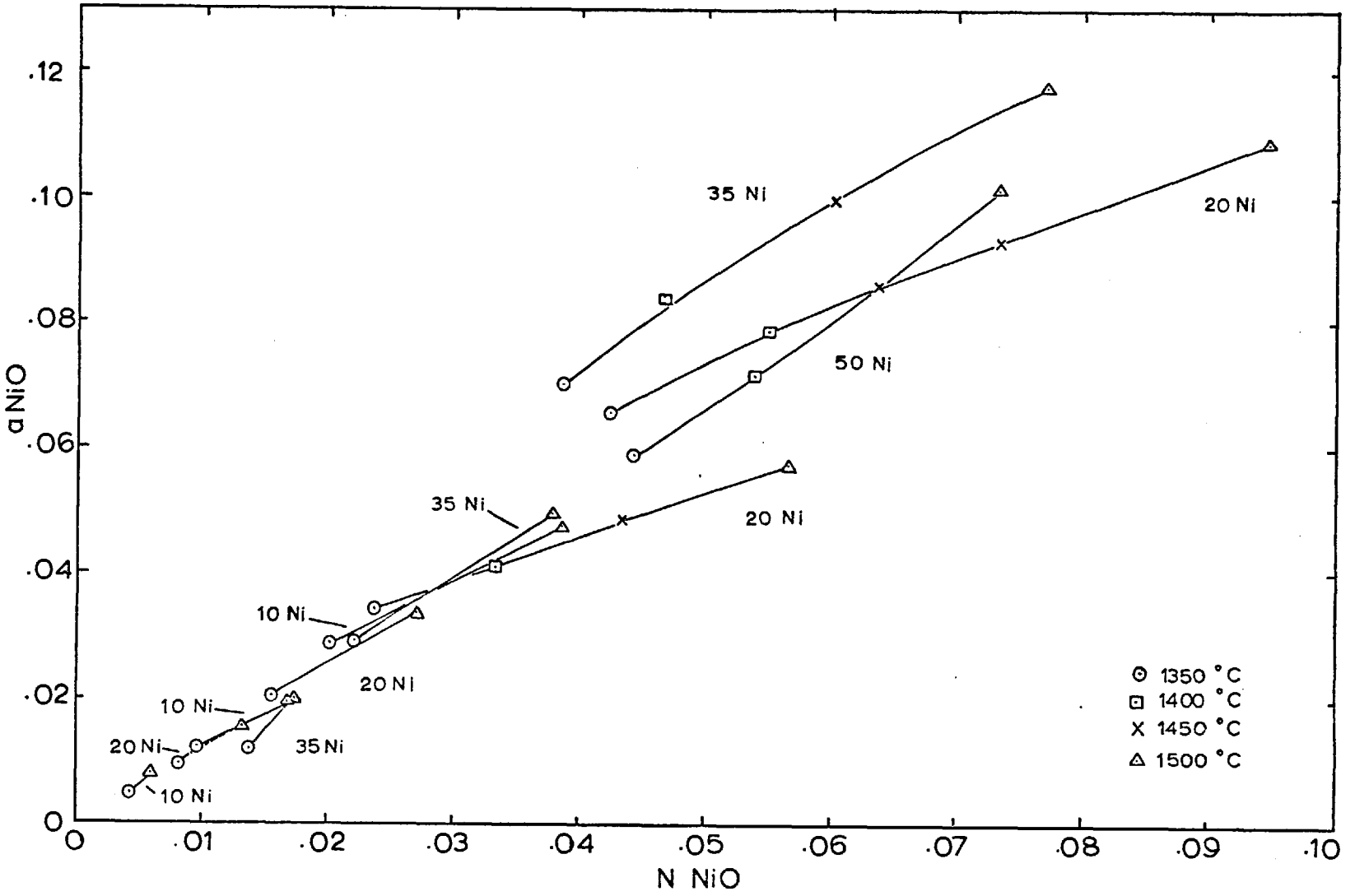

FIG. 3.23

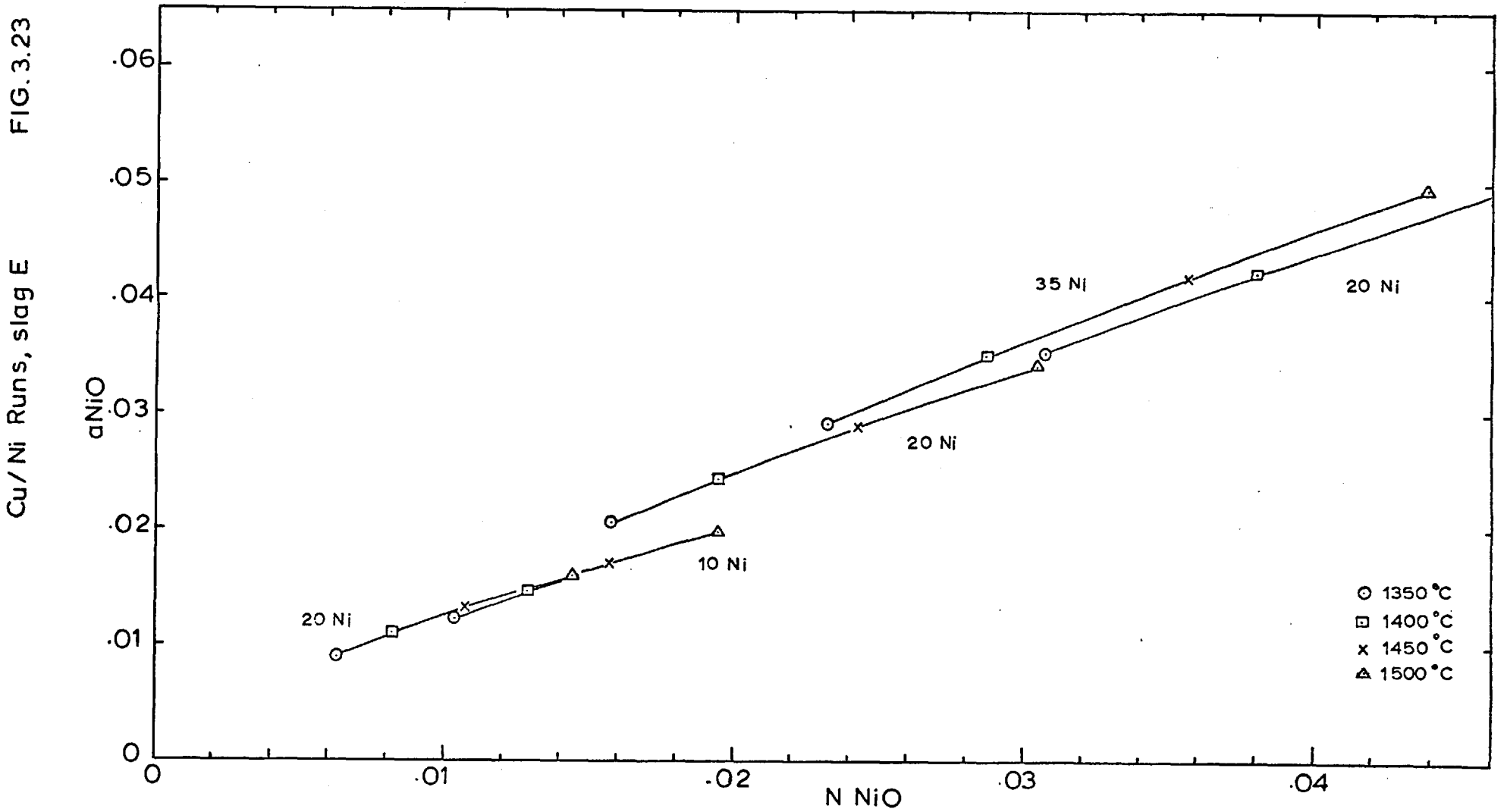
Cu/Ni Runs, slag E
aNiO
N NiO
0
.01
.02
.03
.04
.05
.06
35 Ni
20 Ni
20 Ni
20 Ni
10 Ni
1350 °C
1400 °C
1450 °C
1500 °C

Cu/Ni Runs, slag E FIG. 3.24

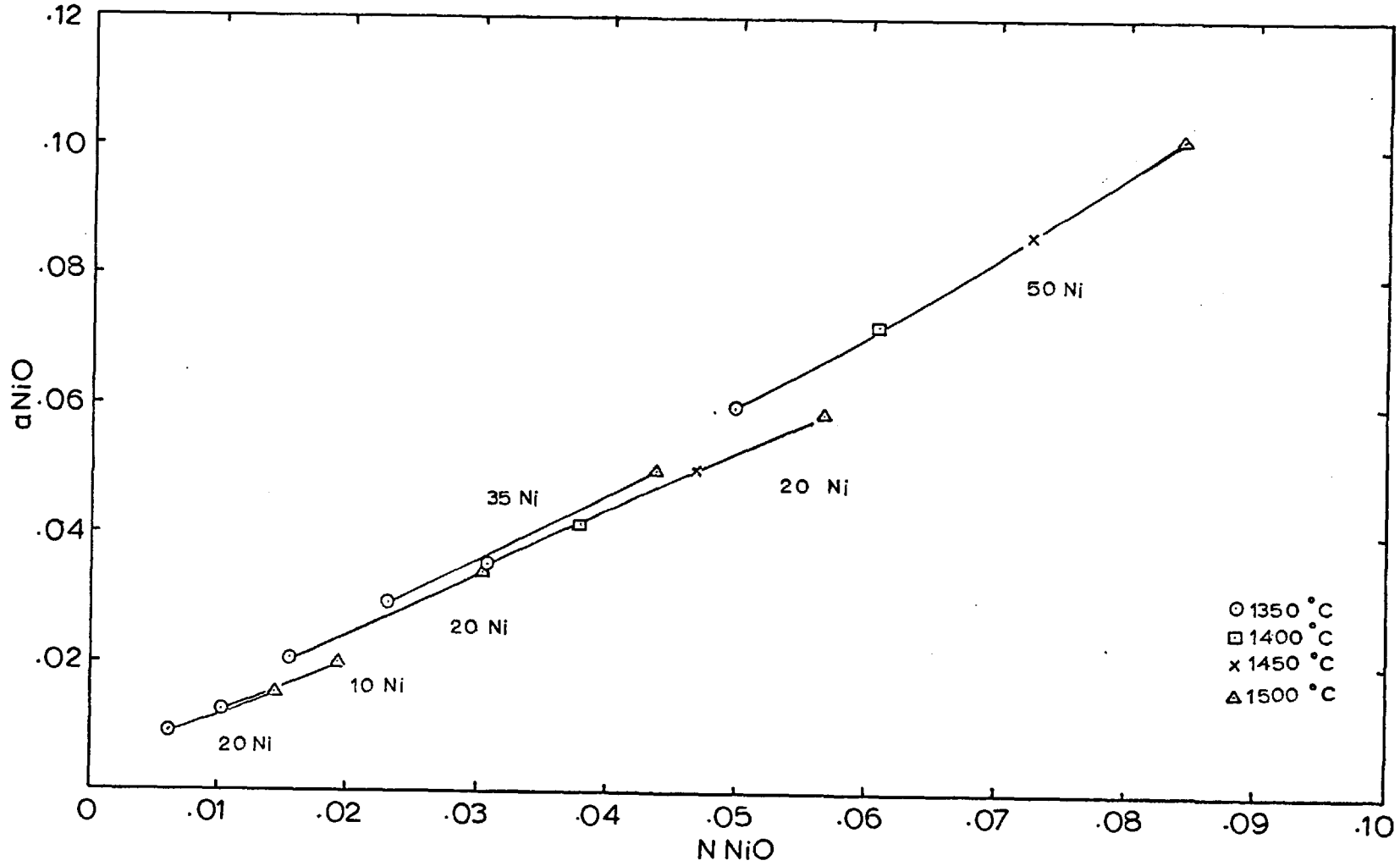

FIG. 3.25 Combination of Cu/Au and Cu/Ni Runs

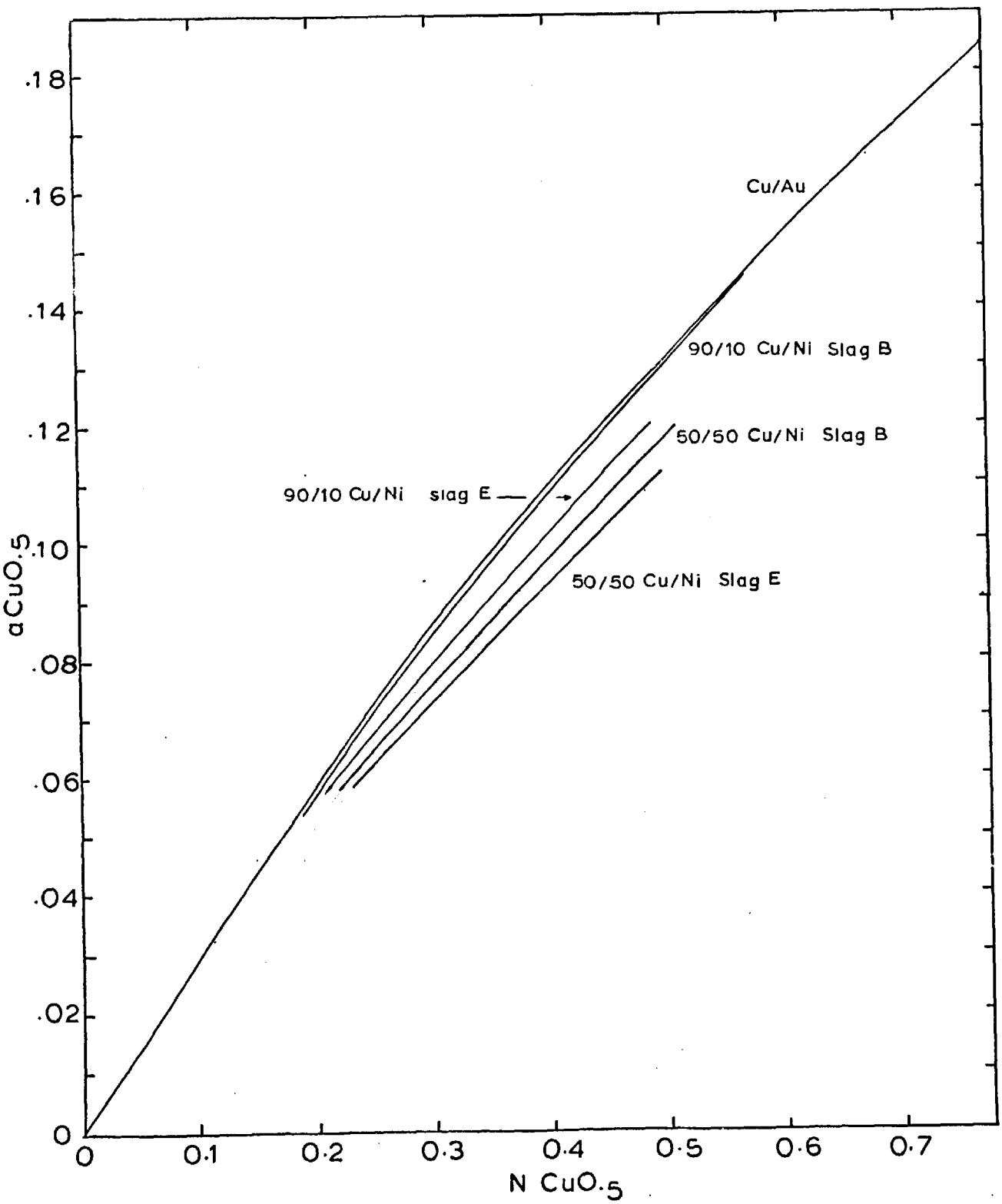

Cu/Ni Runs, slags B & E, 1400 & 1450 °C FIG. 3.26

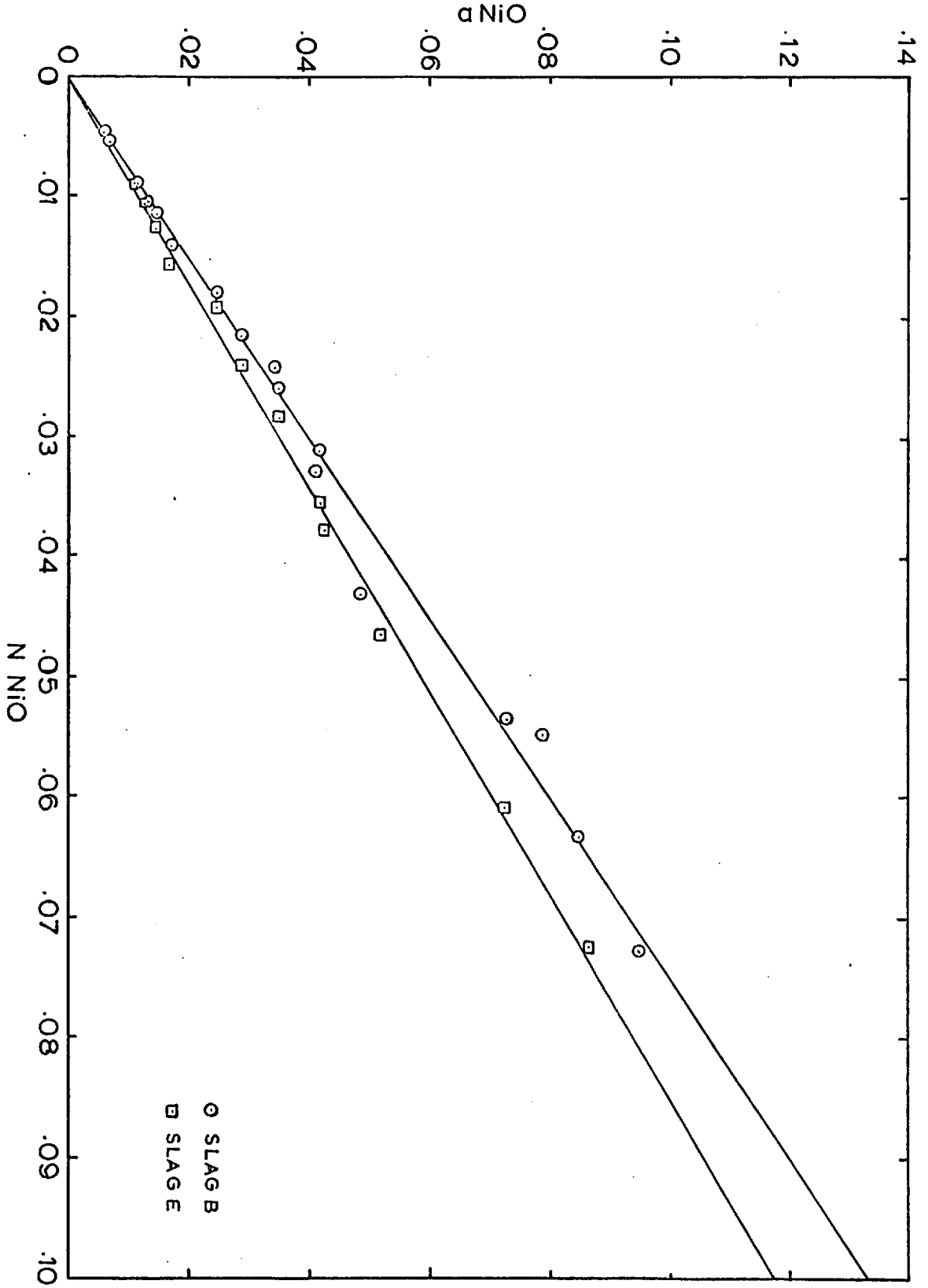

Activity Coefficients of $CuO_{.5}$ and NiO

FIG. 3.27

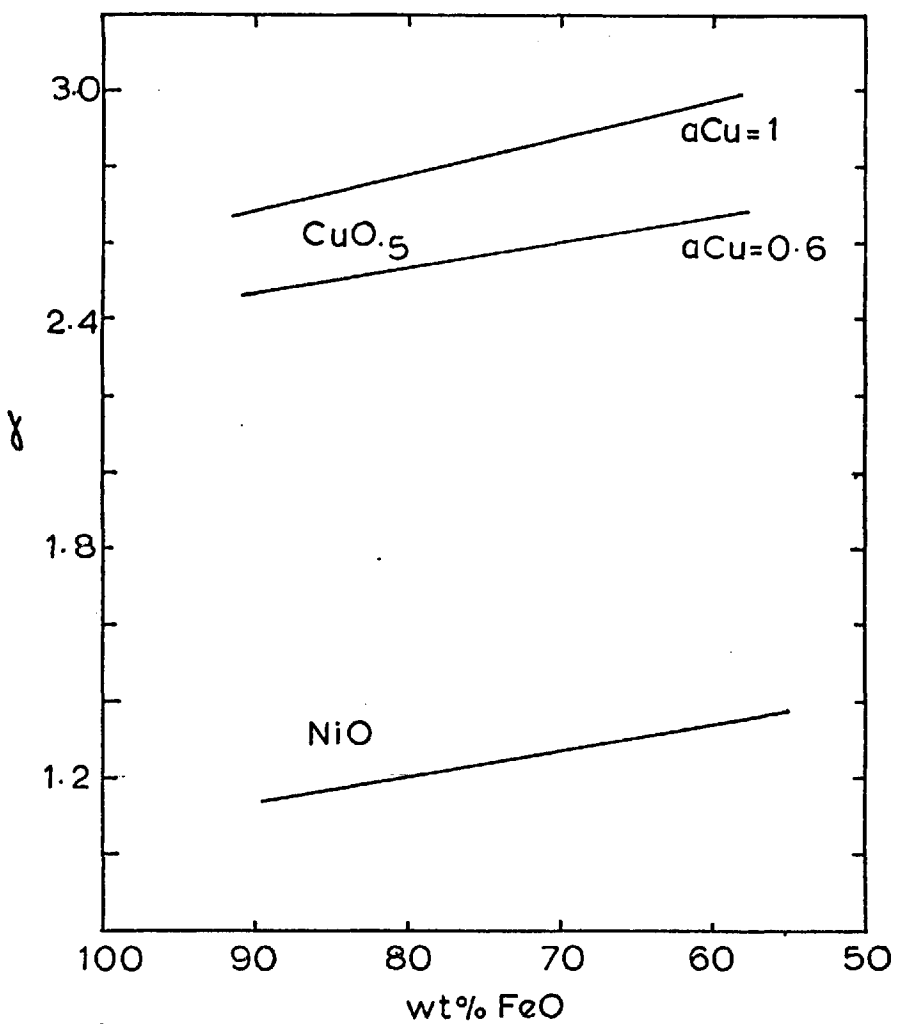

Cu Contents of slags FIG 3.28

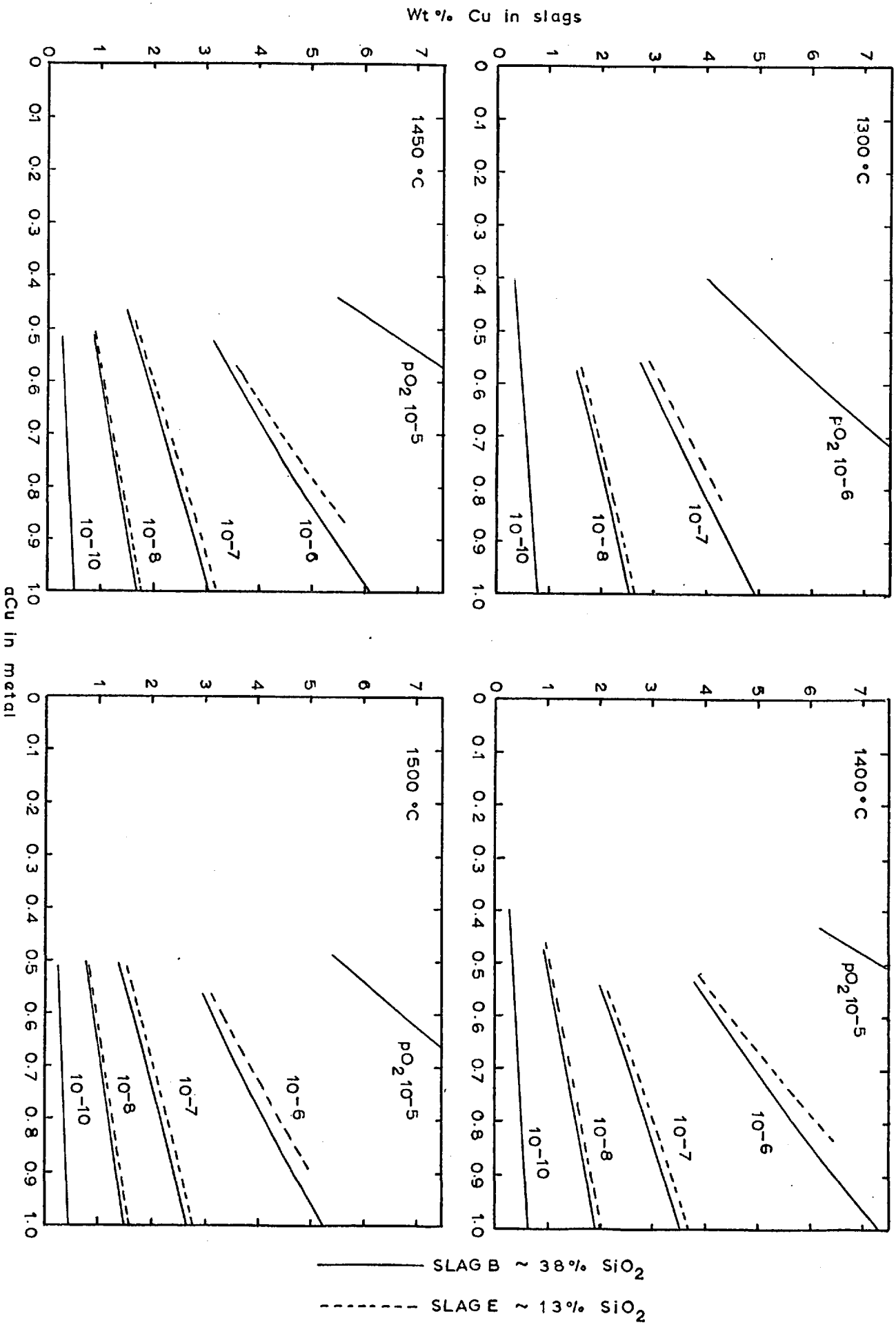

Ni Contents of slags FIG. 3,29

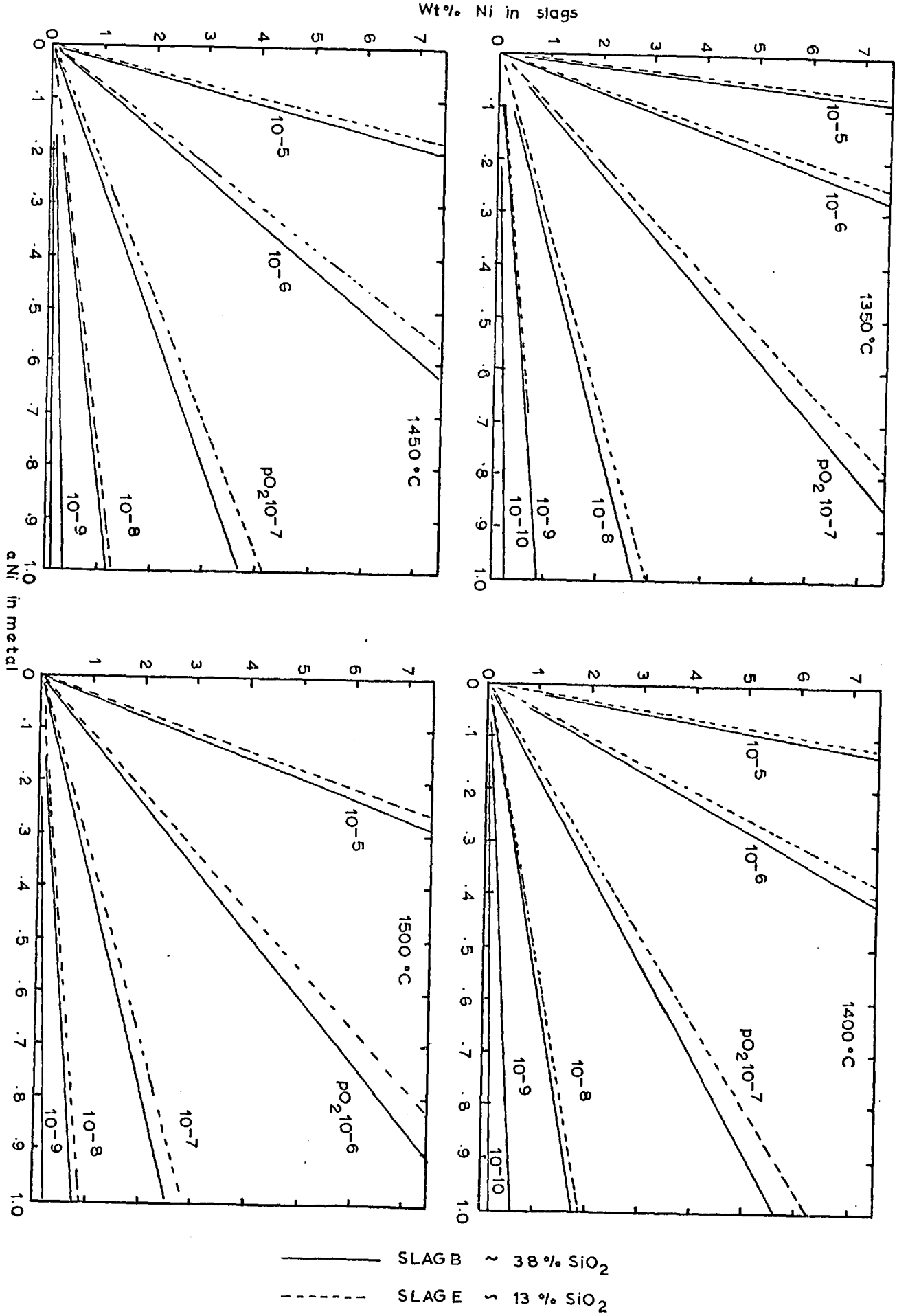

CHAPTER 4.

DISCUSSION.

Choice of $CuO._5$ as Species for Copper in Slag

Copper commonly forms two oxides, CuO and Cu_2O. At high temperatures and in contact with copper metal, Cu_2O is much more stable than CuO. Using data from JANAF tables,[121] at 1600°K under conditions where aCu = 1 and $aCuO._{5(\text{relative to liquid})} = 0.20$, the activity of CuO (relative to solid) is ~ 0.0018. The presence of any copper in the cupric state has therefore been ignored.

$CuO._5$ rather than Cu_2O has been chosen as the thermodynamic species for cuprous oxide. The choice emphasises the ionic nature of the slag, with Cu_2O forming two separate Cu^+ ions rather than a Cu_2^{2+} group. Lumsden[32] showed that properties of iron silicate slags could be more conveniently expressed if the ferrous oxide species was taken as $FeO_{1.5}$ rather than Fe_2O_3, reflecting the presence of single Fe^{3+} ions.

Previous workers[67,70,72] have shown that dissolution of cuprous oxide is consistent with cuprous oxide forming $2Cu^+$ rather than Cu_2^{2+}. Two possibilities are:

$$2Cu + \tfrac{1}{2} O_2 = Cu_2O \qquad (a)$$

$$Cu + \tfrac{1}{4} O_2 = CuO._5 \qquad (b)$$

The amount of copper in the slag is directly proportional to $pO_2^{\frac{1}{4}}$ and aCu, and not $pO_2^{\frac{1}{2}}$ and aCu^2. Use of $aCuO._5$ gives a constant value for $\gamma CuO._5$ as N $CuO._5$ approaches zero, whilst γCu_2O approaches zero as N Cu_2O approaches zero. Thus equation (b) is preferred to equation (a).

General Discussion

Considering the wt% vs. T°C plots for the Cu/Au runs, Figs. 3.2 to 3.5, pages 84 to 87, 85-90% of the points tend to lie within $\pm$ 4% of the lines drawn. The combination of the results from these curves to give the $aCuO._5$ vs. N $CuO._5$ curve, Fig. 3.18 page 112, gives a scatter of about $\pm$ 2%. These results show considerably less scatter than those of Ruddle et al,[68] and as little, if not less scatter than those of Altman and Kellogg.[72] This curve is, of course, the result of many more slag analyses than used by the other workers. A single line has been drawn to represent all the points. The effect of slag composition is discussed later. The line is linear up to about 0.03 mol fraction $CuO._5$ (about 3 wt% Cu in the slag) and passes through the origin, suggesting that the choice of $CuO._5$ is reasonable.

The position of the $aCuO._5$ vs. N $CuO._5$ curve seems to be independent

of temperature over the temperature range studied. The relationship

$$\frac{\partial \ln a\mathrm{CuO}_{.5}}{\partial \frac{1}{T}} = \frac{\Delta \bar{H}}{R}$$

where $\Delta \bar{H}$ is the partial molar heat of solution of $\mathrm{CuO}_{.5}$ in the slag, is not strictly applicable since the slag composition is not kept constant. However, to a first approximation, $\Delta \bar{H}$ seems to be zero.

The scatter for the Cu/Ni runs, Figs. 3.6 to 3.17, pages 88 to 89, increases from about $\pm$ 5% for the 10% nickel alloy to about $\pm$ 12% for the 50% alloy. This increase in scatter is thought to arise from the increasing difficulty of removing slag samples as the nickel content of the alloy rises. At high nickel contents, the slag does not detach neatly from the drop; the metal has a tendency to stay with the slag on withdrawing the quenching rod.

Values of $a\mathrm{CuO}_{.5}$ and aNiO calculated from the individual runs are plotted against mol fraction $\mathrm{CuO}_{.5}$ and NiO respectively for slags B and E in Figs. 3.19 to 3.24, pages 114 to 119.

The $a\mathrm{CuO}_{.5}$ and aNiO vs. mol fraction curves do not match up as well as those from the Cu/Au runs, (Fig. 3.18, page 112). This can only partly be explained by the increased scatter in the points for the individual runs. The relative position of the curves depends also on the pyrometer calibration for the four Cu/Ni alloys, the accuracy of the activity values taken for Cu and Ni and the average analysis values taken to represent the alloy composition, and the effect of a wide range of slag composition on the activity coefficients of $\mathrm{CuO}_{.5}$ and NiO.

It is difficult to assess the accuracy of the pyrometer calibrations. Readings are reproducible to within about $\pm$ 2°C during the runs. It is nevertheless possible that the absolute error in the temperature readings could be $\pm$ 5-10°C. An error of 5°C would give a 3% error in the value of $a\mathrm{CuO}_{.5}$.

The nickel activities recommended by Elford[123] are a maximum of about 2% higher than those recommended by INCRA[125] and a maximum of 4-5% below those recently measured by Kulkarni and Johnson.[126] The copper activities are a maximum of 3% higher than INCRA and 3% higher than ref. 124. The alloy analyses within a run generally show less variation that this.

The results for the 35 wt% Ni runs at high and low pO_2 (i.e. N35C(a) and N35B(b)) are considered to be anomalous; no satisfactory explanation has been found for their position relative to the other results (see Figures 3.19, 3.21 and 3.22, pages 114, 116 and 117). The results from these two runs are not generally considered further in the discussion.

In figure 3.25, page 120, the results for $aCuO._5$ from the Cu/Au alloys are combined with the results from the Cu/Ni runs in a schematic form to represent the general form of the results. The agreement between the two sets is good, and two trends are noticeable; the lowering of the $CuO._5$ activity coefficient with increasing iron content of the slag, and the lowering of the $CuO._5$ activity coefficient with increasing copper metal activity. In the aNiO vs. N NiO curves (Figures 3.21 to 3.24, pages 116 to 119), there is a slight suggestion that γNiO is lowered as the nickel activity is lowered in slag E, but this is not noticeable in slag B.

In drawing the wt% metal in slag vs. temperature curves (Figures 3.2 to 3.17), from which the activity of metal oxide curves are derived, the position for the two ends of the curves, at the highest and lowest temperatures of the run, are less well defined than the position of the middle parts of the curve. With this in mind, the points at 1400° and $1450^{\circ}C$ have been taken from Figure 3.22, page 117, for slag B and Figure 3.24, page 119 for slag E and combined together in Figure 3.26, page 121, to show the effect of slag composition on the activity coefficient of NiO. The activity coefficient is lowered by an increase in iron content of the slag, and remains appreciably constant for a given slag composition up to at least a nickel oxide mol fraction of 0.07 (7 wt% Ni).

For the Cu/Au alloys, the activity coefficients of $CuO._5$ in slags B,C,D and E in the linear part of the curve are 2.96, 2.92, 2.87 and 2.74 respectively. $\gamma CuO._5$ falls to about 2.5 in slag E when aCu is about 0.6. These suggested activity coefficients are shown in Figure 3.27, page 122. From Figure 3.26, page 121, it can be seen that the activity coefficient for NiO is 1.33 in slag B and 1.17 in slag E. These are also shown in Figure 3.27. On a weight % basis, the solubility of the nickel in the slag can be expressed by:-

wt% Ni in slag = 65.3.aNiO for Slag B.

wt% Ni in slag = 72.0.aNiO for Slag E.

and for copper in the slag:

wt% Cu in slag = $32.0.aCuO._5$ for high aCu and high silica slags

wt% Cu in slag = $36.0.aCuO._5$ for aCu = 0.6 and low silica slags

The equations apply up to 7 wt% nickel and 3 wt% copper in the slag.

Within the experimental error, the position of the aNiO curves seem independent of temperature as in the case of $aCuO._5$. The positions of the NiO curves are affected by the choice of the entropy of fusion of NiO. A low entropy of fusion would give higher activity coefficients and would show γ decreases with increasing temperature. For $\Delta S_{fusion} = 5$ cal/deg/mol instead of 6 cal/deg/mol, for instance, aNiO and γNiO would be multiplied by 1.217, 1.192, 1.169 and 1.147 at 1350, 1400, 1450 and 1500°C.

Two points require further discussion. Firstly the absolute magnitude of the activity coefficients for copper and nickel oxide, and secondly the lowering of the activity coefficients with increasing iron content and decreasing metal activity.

The free energy of mixing of a number of binary silicates is shown in Figure 4.1, page 130. The melts decrease in stability in the same order as the oxides and orthosilicates, formed from the respective metals, decrease in stability, although lead is somewhat anomalous.

On this basis, the free energy of mixing curve for NiO and SiO_2 would be more positive than the $FeO-SiO_2$ line, and that for Cu_2O-SiO_2, more positive still.

The heats of formation of a number of solid orthosilicates of metals from the first transition series have been measured[83] i.e. ΔH_f^o for the reaction

$$2MO_{(s)} + SiO_{2(s)} = 2MO.SiO_{2(s)}$$

The values are (ΔH_f^o for Ca_2SiO_4 has also been included for comparison):

$2CaO.SiO_2$	ΔH_{298}	- 30.0 Kcal.
$2MnO.SiO_2$	ΔH_{298}	- 11.8 Kcal.
$2FeO.SiO_2$	ΔH_{298}	- 8.2 Kcal.
$2CoO.SiO_2$	ΔH_{298}	- 4.3 Kcal.
$2NiO.SiO_2$	ΔH_{298}	- 3.15 Kcal.
$2CuO.SiO_2$	ΔH_{298}	+ 3-4 Kcal.

Free Energies of Mixing in Some Binary Silicates FIG. 4.1

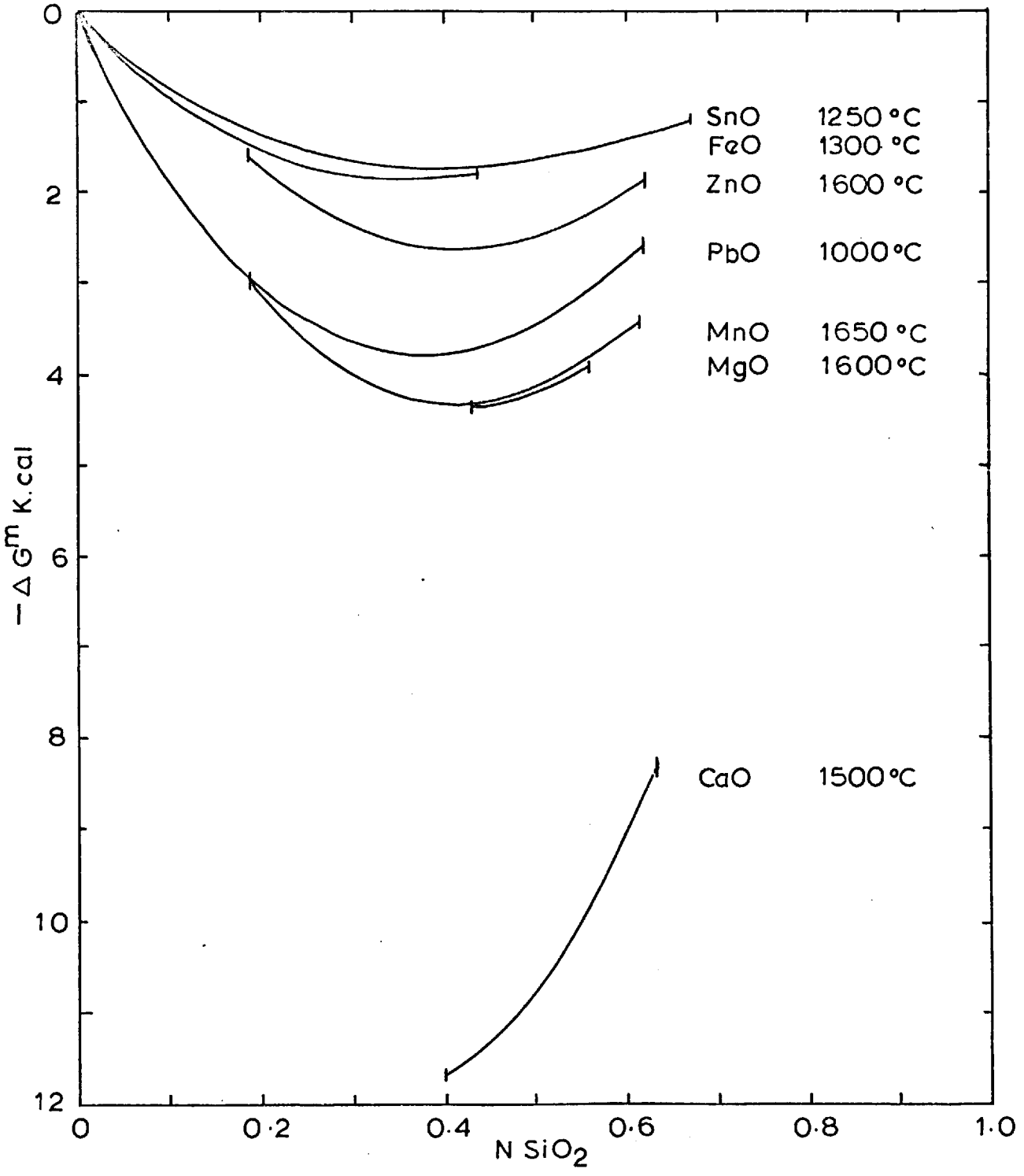

The value for the heat of formation of copper orthosilicate is an estimation by Navrotsky,[82] who suggested copper silicates have small positive free energies and enthalpies of formation. The Cu_2O phase diagram, Fig. 1.7, page 21, shows no intermediate compounds and a wide range of immiscibility between Cu_2O-rich liquid and solid SiO_2.

This decrease in enthalpy in the transition series order Mn, Fe, Co, Ni, Cu suggests a decreasing stability of the $Si\text{-}O^-$ - metal bond compared with the $M\text{-}O^{2-}$ bond, and suggests a decreasing tendency for the metal to associate with the $Si\text{-}O^-$ bonds in the silicate lattice and an increasing tendency to remain bonded to O^{2-} ions in the oxide lattice. In the crystaline solid state there is no choice between $Si\text{-}O^-$ bonds and O^{2-} bonds, but on melting, there is a possibility of choice between the two bond types. As discussed in Chapter 1., a strong interaction between the metal cation and $Si\text{-}O^-$ bonds tends to prevent polymerization of the melt, leaving few O^{2-} ions, and a low metal oxide activity. Increasing preference for O^{2-} compared with $Si\text{-}O^-$ bonds will allow polymerization of the melt and give a high metal oxide activity. Thus the activity of metal oxides in binary silicate melts would be expected to increase in the order $MnO < FeO < CoO < NiO$.

Activities in binary melts have been measured for $MnO\text{-}SiO_2$,[127] $FeO\text{-}SiO_2$,[127] and $CoO\text{-}SiO_2$[128] systems and are shown in Fig. 4.2, page 132 (activities are relative to the liquid oxide). The activities do increase in the order MnO, FeO, CoO and it would be expected that the NiO activities would be higher still. Activities for NiO and Cu_2O[16] calculated from the phase diagram are included, although it is not valid to compare aCu_2O or $aCuO._5$ directly because of the valency difference. The NiO liquidus in the $NiO\text{-}SiO_2$ phase diagram, Fig. 1.8 page 21, has been estimated and not experimentally determined and is very tentative. Greatest weight is attached to the low temperature points.

Activities in the present work were, of course, measured in $FeO\text{-}SiO_2$ melts and not in melts with silica alone. Low concentrations of the metal in the $FeO\text{-}SiO_2$ melt would not be expected to affect the degree of polymerization of the melt or the O^{2-} ion activity, but it is expected that the activities of the metal oxide in the ternary melt are a reflection of the degree of association of the cation with either $Si\text{-}O^-$ or O^{2-} ions. Assuming no interaction between Fe ions and the second metal, then activity coefficients of the metal oxide in $MO\text{-}FeO\text{-}SiO_2$ melts would be expected to increase in the order Ca, Mn, Fe, Co, Ni, Cu. activity

Activities in Binary Silicate Melts FIG. 4.2

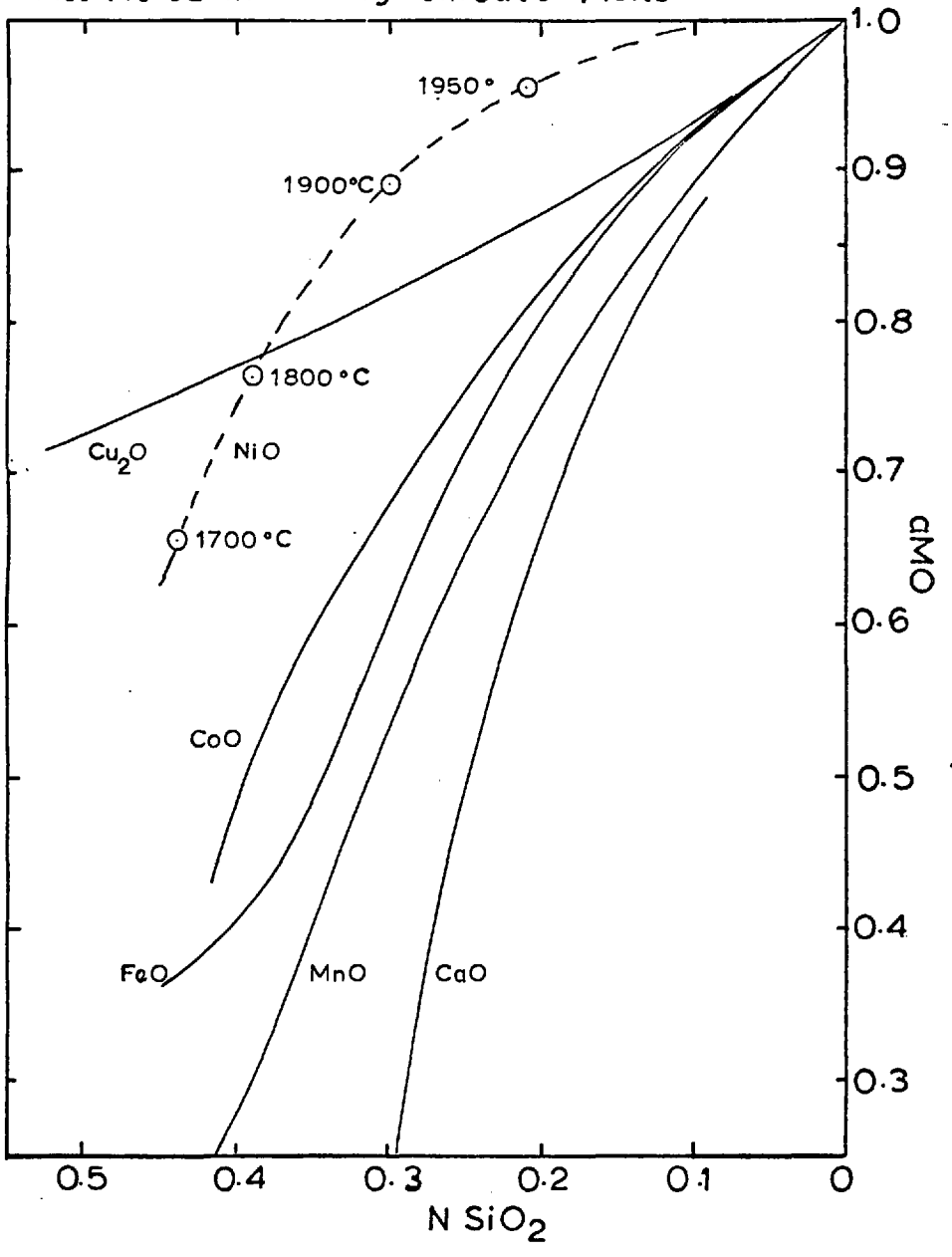

Activity Coefficients in Iron Silicate Melts FIG. 4.3

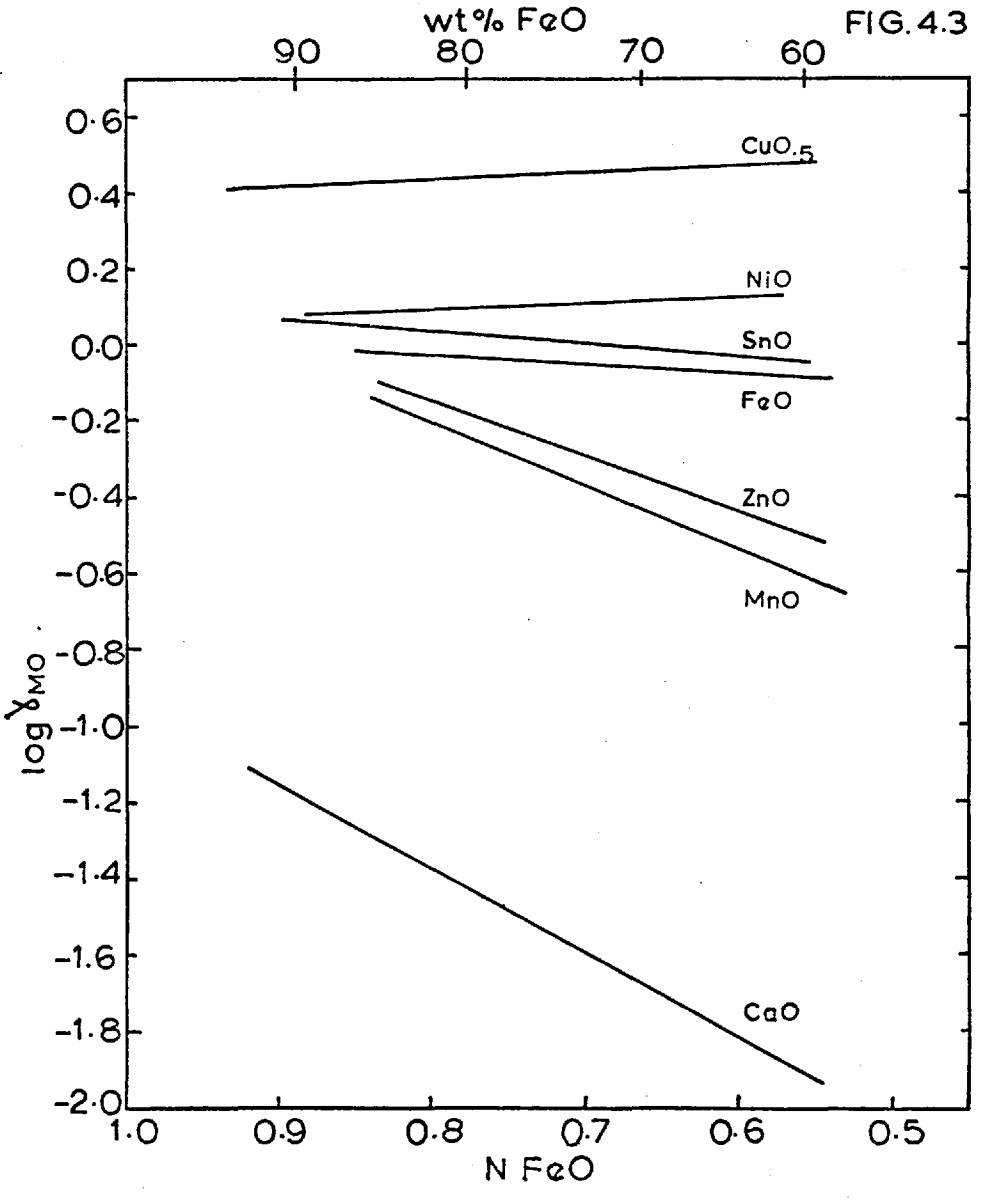

coefficients for CaO,[18] MnO,[129] FeO,[30] and NiO and $CuO._5$ from this work, taken from measurements at low MO levels where possible, are plotted against $FeO-SiO_2$ melt composition in Fig. 4.3, page 132. Also included are activity coefficients for ZnO [33] and SnO,[130] whose position can be compared with their position in the free energy of mixing curves, Fig. 4.1, page 130. It can be seen that the measured values of γ_{NiO} and $\gamma_{CuO._5}$ are consistent with the above arguments.

In this respect, the results of Ray[131] are of some interest. Ray measured activities of FeO, CoO, NiO and Cu_2O in 18.4 mol% Na_2O - 31.6 mol% K_2O - 50.0 mol% SiO_2 melts at about 1000°C, in concentration and galvanic cells. The results give 'Henrian' activity coefficients relative to the solid oxides as γ_{FeO}; 1.1 ± 0.4, γ_{CoO}; 5.9 ± 0.7, γ_{NiO}; 12.3 ± 4.7 and γ_{Cu_2O}; 8.7. If Cu_2O is converted to $CuO._5$, then $\gamma_{CuO._5}$ is about 14. Converting these to a liquid oxide standard state gives:

$$\gamma_{FeO} = 0.56$$

$$\gamma_{CoO} = 0.83$$

$$\gamma_{NiO} = 1.19$$

$$\gamma_{CuO._5} = 9.0$$

That is, the activity coefficients in the Na_2O- K_2O- SiO_2 melts increase in the order found in the $FeO-SiO_2$ melts.

It is interesting to consider the effect on γ_{NiO} and $\gamma_{CuO._5}$ in iron silicate melts of the addition of a strong depolymerizing cation such as Ca^{2+}. Taylor and Chipman showed that γ_{FeO} was raised by the addition of CaO. This effect was discussed in the first Chapter. A similar effect has been found for γ_{MnO},[36] γ_{ZnO}[132] and γ_{SnO}.[130] It is to be expected that the activity coefficients of $CuO._5$ and NiO will also be raised by CaO additions. No information is available for NiO, but Bailey[49] reports a marked lowering of copper content of a slag of composition 38% SiO_2, 16% Fe, 19% CaO, 17% Al_2O_3 and 4% K_2O compared with a silica saturated iron silicate slag.Any raising of the activity coefficient would be helpful in reducing losses of copper or nickel in the slag during smelting.

The tendency for the activity coefficients of $CuO._5$ and NiO to be lowered by increasing iron content of the slag and decreasing metal activity can be explained by the tendency for copper and nickel oxides to associate with Fe_2O_3 in the melt to form ferrites.

Heats of formation of $CuFeO_2$, $NiFe_2O_4$ and Fe_3O_4, taken from ref. 133 are given below.

$$FeO\ (stoichiometric) + Fe_2O_3 = Fe_3O_4 \quad \Delta H_{298} \quad - 5.3\ Kcal$$

$$\tfrac{1}{2}\ Cu_2O + \tfrac{1}{2}\ Fe_2O_3 = CuFeO_2 \quad \Delta H_{298} \quad - 8.7\ Kcal$$

$$NiO + Fe_2O_3 = NiFe_2O_4 \quad \Delta H_{298} \quad - 4.1\ Kcal$$

The heats of formation of copper and nickel ferrites are of the same order of magnitude as that of magnetite, with that of copper ferrite (delafossite) somewhat more negative than that of nickel ferrite.

Ferrite formation will be favoured by high copper or nickel oxide activity and high Fe_2O_3 activity, given by high oxygen potentials or slags of high iron content. The lower the metal activity in the alloy, the higher will be the oxygn potential required to produce the same metal oxide activity. Thus at constant $aCuO._5$ or aNiO, the lower the metal activity in the alloy, the higher the Fe_2O_3 activity will be in the slag. This is in agreement with the conditions under which the activity coefficients are found to be lowered experimentally.

Using the room temperature data from ref. 133 and specific heat and other data from Kubaschewski[118] the following equations were derived for the experimental temperature range

(a) $[Ni] + 2[Fe]_\gamma + O_2 = [NiFe_2O_4] \qquad \Delta G_T^o = -255{,}458 + 82.103\ T$

(b) $(Cu) + [Fe]_\gamma + O_2 = [CuFeO_2] \qquad \Delta G_T^o = -120{,}868 + 36.555\ T$

combination of (a) and (b) with data from Table 3.2, page 61, gives:

(c) $2(FeO) + 2(NiO) = [NiFe_2O_4] + (Ni) \qquad \Delta G_T^o = -50{,}208 + 26.344\ T$

(d) $3(FeO) + (NiO) = [Fe_3O_4] + (Ni) \qquad \Delta G_T^o = -51{,}001 + 24.116\ T$

(e) $(FeO) + 2(CuO._5) = [CuFeO_2] + (Cu) \qquad \Delta G_T^o = -36{,}728 + 15.527\ T$

(f) $3(FeO) + 2(CuO._5) = [Fe_3O_4] + 2(Cu) \qquad \Delta G_T^o = -67{,}386 + 29.752\ T$

These equations are presented in a graphical form in Figs. 4.4, page 135 and 4.5, page 136, to show the conditions for the formation of solid $NiFe_2O_4$, Fe_3O_4 and $CuFeO_2$ at several values of metal oxide activity and two temperatures (1350 and 1450°C). The condition for formation of solid NiO is also shown. The curves illustrate that copper or nickel ferrite formation is favoured by high iron slag contents (represented by high aFeO) and, at constant $aCuO._5$ or aNiO, low metal activity in the alloy. The curves also show that while $CuFeO_2$ and $NiFe_2O_4$ reach an appreciable activity in the melt under the experimental conditions used, solid Fe_3O_4 is more likely

Formation of $NiFe_2O_4$, Fe_3O_4 and NiO

FIG. 4.4

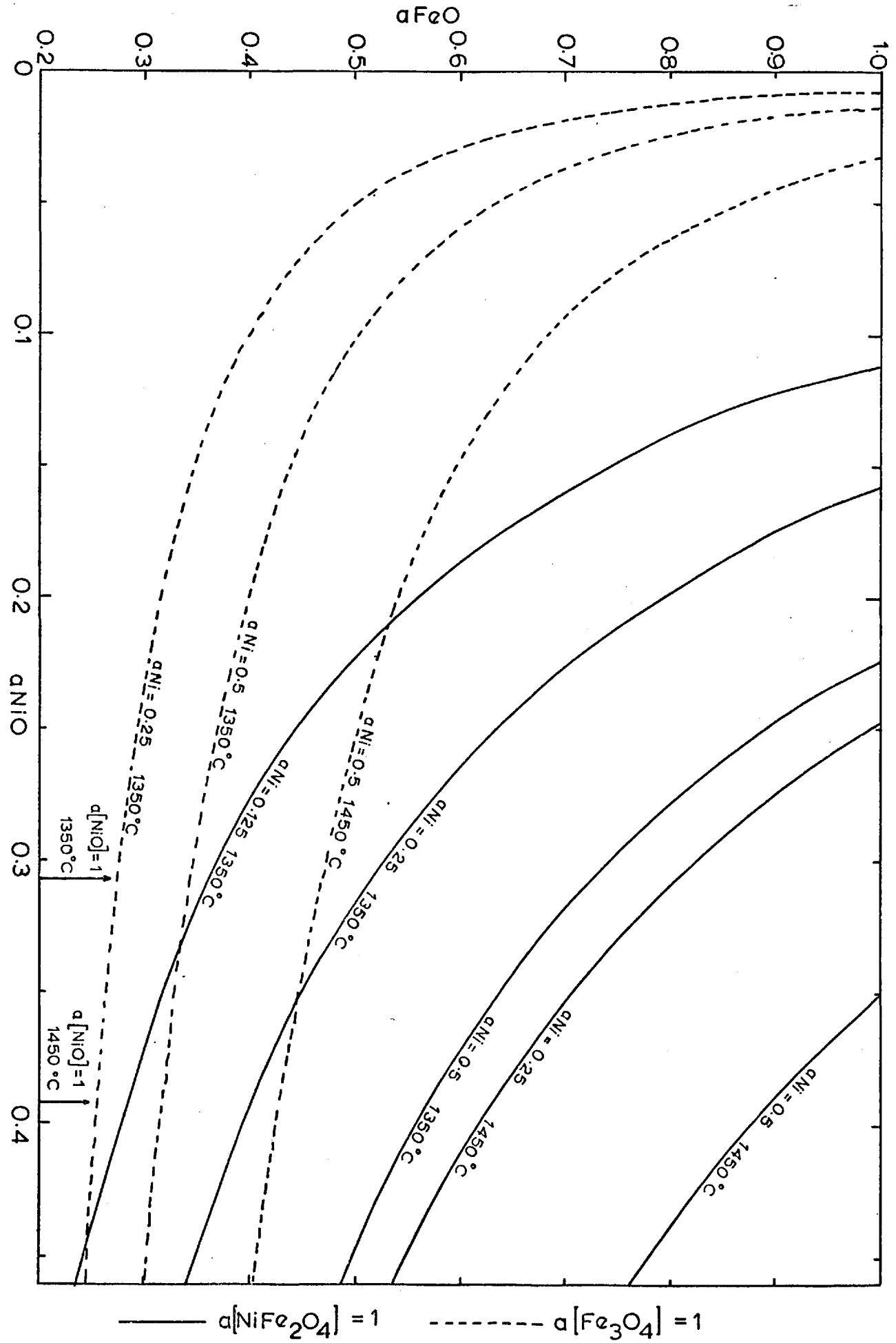

Formation of $FeCuO_2$ and Fe_3O_4 FIG. 4.5

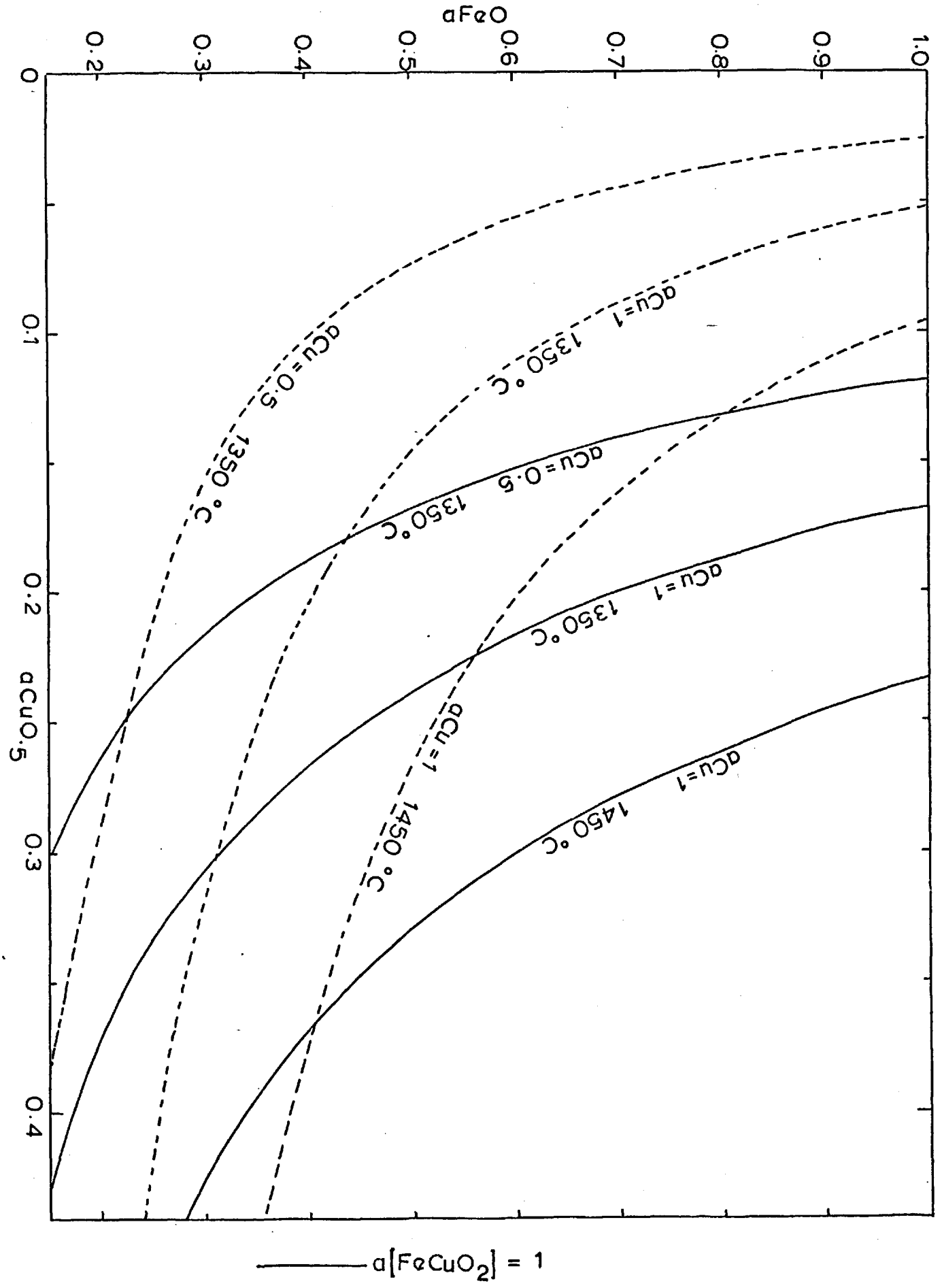

to form than $CuFeO_2$, NiO or $NiFe_2O_4$.

A complete range of solid solutions is reported between Fe_3O_4 and $NiFe_2O_4$,[134] and Fe_3O_4 and $CuO.Fe_3O_4$.[135] At high temperatures, where Cu_2O is more stable than CuO, substitution of Cu_2O into Fe_3O_4 occurs until the spinel becomes unstable with respect to a Cu_2O-rich liquid phase.[133] Thus formation of a solid compound in the experimental melts can occur at aFe_3O_4 less than unity by substitution of Cu or Ni into Fe_3O_4 to form a Cu/Fe/O or Ni/Fe/O spinel.

Further evidence for solution of copper in solid magnetite comes from Altman and Kellogg,[72] who report about 1.8 wt% copper in true solution in magnetite crystals after equilibration with a copper/gold alloy. Huang and Hayward[136] added varying amounts of Cu_2O to a 47.5% FeO, 42% SiO_2, 10.5% CaO melt at 1200°C, and analysed the resulting phases in the solidified slag by X-ray diffraction. They found $Cu_2O.Fe_2O_3$ crystals present on adding more than about 10 wt% Cu_2O to the melt, but did not consider the possibility of substitution of copper into magnetite crystals. The diffraction patterns of magnetite and $Cu_2O.Fe_2O_3$ were reported to be very similar and the presence of any copper in the magnetite may well have been missed. It has been suggested that the naturally occuring mineral delafossite has a composition approximating to $3Cu_2O.Fe_3O_4$ and not $Cu_2O.Fe_2O_3$ as previously thought.[135]

The curves in Figs. 4.4 and 4.5, suggest that the low silica slags (slag E) at 1350°C would be very near magnetite saturation under the experimental conditions used. It was noticed experimentally that these slags often became fairly solid below about 1300°C and were 'sticky' and difficult to sample below about 1360°C.

Formation of a solid phase is not thought to account for the scatter for the high nickel Ni/Cu runs unless an $Fe(Fe(NiFe))O_4$ phase is formed at much lower oxygen potentials than Fe_3O_4 or a copper-substituted magnetite would form, since copper-containing slags were taken to conditions more likely to produce solid phases without producing a scatter in the results.

Ferrites are also reported for Co, Zn, Mn and Ca.[133] For metals which have relatively large interactions with silica, the effect on the activity coefficient of any tendency for ferrite formation with increasing iron slag content would be largely swamped by the effect of decreasing silica

content. Thus γ_{NiO} and $\gamma_{CuO.5}$ are lowered by higher iron contents, while γ_{CaO} continues to increase (Fig. 4.3 page 132). The intermediate case of ZnO is interesting. Richards and Thorne[33] measured ZnO activities in $FeO-SiO_2$ melts saturated with iron, giving very low Fe_2O_3 contents, and found γ_{ZnO} increased with increasing FeO/SiO_2 ratio. Lange,[132] who may have used higher oxygen potentials, found γ_{ZnO} first increased, and then decreased with increasing FeO/SiO_2 ratio.

Calculation of Iron Oxide Activities

In view of the preceding section, it is of interest to have some idea of the activity of the iron oxide species in the slags. The calculations depend largely on knowing the iron content of the alloy samples. No great accuracy can be expected because of the difficulty of analysing the very low iron contents, and because the experiment was not designed for accurate sampling of the metal phase.

From the analysis of the iron content of the Cu/Au alloys, and using the activities of Fe derived by Altman and Kellogg[72] (A+K) for their slags, it should be possible to calculate rough values of activities of iron oxides in the slags from the Cu/Au runs, assuming the high silica slags (slag B) correspond in composition to A+K's silica saturated slags. A+K calculated aFe in equilibrium with their copper-containing slags at four temperatures (from 1224-1287°C) and over a range of oxygen partial pressures.

The variation of aFe with pO_2 in silica saturated slags was shown by Michal and Schuhmann[55] to be of the form

$$\log aFe = \frac{A}{T} + B \log pO_2 + C$$

Log pO_2 was plotted against T for a series of values of aFe derived from A+K's work. The result was a series of straight lines which could be extrapolated , with some reservation, up to 1450°C. From these curves, values of pO_2 corresponding to the aFe values were found at 1300, 1350, 1400 and 1450 and converted to values of aFe at regular pO_2 intervals. These are given in Tables 4.1 and 4.2, pages 144 and 145.

The analytical results of wt% Fe in the Cu/Au alloys from this present work (tables pages 66 to 69) were plotted for each run against temperature. The best straight line was drawn through the points for each run, and values of wt% Fe were taken at 1300, 1350, 1400 and 1450°C. The results are given in tables pages 103-105. These wt% Fe values were plotted against their corresponding pO_2 values, also given in the tables, and the points for slags B, C, D and E joined up to give a series of curves at 1300, 1350, 1400 and 1450°C, shown in Figs. 4.6 to 4.9, pages 140 and 141.

The assumption is now made that the curves for slag B represent a silica saturated slag and the wt% Fe vs. pO_2 curve for slag B can be identified with the aFe vs. pO_2 curve derived from A+K's work. Thus a curve of aFe vs. wt% Fe in the Cu/Au alloy can be drawn, Fig. 4.10, page 142.

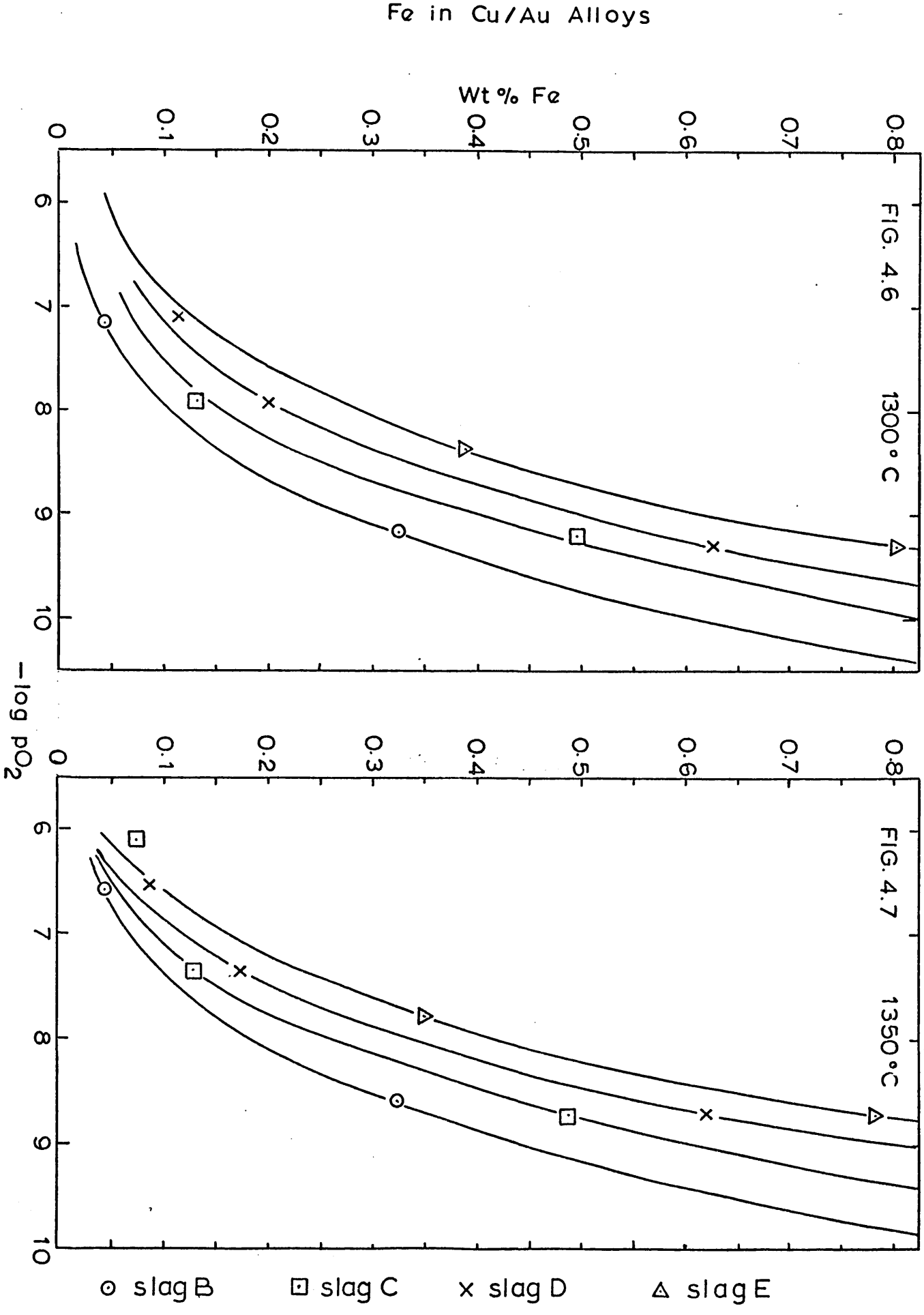
Fe in Cu/Au Alloys
Wt % Fe
0
0.1
0.2
0.3
0.4
0.5
0.6
0.7
0.8
6
7
8
9
10
−log pO2
FIG. 4.6
1300°C
FIG. 4.7
1350°C
⊙ slag B
⊡ slag C
× slag D
△ slag E

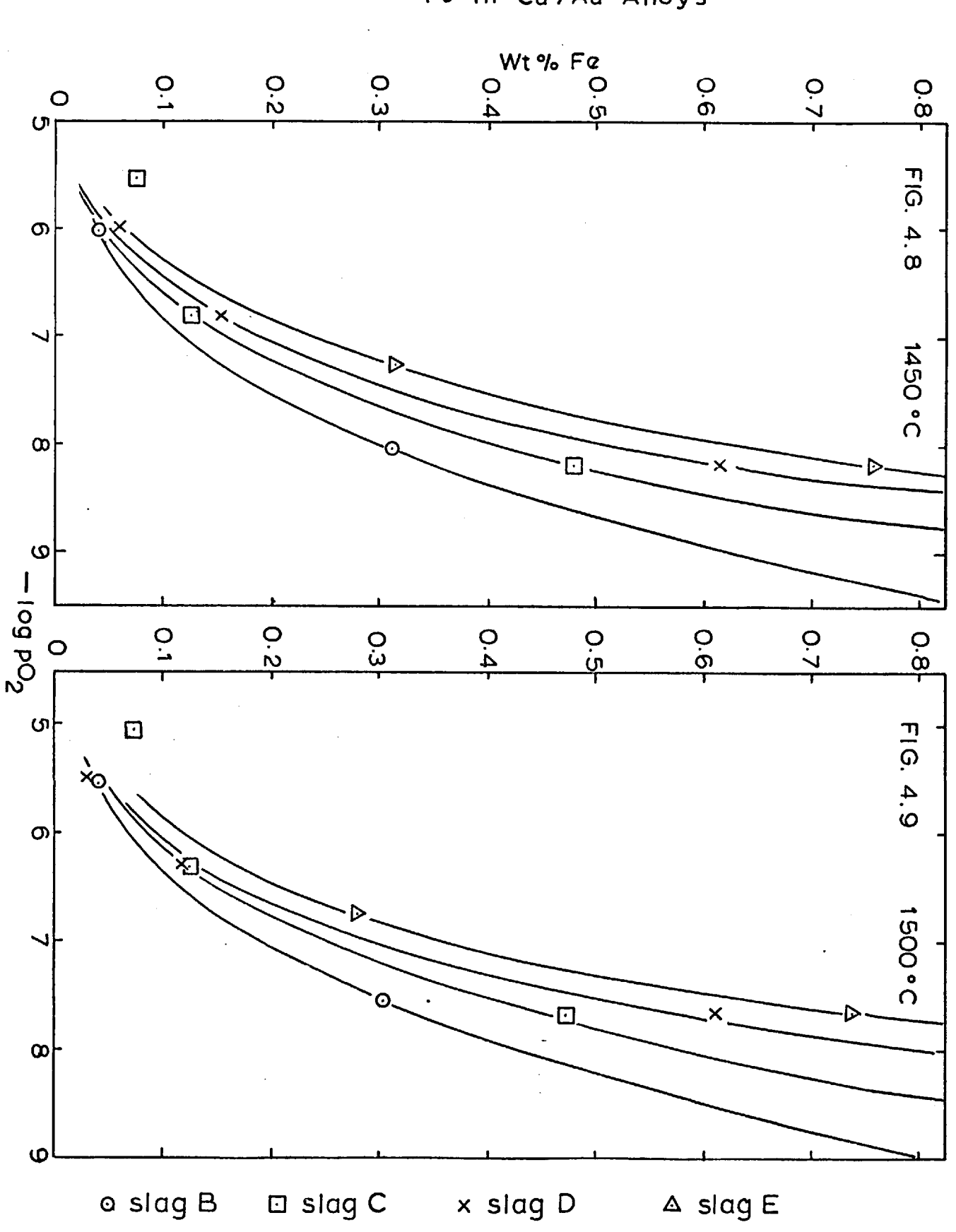
Fe in Cu/Au Alloys
Wt % Fe
0
0.1
0.2
0.3
0.4
0.5
0.6
0.7
0.8
5
6
7
8
9
− log pO_2
FIG. 4.8 1450 °C
FIG. 4.9 1500 °C
o slag B
□ slag C
x slag D
Δ slag E

Fe in Cu/Au alloys FIG. 4.10

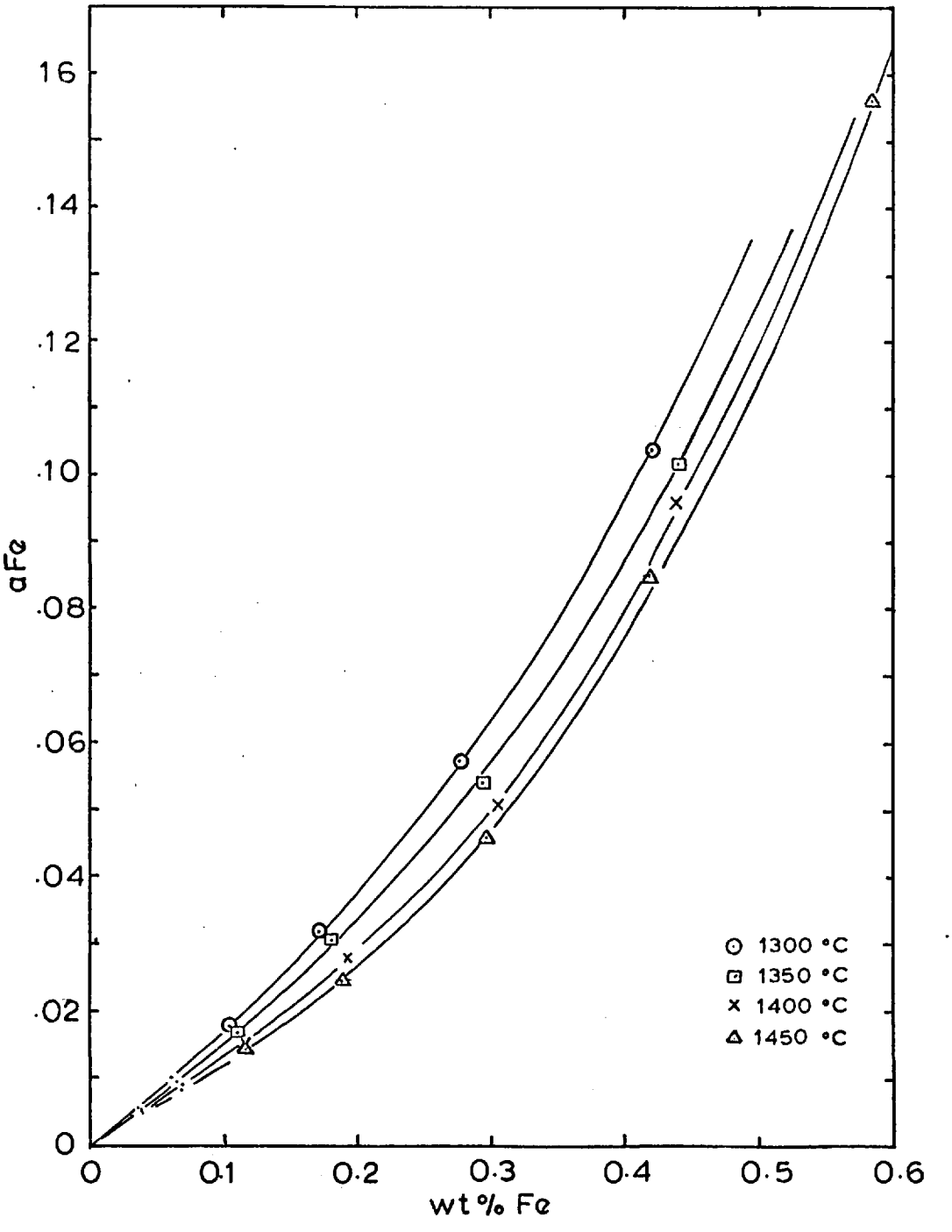

If we assume the oxygen content of the Cu/Au alloys does not affect the activity of iron in the alloy, then it would seem possible to read off aFe for the slags C, D and E directly from the curves in Fig. 4.10, using wt% Fe values from Figs. 4.6-4.9. This procedure does not yield sensible results when aFeO is calculated from the derived aFe values for slags C, D and E.

This procedure assumes that the change in composition of slags B, C, D and E with pO_2 'parallels' the change in composition of a silica saturated slag with pO_2, and this is unlikely to be true. With the few points available for drawing the Figs. 4.6 to 4.9 curves, curve B is drawn as much by reference to the other curves as by the use of the points belonging to it. The effect of oxygen content on the activity coefficient of iron is examined later. Slag B slags do, however, correspond closely in composition to A+K's silica saturated slags. Fig. 4.10 is therefore retained, but an alternative procedure is used for reading aFe values for slags C, D and E.

It is assumed that at constant pO_2, iron obeys Henry's law in the copper/gold alloys. Selecting a certain pO_2, values of wt% Fe for slags B, C, D and E are read from curves Figs. 4.6 to 4.9. The aFe corresponding to the wt% Fe for slag B is read from curve 4.10, and is used as the basis for a straight line Henry's law plot of aFe vs. wt% Fe for this particular pO_2. Activities of Fe for slags C, D and E at this pO_2 can then be read from this line.

Using the free energy equation given in table 3.2, page 61,for the reaction $[Fe]_\gamma + \frac{1}{2} O_2 = (FeO)$, activities of FeO have been calculated from the derived values of aFe. Results of aFe and aFeO are given in Table 4.1 and 4.2, page 144 and 145.

This treatment assumes two major factors; that the slag B slags have a similar composition to A+K's silica saturated slags at the same pO_2 and that the ratio of wt% Fe in the slags B, C, D and E is correct at the same pO_2. It also assumes that Henry's law holds up to about 1 wt% Fe in some cases. The results suggest that this latter is not valid above about 0.5 to 0.6 wt% Fe. This treatment also roughly allows for the effect of oxygen content on the iron activity, assuming to a first approximation a constant oxygen metal content at the same pO_2 for different slags.

Consideration of the wt% Fe vs. pO_2 curves, Figs. 4.6 to 4.9, suggests that the ratio of wt% Fe in slags B, C, D and E will be most reliable at pO_2 values of about 10^{-9}, $10^{-8.5}$, 10^{-8} and $10^{-7.5}$ at 1300, 1350, 1400 and 1450°C respectively. Slag analyses and aFeO values at these oxygen pressures and temperatures are given in Table 4.3, page 146. The aFeO values have

TABLE 4.1 Cu/Au Runs, Wt.% Fe and aFe in Alloys and aFeO in Slags.

		SLAG B			SLAG C			SLAG D			SLAG E		
T^oC	log pO_2	Fe	aFe	aFeO	Fe	aFe	aFeO	Fe	aFe	aFeO	Fe	aFe	aFeO
1300	-7.0	0.035	0.0045	0.297	0.064	0.0081	0.538	0.098	0.012	0.826	0.121	0.015	1.000
1300	-7.5	0.062	0.0087	0.324	0.100	0.014	0.520	0.148	0.021	0.773	0.186	0.026	0.971
1300	-8.0	0.103	0.016	0.340	0.154	0.024	0.503	0.226	0.035	0.739	0.283	0.044	0.928
1300	-8.5	0.170	0.030	0.349	0.250	0.043	0.511	0.352	0.061	0.721	0.426	0.074	0.874
1300	-9.0	0.276	0.054	0.356	0.402	0.078	0.516	0.504	0.092	0.647	0.632	0.122	0.810
1300	-9.5	0.418	0.095	0.356	0.592	0.135	0.503	0.710	0.161	0.602	0.975	0.222	0.827
1350	-6.5	0.037	0.0043	0.293	0.050	0.0057	0.395	0.062	0.0071	0.490	0.089	0.010	0.704
1350	-7.0	0.065	0.0083	0.321	0.091	0.012	0.450	0.118	0.015	0.587	0.159	0.020	0.784
1350	-7.5	0.110	0.015	0.327	0.151	0.021	0.448	0.203	0.028	0.604	0.256	0.035	0.761
1350	-8.0	0.179	0.028	0.339	0.262	0.042	0.509	0.335	0.053	0.650	0.416	0.066	0.806
1350	-8.5	0.294	0.052	0.354	0.405	0.070	0.484	0.510	0.089	0.610	0.635	0.110	0.758
1350	-9.0	0.440	0.092	0.356	0.595	0.125	0.483	0.810	0.170	0.658	0.970	0.204	0.788

TABLE 4.2 Cu/Au Runs, Wt.% Fe and aFe in Alloys and aFeO in Slags.

		SLAG B			SLAG C			SLAG D			SLAG E		
T^oC	log pO_2	Fe	aFe	aFeO	Fe	aFe	aFeO	Fe	aFe	aFeO	Fe	aFe	aFeO
1400	-6.5	0.068	0.0076	0.313	0.091	0.010	0.418	0.108	0.012	0.496	0.117	0.013	0.529
1400	-7.0	0.117	0.014	0.325	0.156	0.018	0.425	0.186	0.022	0.511	0.240	0.028	0.658
1400	-7.5	0.192	0.026	0.337	0.260	0.035	0.455	0.310	0.041	0.538	0.390	0.052	0.678
1400	-8.0	0.305	0.048	0.352	0.400	0.062	0.459	0.505	0.078	0.576	0.620	0.097	0.711
1400	-8.5	0.437	0.086	0.356	0.620	0.122	0.503	0.775	0.152	0.629	1.000	0.196	0.812
1450	-6.0	0.068	0.0066	0.301	0.085	0.0082	0.375	0.095	0.0092	0.420	0.115	0.011	0.510
1450	-6.5	0.116	0.013	0.322	0.148	0.016	0.407	0.152	0.016	0.415	0.209	0.022	0.571
1450	-7.0	0.187	0.023	0.332	0.250	0.030	0.436	0.297	0.036	0.520	0.358	0.044	0.629
1450	-7.5	0.295	0.043	0.345	0.392	0.056	0.456	0.457	0.066	0.533	0.610	0.088	0.709
1450	-8.0	0.417	0.077	0.352	0.575	0.106	0.485	0.820	0.152	0.691	1.150	0.214	0.974

TABLE 4.3 Cu/Au Runs, FeO Activities and Slag Compositions.

			SLAG B			SLAG C			SLAG D			SLAG E		
$T^{\circ}C$	log pO_2	Cu_2O	aFeO	SiO_2	FeO	aFeO	SiO_2	FeO	aFeO	SiO_2	FeO	aFeO	SiO_2	FeO
1300	-9.00	1.50	0.35	37.0	61.5	0.51	32.5	66.0	0.60	27.0	71.5	0.80	14.0	84.5
1350	-8.50	1.75	0.35	37.0	61.0	0.48	32.5	65.5	0.60	27.5	71.0	0.75	14.0	84.0
1400	-8.00	2.00	0.35	37.5	60.0	0.45	32.5	65.5	0.56	27.5	70.5	0.70	14.5	83.5
1450	-7.50	2.40	0.34	38.5	59.0	0.44	32.5	65.0	0.53	27.5	70.0	0.69	14.5	83.0

been plotted against wt% FeO in the slag in Fig. 4.11, page 148, on the basis that wt% FeO = 100 - (wt% species other than iron oxides). Included on the same basis are the results of Schuhmann's ternary integration of the $FeO-Fe_2O_3-SiO_2$ system at 1350°C,[57] taken at pO_2 equals $10^{-8.5}$, and the results for the $FeO-SiO_2$ system at iron saturation at 1300°C and about 1850°C.[59] The results are in reasonable agreement with Schuhmann's results for the copper free system, although the points from this work represent slags with only about 2% copper content.

The activity coefficient of Fe in the Cu/Au alloy in the presence of oxygen, γ_{Fe}, is given approximately by:

$$\ln \gamma_{Fe} = \ln \gamma^{o} + N_{Fe} \epsilon^{Fe}_{Fe} + N_{O} \epsilon^{O}_{Fe}$$

where γ^{o} is the activity coefficient of Fe in the Cu/Au alloy in the absence of oxygen, and ϵ^{Fe}_{Fe} and ϵ^{O}_{Fe} are interaction coefficients. Estimates of ϵ^{O}_{Fe} are given below: (reference 137)

T°C	ϵ^{O}_{Fe}
1200	- 565
1300	- 413
1400	- 279
1500	- 160

Tankins [138] estimates ϵ^{Fe}_{Fe} to be zero. Estimates of the effect of oxygen on γ_{Fe} in the present work now depends on knowing the oxygen content of the metal. Oxygen contents were not measured in this work, but were measured by Ruddle et al.[68] Calculations using Ruddle's oxygen contents at known pO_2 and temperature suggest that in this present work the effect of oxygen on γ_{Fe} will be small enough to ignore at iron contents above 0.1 wt% Fe. The effect of oxygen will be greater at the lower temperatures. At 1300°C, for 0.1 wt% Fe in the metal, $N_O = 0.00015$, so:

$$\ln \gamma_{Fe} = \ln \gamma^{o} - 0.00015.565$$

$$\gamma_{Fe} = 0.94.\gamma^{o}$$

Activity coefficients of iron were taken from Fig. 4.10, page 142, at 0.125 wt% Fe. The results are given below, together with the extrapolated value at the melting point of iron.

T°C	γ_{Fe} (N Fe → zero)
1300	14.6
1350	13.2
1400	11.3
1450	10.3

FIG. 4.11

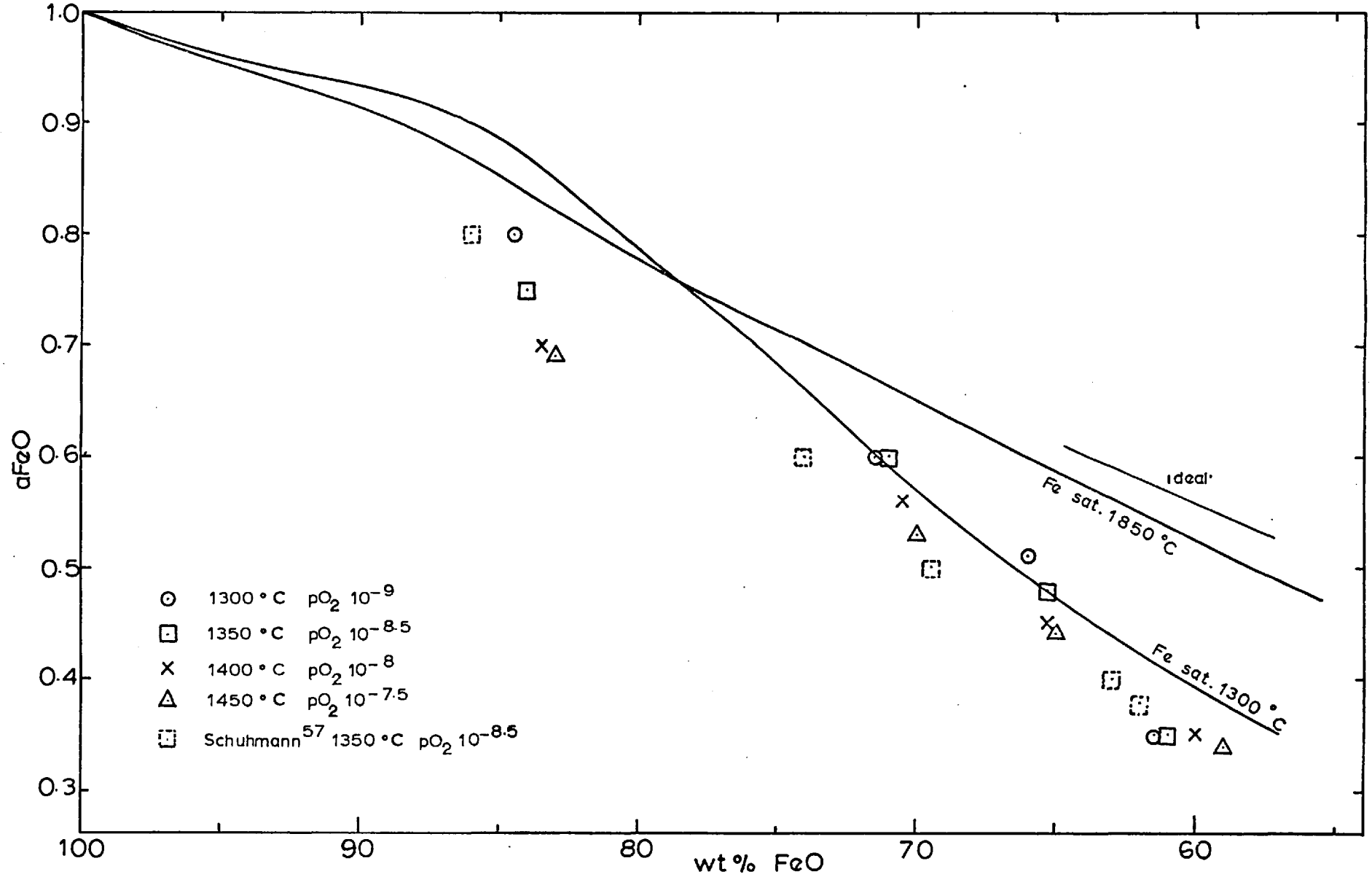
aFeO in slags
aFeO
1.0
0.9
0.8
0.7
0.6
0.5
0.4
0.3
100
90
80
70
60
wt % FeO
ideal
Fe sat. 1850 °C
Fe sat. 1300 °C
1300 °C pO2 10-9
1350 °C pO2 10-8.5
1400 °C pO2 10-8
1450 °C pO2 10-7.5
Schuhmann57 1350 °C pO2 10-8.5

From a plot of ln γ_{Fe} against $\frac{1}{T}$, Fig. 4.12, page 150, the partial molar heat of solution of Fe in the 10% Au/Cu alloy at infinite dilution relative to solid iron, was calculated to be + 12,996 cal. Assuming a heat of fusion of 3,300 cal, $\Delta\bar{H}_{Fe}$ relative to liquid is about + 9,700 cal.

For pure copper, Hultgren et al[125] recommend $\Delta\bar{H}_{Fe}$ as + 9,300 cal at 1550°C, and γ_{Fe}, extrapolated to 1536°C, as 10.9 (relative to solid or liquid).

Altman and Kellogg[72] found no significant variation of γ_{Fe} with temperature over the range 1224-1286°C and give γ_{Fe} as 14.1 in their 55 wt% Au/Cu alloy and 22.6 for their 71 wt% Au/Cu alloy. (relative to solid Fe).

In view of the derivation of the activity coefficients, the agreement with other work is better than expected.

If it is assumed that FeO activities in the slags from the Cu/Ni runs follow the relationship between aFeO and wt% FeO shown in Fig. 4.11, page 148, then it is possible to estimate iron activities in the Cu/Ni alloys.

The iron contents of the Cu/Ni alloys equilibrated with slags B and C, given in tables pages 80 to 82, were plotted against temperature, and the best straight line drawn through the points for each run. Values of wt% Fe were taken at 1350, 1400, 1450 and 1500°C for each run and plotted against log pO_2 to produce a series of curves similar to those for the Cu/Au runs, Figs. 4.6 to 4.9, pages 140 and 141. Values of wt% Fe were taken from these curves at a series of pO_2 values. Values of wt% FeO in the slag at these pO_2 values were derived from the tables, pages 106 to 110, and values of aFeO estimated from the results of Schuhmann[57] for these slags. Iron activities were then calculated , knowing aFeO and pO_2. The calculated values of aFe are plotted against wt% Fe in alloy for the 10% Ni, 20% Ni, 35% Ni and 50% Ni alloys at 1350, 1400, 1450 and 1500°C in Figs. 4.13 to 4.16, pages 151 and 152. Activity coefficients for Fe in the alloys, relative to solid Fe, have been calculated and are given in Table 4.4, page 153. Values for γ_{Fe} in pure copper[125] and pure nickel[124] have been included for comparison.

γ_{Fe} in Cu/Au alloys FIG. 4.12

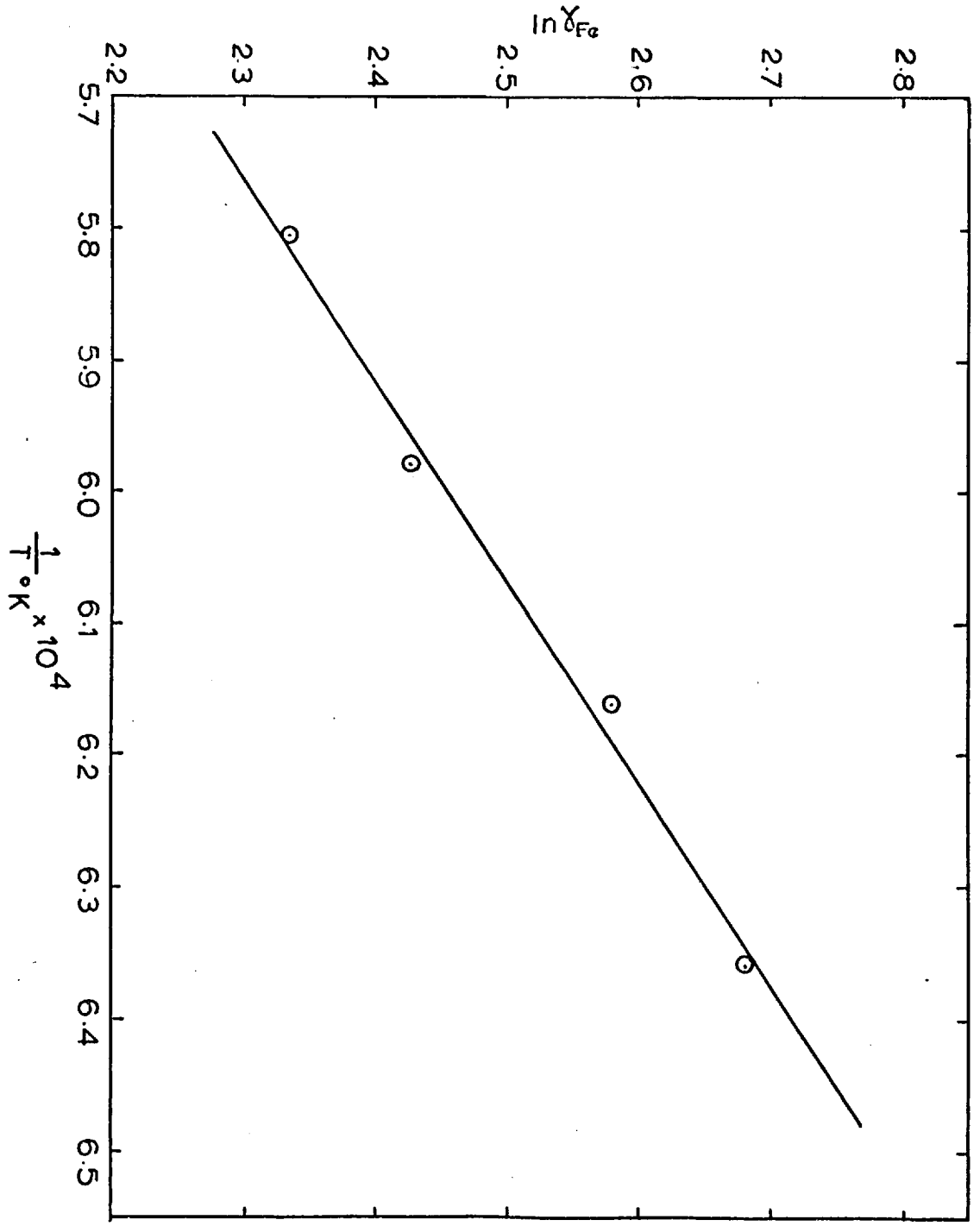

Fe in Cu/Ni alloys

FIGS. 4.13
4.14

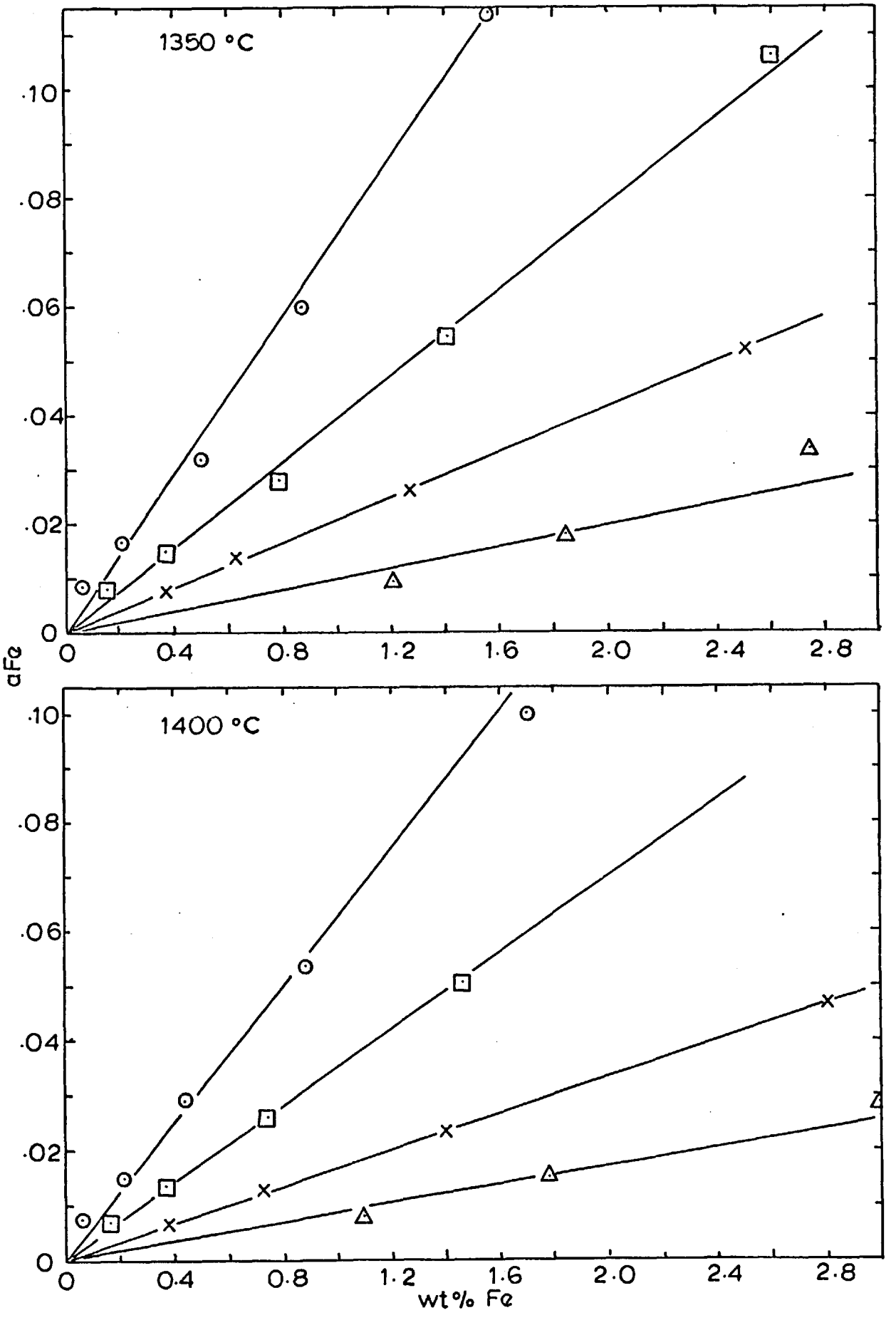

Fe in Cu/Ni alloys

FIGS. 4.15
4.16

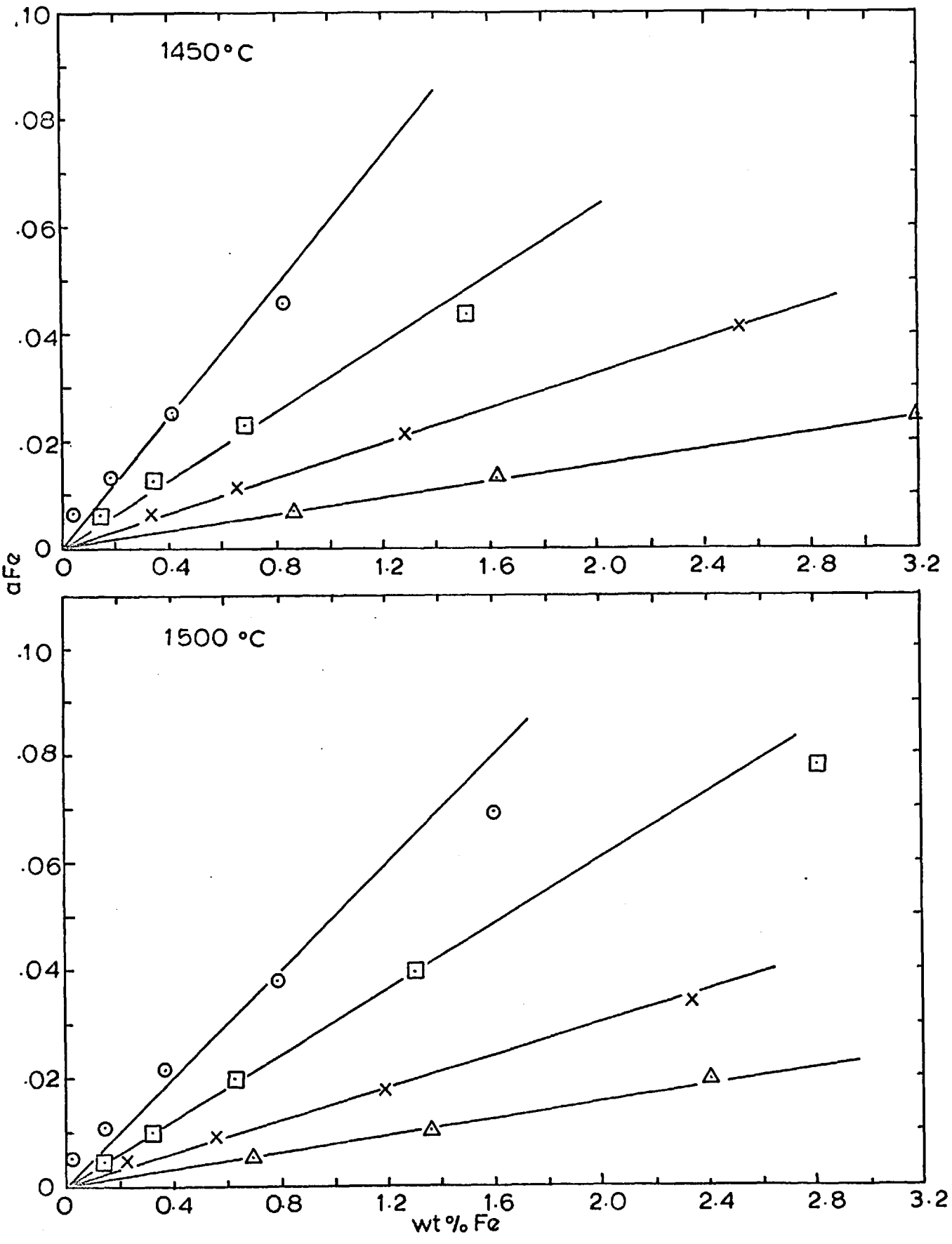

γ_{Fe} (relative to solid Fe) in Cu/Ni Alloys TABLE 4.4

Wt.% Ni	1350°C	1400°C	1450°C	1500°C	1600°C
0	16.0	14.2	12.8	11.5	-
10	6.54	5.73	5.54	4.54	-
20	3.54	3.20	2.88	2.75	-
35	1.91	1.52	1.47	1.36	-
50	0.91	0.82	0.73	0.73	-
100	-	-	-	-	0.39

Comparision With Other Work

The results for high silica slags from this work can be compared with those of Altman and Kellogg [72] and Ruddle et al.[68] The three sets of results are shown in Fig 4.17, page 155. The agreement is good, and the results show remarkable consistency over a temperature range of 1226°C (Altman and Kellogg) to 1500°C (this work). Ruddle's results show slightly higher copper slag contents at low $aCuO._5$, and lower copper contents at high $aCuO._5$ levels. However, Ruddle's results are not at all well defined at high $aCuO._5$ levels, and the slags were equilibrated with pure copper, so the higher copper slag contents at low $aCuO._5$ could possibly be explained by local precipitation of copper as described by Richardson and Billington.[67]

Altman and Kellogg equilibrated their slags with Cu at an activity of 0.73. The results fall slightly to the right of the results from this work intermediate $aCuO._5$ levels. Their curve above 4.5 wt% Cu is based on four points only.

Toguri and Santander[70] used slags containing about 6% Al_2O_3 and 34% SiO_2. The presence of Al_2O_3 may possibly explain the lower solubility of copper in their slags. The slags were equilibrated with Cu/Au alloys of activities ranging from 0.25 to 1.0. The results for $aCu \geqslant 0.88$ are consistently to the right of the line drawn, again suggesting possible local precipitation of copper in the slags. In the present work, results for high copper activities tend to fall to the left of lower copper activity results. It is possible that the levitation forces inhibit the formation or presence of metal droplets in the slag. Toguri and Santander propose the relationship

$$\text{wt\% Cu in slag} = 29.73\ (aCu_2O)^{\frac{1}{2}}.$$

Since $aCu_2O^{\frac{1}{2}} = aCuO._5$, this can be compared with wt% Cu = 32.0 $aCuO._5$ in the present work.

Also shown in Figure 4.17 are the results reported by Bailey[49] for an industrial slag of composition 38% SiO_2, 16% Fe, 19% CaO, 17% Al_2O_3, 4% K_2O. The addition of CaO and Al_2O_3 have shown a remarkable lowering of the slag copper content.

It is of some importance to see whether the copper solubility results obtained for sulphur-free systems can be applied to matte/slag systems. Unfortunately there are few reliable matte/slag equilibrium measurements which can be used for comparison.

Comparison with other work FIG. 4.17

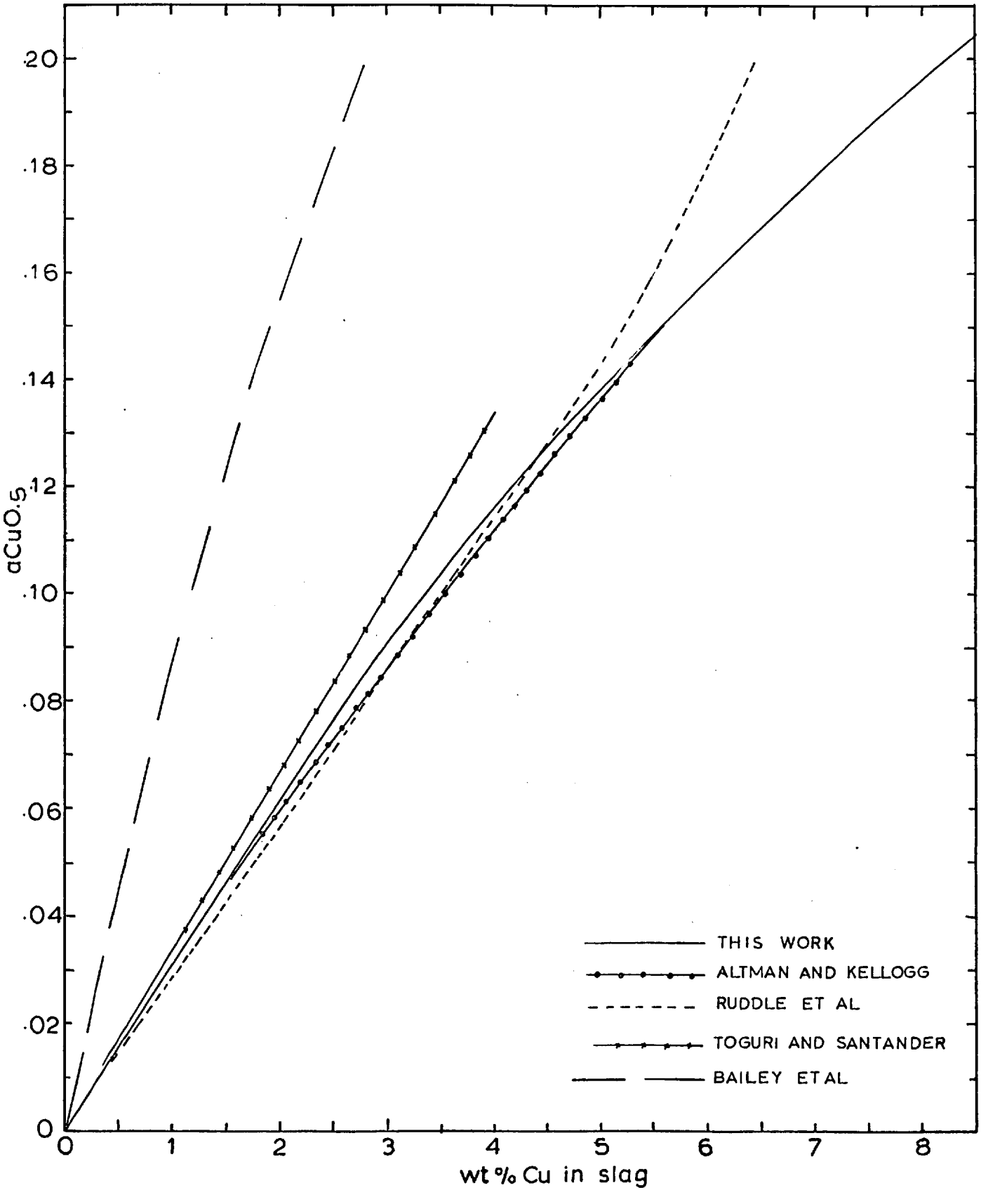

Yazawa and Kameda[41] equilibrated various FeS/Cu_2S mattes with slags of composition 43% SiO_2, 45.5% FeO and 11.5% CaO in iron crucibles, and measured the equilibrium copper level in the slag. If the equilibrium is expressed

$$(Cu_2O) + [FeS] = (FeO) + [Cu_2S]$$

then assuming to a first approximation that $aCu_2S = N\ Cu_2S$, $aFeS = N\ FeS$ and aFeO is about 0.40, aCu_2O can be calculated. This has been done by Toguri and Santander,[70] and using their relationship

$$\text{wt\% Cu in slag} = 29.73.aCu_2O^{\frac{1}{2}}.$$

Copper contents of the slag were predicted. The predicted copper contents are in excellent agreement with experimental results. Figure 4.18, page 158.

Sehnalek and Imris[51] equilibrated Cu/Fe/S mattes with silica saturated iron slags at 1200°C under three sets of conditions; under an N_2-S_2-SO_2 atmosphere arranged to give a constant pO_2 of 5.10^{-10} atm. and a pS_2 ranging from about 6.10^{-5} atm. to 5.10^{-1} atm.; under an N_2-S_2-SO_2 atmosphere arranged to give a constant pS_2 of 9.10^{-4}atm. and a pO_2 ranging from 9.10^{-10} to $1.3 . 10^{-8}$ atm., and finally under conditions of co-saturation with both silica and magnetite under an N_2-SO_2 atmosphere with pSO_2 varying from 1 atm. to 0.01 atm.

In the first and second set of experiments, the slags were analysed for copper, iron, silica and sulphur, and the mattes for copper only.The slags contained up to 5% sulphur.

From the equations:

$$4Cu + S_2 = 2Cu_2S \quad \Delta G_T^o = -50,920 + 6.00T$$

$$4Cu + O_2 = 2Cu_2O \quad \Delta G_T^o = -58,520 + 20.976T$$

then for $2Cu_2O + S_2 = 2Cu_2S + O_2$, $\Delta G_T^o = + 7,600 - 14.976T$ at 1200°C, $\Delta G = -14,460$ cal.

pS_2 and pO_2 are known from the experiment. If the matte is considered to be a Cu_2S/FeS mixture, then the mol fraction of Cu_2S can be calculated. Assuming that the activity of Cu_2S is equal to its mol fraction, then aCu_2O can be calculated, hence $aCuO_{.5}$.

In the third set of experiments, the matte is almost pure Cu_2S, with about 0.25 wt% Fe and 0.5% oxygen. In principle, activities of Cu_2O can be calculated from the relationship

$$6Cu + SO_2 = Cu_2S + 2Cu_2O \quad \Delta G_T^o = 2,200 + 6.716T$$

$$\Delta G = 12,113 \text{ cal at } 1200^oC.$$

aCu_2S can be taken as unity, but the calculation of aCu_2O is very sensitive to the value taken for aCu. The results of Schuhmann and Moles[53] show that aCu varies rapidly around the Cu_2S composition with small changes in the Cu/S ratio. The activity of copper has been taken as constant at 0.7, but great accuracy cannot be expected from the calculations.

Activities of $CuO._5$ have been calculated for the three sets of experiments, and using the relationship between $aCuO._5$ and wt% Cu in slag found in this work, values of wt% Cu in slag have been predicted. These are compared with the experimentally determined values of wt% Cu in Figures 4.19, 4.20 and 4.21, pages 158 and 159. The agreement is excellent over a wide range of conditions, and copper contents from about 0.1 wt% to 9 wt%. Even allowing for the possibly inaccurate assumptions, it seems from these calculations and those of Toguri and Santander, that copper solubility in slags can be described in terms of cuprous oxide formation for both metal/slag systems and industrial matte/slag systems, and that $\gamma CuO._5$ is not affected significantly by the presence of sulphur in the slag.

The only data that has been found for NiO in slags which can be compared with the results from the present work, are those of Bardenheuer and Brauns.[75] They measured the partition of nickel between a Ni/Fe alloy bath, varying from 70-20 wt% Ni in composition, and a silica saturated slag at 1620°C. The maximum nickel slag content was 1% Ni. From the relationship

$$\frac{aFeO \,.\, aNi}{aNiO \,.\, aFe} = K$$

and assuming aFeO = 0.3, and calculating aNi and aFe from the data recommended by Hultgren et al,[124] activities of NiO can be calculated. Defining the activity coefficient as aNiO/wt% Ni in slag, activity coefficients of about 0.4 for 70 to 40 wt% Ni in the alloy, 0.6 at 30% Ni and 1.3 at 20% Ni were calculated. These can be compared with a constant value of 1.53, defined on the same basis, from this work. The agreement is poor, but not enough is known about the German work to offer any explanation.

Comparison with matte/slag systems

FIG. 4.18

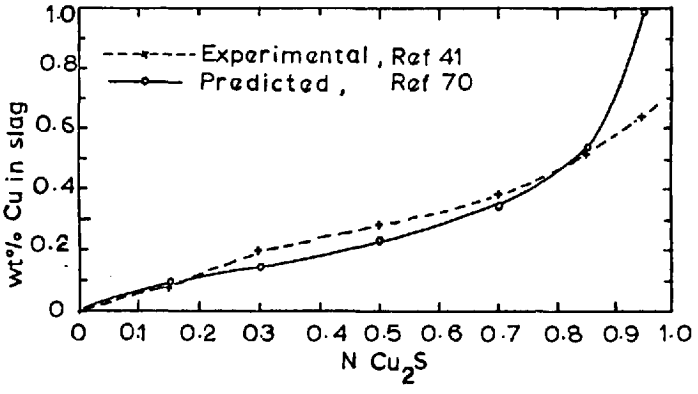

FIG. 4.19

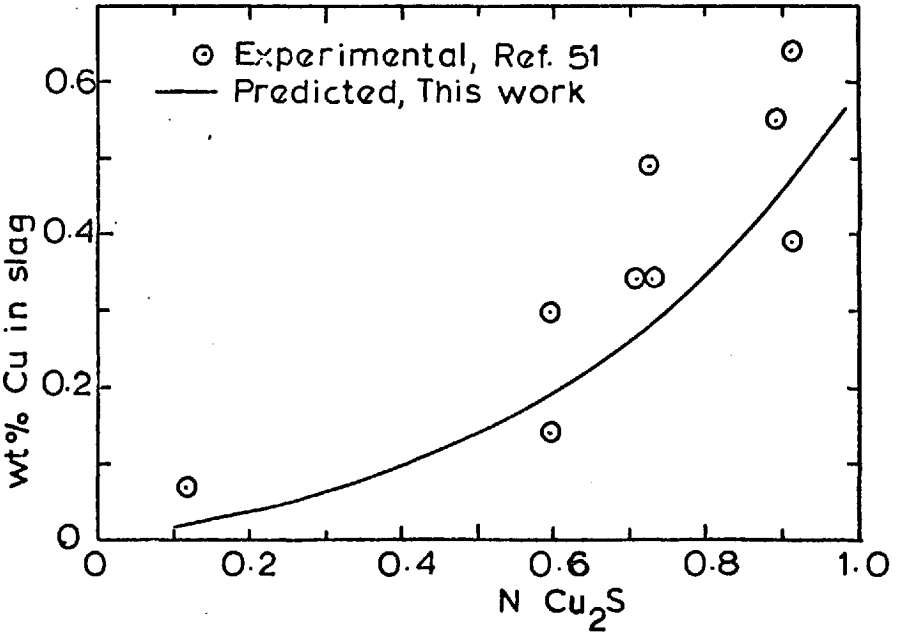

FIG.4.20

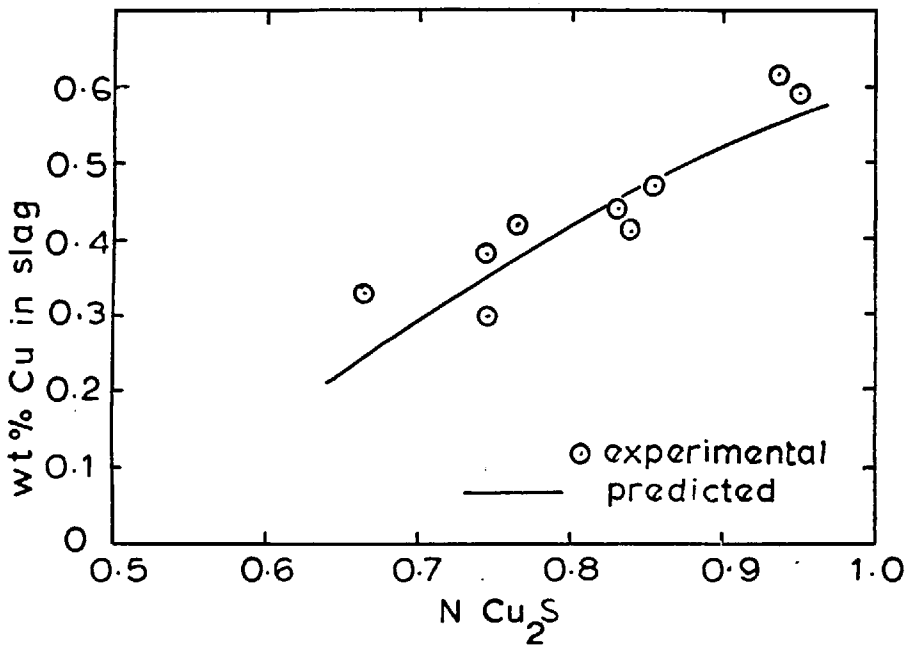

FIG 4.21

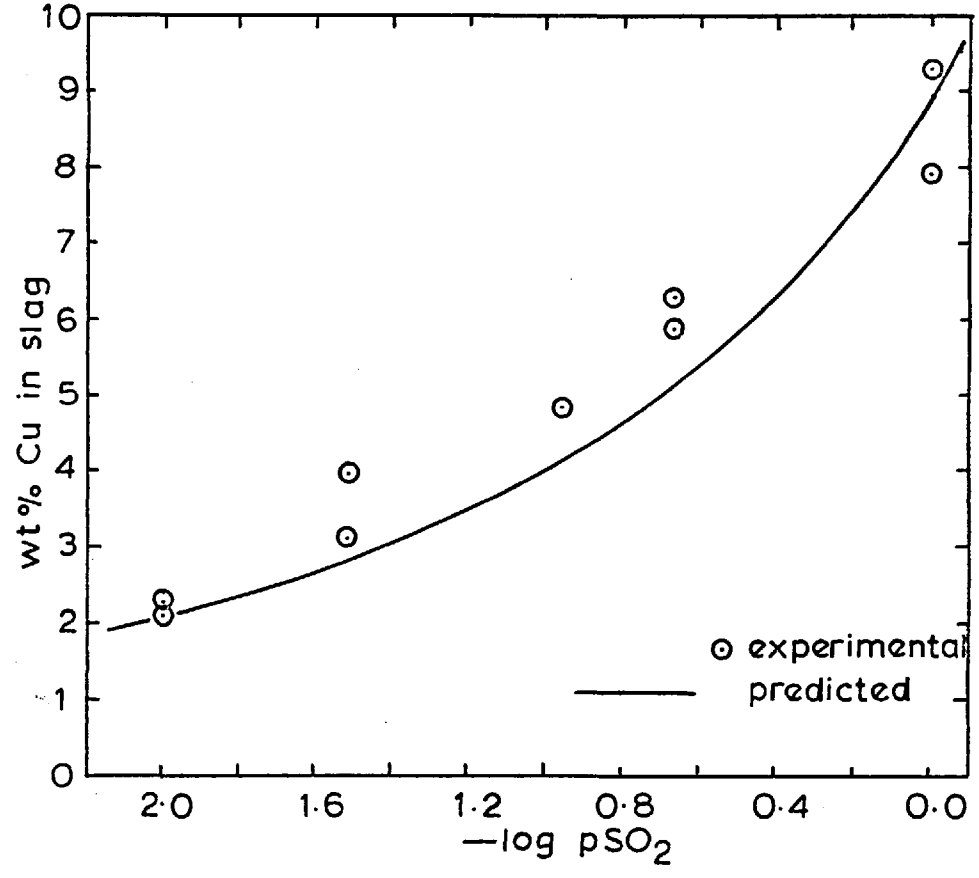

Suggestions for Further Work

Industrial slags commonly contain metal oxides which were not present in the slags used in this work, particularly CaO and Al_2O_3. An investigation into the effect of these oxides on the activity coefficients of $CuO._5$ and NiO would be a logical extension of this work. The levitation technique developed here would seem admirably suited to such an investigation, and careful metal sampling would possibly allow reasonably accurate measurements of iron oxide activities in the slags.

Although the industrial need for measurements of activities of CoO in iron silicate slags is not great, it would be of interest to compare the CoO activities with the NiO activities measured here.

For industrial application of this work, the outstanding need is to show conclusively whether or not soluble copper in the slag can be described in terms of cuprous oxide formation, and to determine the effect of sulphur on the activity coefficient of $CuO._5$.

CHAPTER 5.

CONCLUSIONS.

CONCLUSIONS

Relationships between $aCuO_{.5}$ and copper contents of iron silicate slags and between aNiO and nickel contents of iron silicate slags have been derived. Changing the iron/silica ratio in the slags has only a small effect on $\gamma_{CuO_{.5}}$ and γ_{NiO}. The changes which do occur can be explained in terms of a tendency for $CuO_{.5}$ and NiO to associate with Fe_2O_3 in the melt to form ferrites. Consideration of properties of other metals from the first transition series, in relation to those of Ni and Cu, suggest that the values obtained for $\gamma_{CuO_{.5}}$ and γ_{NiO} are reasonable ones. Although not investigated in this work, it is supposed that the values of $\gamma_{CuO_{.5}}$ and γ_{NiO} would be higher in industrial slag containing significant quantities of CaO and Al_2O_3.

Predictions of copper contents in slags in matte/slag systems using the relationships between $aCuO_{.5}$ and wt% Cu in slag for metal/slag systems derived here, suggests that soluble copper slag contents in matte/slag systems can be described in terms of cuprous oxide formation, and that sulphur in the slag has only a small effect on $\gamma_{CuO_{.5}}$.

Agreement between this work and the results of other work obtained using more conventional equilibration techniques is good. In some systems at least, therefore, levitation techniques can be used in thermodynamic studies of gas/metal/slag equilibria. Sensible values of aFeO in slags equilibrated with Cu/Au alloys were derived and activity coefficients of Fe in Cu/Au and Cu/Ni also obtained. These values are not thought to be of a high degree of accuracy, but better metal sampling techniques might allow more accurate values to be obtained.

The advantages of using levitation techniques for these studies are that only short equilibration times are needed; a few minutes compared with many hours by conventional equilibration techniques, and the problem of finding suitable container material for the melts is eliminated. Furthermore, excluding the H.F. generator, the apparatus is relatively inexpensive and operates at room temperature. The disadvantages are that only small samples are obtainable, temperature control and measurement is difficult and many systems are not amenable to a levitation technique.

ACKNOWLEDGEMENTS

I would mainly like to thank Dr. Jeffes for his helpful supervision and guidance throughout the past three years.

Also, I would like to thank Dr. R. Thompson and the Borax Research Centre for the understanding attitude they have shown.

Thanks are due to Miss. J. White and Mrs. J. Baker for their contributions to the typing.

Thanks are especially due to my wife June for the major part of the typing and her unfailing help and encouragement throughout this work.

I am indebted to the Science Research Council for their financial support.

REFERENCES.

1. Jeffes J.H.E. and Diaz C. Trans. Inst. Min. Metall., 80, 1969, C1-6.

2. Themelis N.J. and Spira P. Canadian Patent 758 020, 1969.

3. Worner H.K. In "Advances in Extractive Metallurgy" (London: Institution of Mining and Metallurgy , 1968), 245-63.

4. Sproule K., Harcourt G.A.., Renzoni L.S. In "Extractive Metallurgy of Copper, Nickel and Cobalt". Interscience, New York, 1960, p.33.

5. Queneau P., O'Neill C.E., Illis A., Warner J.S., J. Metals, July 1969, p.35.

6. Op. cit., ref. 4, (a) pp 263-286, (b) pp 287-300, (c) pp 301-313.

7. Op. cit., ref. 3, Moussoulos J., p.264.

8. Schenck H. The Physical Chemistry of Steelmaking, English translation by B.I.S.R.A., London, 1945.

9. The Physical Chemistry of Melts, London: Institution of Mining and Metallurgy, 1953.

10. Bodsworth C. Physical Chemistry of Iron and Steel Manufacture, London: Longmans, 1963.

11. Richardson F.D. In "The Physical Chemistry of Steelmaking." Wiley and Sons, New York, 1958, pp 55-62.

12. Richardson F.D. In "The Physical Chemistry of Melts", London: Inst. Min. Metall., 1953, pp 87-88.

13. Richardson F.D. In "The Vitreous State". Glass Delegacy of the University of Sheffield, Sheffield, England, 1955, pp 63-84.

14. Fincham C.J.B. and Richardson F.D. Proc. Roy. Soc., A223, 1954, p 40.

15. Toop G.W. and Samis C.S. Trans. Met. Soc. A.I.M.E., 224, 1962, pp 878-87.

16. Toop G.W. and Samis C.S. Can. Met. Quart., 1, (2), 1962, pp 129-52.

17. Temkin M. Acta Physiochim., 20. 1945, p 411.

18. Elliott J.F. Trans. A.I.M.E., 203, 1955, p 485.

19. Masson C.R. Proc. Roy. Soc., A287, 1965, p 201.

20. Meadowcroft T.R. and Richardson F.D. Trans. Faraday Soc., Vol. 61., Part 1., 1965, pp 54-70.

21. Cripps-Clark C.J. Sridhar R. Jeffes J.H.E. and Richardson F.D. The Richardson Conference, London, 1973.

22. Masson C.R., Smith I.B. and Whiteway S.G. Can. J. Chem., 48, (9), 1970, pp 1456-1464.

23. Gaskell D.R. Metallurgical Transactions, Vol. 4, Jan. 1973, P 185.

24. Lentz C.W. Inorg. Chem., 3, 1964, pp 574-579.

25. Götz J. and Masson C.R. J. Chem. Soc., A 1971, 686-688.

26. Gaskell D.R., McLean A. and Ward R.G. Trans. Faraday Soc., Vol. 65, Part 6, 1969, pp 1498-1508.

27. Temkin M. Zh. Fiz. Khim. (USSR), 20, (1), 1946, pp 105-10.

28. Herasymenko P. Trans. Faraday Soc., 34, 1938, p 124.

29. Flood H., Førland T., Grjotheim K. "The Physical Chemistry of Melts", London: Inst. Min. Metall., 1953, pp 46-59.

30. Bodsworth C., J.I.S.I., 193, 1959, p 13.

31. Davidson I.M. and Bodsworth C., J.I.S.I., 195, 1960, P 163.

32. Lumsden J. In "The Physical Chemistry of Process Metallurgy", Interscience, 1961, p 263.

33. Richards A.W. and Thorne D.F.J. ibid, p 277.

34. Richardson F.D. Trans. Faraday Soc., 52, 1956, p 1312.

35. Abraham K.P. and Richardson F.D. In "The Physical Chemistry of Process Metallurgy", Interscience, 1961, p 263.

36. Abraham K.P., Davies M.W. and Richardson F.D., J.I.S.I. Sept. 1960. p 82.

37. Ruddle R.W. "The Physical Chemistry of Copper Smelting", London: Inst. Min. Metall., 1953.

38. Evans G.L. Mining Mag., 88, pp 9-16, 85-93, 145-51, 206-18, 1953.

39 Yannopoulos J.C. Can Met. Q., Vol. 10, No. 4, 1971.

40. Spira P. and Themelis N.J., J. Metals, April 1969, p 35.

41. Yazawa A. and Kameda M., Tech. Repts., Tokohu Univ., 19, (1), 1954, pp 1-22.

42. Korakas N. Doctorial Thesis, Liege Univ., 1964.

43. Bor F.Y. and Tarassoff P. Can. Met. Q., Vol. 10, No. 4, 1971.

44. Wiese W. Erzmetall. 16, 1963, 452.

45. Montil'O I.A. et al. Tr., Ural. Nauch. - Issled. Proekt. Inst. Mednoi Prom. 10, 1967, p 228.

46. Tseidler A.A. "Metallurgy of Copper and Nickel", Moscow, 1958. Israel Programme for Scient. Translations, Jerusalem 1964, pp 47-48, 43-44, 51-52.

47. Wanjukoff, W.A. Metallurgia, 9, 1912, p 1.

48. Scobie A.G., C.I.M. Trans. 49, 1946, 557.

49. Bailey J.B.W., Brown N.E., Garner F.A. and Ward S.G. In "Advances in Extractive Metallurgy and Refining", I.M.M., London, Oct. 1971, paper 25.

50. Johansen E.B., Rosenqvist T. and Torgersen P.T., J. Metals, Sept. 1970, p 39.

51. Sehnalek F. and Imris I. op. cit., ref. 49, paper 2.

52. Maurer E., Hammer G. and Mobius H. Arch Eisenhuttenw. 16, 1942, pp 159-65.

53. Schuhmann R. Jr. and Moles O.W. Trans. A.I.M.E., 191, 1951, 401-11.

54. Krivsky W.A. and Schuhmann R. Jr. Trans. A.I.M.E., 209, 1957, p 981.

55. Michal E.J. and Schuhmann R. Jr. Trans. A.I.M.E., 194, 1952, pp 723-8.

56. Schuhmann R. Jr. and Ensio P.J. Trans. A.I.M.E., 191, 1951, pp 401-11.

57. Schuhmann R. Jr. Acta Metallurgica, Vol. 3, 1955, p 219.

58. Bodsworth C., J.I.S.I., 193, 1959, pp 13-24.

59. Distin P.A., Whiteway S.G. and Masson C.R. Can. Met. Quart., 10, 1971, p 73.

60. Taylor C.R. and Chipman J.,Trans. A.I.M.E., 154, 1943, p 228.

61. Winkler T.B. and Chipman J. ibid, 167, 1946, p 111.

62. Fetters K.L. and Chipman J. ibid, 145, 1941, p 95.

63. Richardson F.D. and Fincham C.J.B., J.I.S.I. 178, 1954, p 4.

64. Levin E.M., Robbins C.R., McMurdie H.F. Phase Diagrams for Ceramists, Amer. Ceram. Soc., Ohio, 1964.

65. Schmalzried H., Z. Physik. Chem., (NF), 25, 1960, p 178

66. Zalazinski A.G. et al, Zh. Neorg. Khim., 14, 1969, p 624.

67. Richardson F.D. and Billington. Bull. Inst. Min. Metall., 593, 1956, p 273.

68. Ruddle R.W., Taylor B and Bates A.P. Trans. I.M.M., Sect C, 75, 1966, C1-12.

69. Mihalop P.B. Ph.D. Thesis, University of Birmingham,1969.

70. Toguri J.M. and Santander N.H. Can. Met. Quart., Vol. 8, 1969, pp 167-71.

71. Toguri J.M. and Santander N.H. Met. Trans., Vol. 3, 1972, P 586.

72. Altman R. and Kellogg H.H. Trans. I.M.M., Sect C, Sept. 1972, C163-175.

73. Meyer G.A. Columbia University Thesis 1972.

74. Meyer G.A., Kellogg H.H. and Warner J.S., "Thermodynamics of NiS System", presented at 100th Annual A.I.M.E. Meeting, New York, 1971.

75. Bardenheuer P. and Brauns E. Mitt Kaiser-Wilhelm - Inst. Eisenforsch., 17, 1935, 127-32.

76. Phillips B., Hutta J.J. and Warshaw I. J. Am. Ceram. Soc., 46, (12) 1963, pp 579-83.

77. Ringwood A.E. Geochim. Cosochim. Acta. 10, 1956, 297.

78. Lebedev B.G. and Levitskii V.A. Zh. Fiz. Khim., 35, 1961, pp 2788-2790.

79. Burdese A., Abbattista F. and Damiani R. Metall. Ital., 1963, pp 557-9.

80. Cambell F.E. and Roeder P. Amer. Mineralogist, 53, Jan-Feb. 1968, P 257.

81. Taylor R.W. and Schmalzried H., J. Phys. Chem., 68 (9), 1964, pp 2444-2449.

82. Navrotsky A., J. Inorg. Nucl. Chem., 33, 1971 pp 4035-4050.

83. Spencer J.P., N.P.L. Report Chem. 21, Feb. 1973.

84. Carbo-Novo. J. Ph.D. Thesis, London University, 1969.

85. Muck O. German Patent, No. 422 004, 1923.

86. Okress E.C. et al., J. Appl. Phys., 23, 1952, pp 545-52.

87. Jenkins A.E., Harris B., Baker L.A. Symposium in Metallurgy at High Temperatures and High Pressures, T.M.S. - A.I.M.E. Conf., 1964. Vol. 22. pp 23-43.

88. Peifer W.A., J. Metals, 17, 1965, pp 487-493.

89. Price E.G. M.Sc. Thesis 1961. School of Metallurgy, Univ. N.S.Wales, Australia.

90. Lewis J.C. et al. J. Sci. Instr., 39, 1962, p 569.

91. Oliver B.F. Trans. T.M.S. - A.I.M.E., 227, 1963, P 996.

92. Begley R.T. et al., Rev. Sci. Instr., 30, 1959, p 38.

93. Mills K.C. and Kinoshita K. J. Metals, 16, 1964, P. 107.

94. Jenkins A.E. and Robertson D.G.C. Aust. I.M.M. Monograph No. 2, pp 1-5.

95. Turkdogan E.T. Trans. A.I.M.E., 230, 1964, pp 740-50.

96. Turkdogan E.T. and Mills K.C. Trans A.I.M.E. 230, 1964, pp 750-53.

97. El-Mehairy A.E. and Ward R.G. Trans. A.I.M.E., 227, 1963, p 1226.

98. Shiraishi S.Y. and Ward R.G. Can. Met. Quart, 3, 1964, pp 118-22.

99. Fraser M.E., Lu W.K., Hamielec A.E. and Murarka R. Met. Trans., 2, 1971, pp 817-823.

100. Toop G.W. and Richardson F.D. In "Advances in Extractive Metallurgy", (London: Inst. Min. Metall, 1968) pp 181-205.

101. Glen C.G. Ph. D. Thesis 1968, Univ. of London.

102. Forster A. Ph. D. Thesis 1968, Univ. of London.

103. Distin P.A., Hallett G.D. and Richardson F.D. J.I.S.I., 206, 1968, pp 821-33.

104. Baker L.A., Warner N.A., Jenkins, A.E. Trans. A.I.M.E., 239, 1967 pp 851-864.

105. Baker L.A. and Ward R.G., J.I.S.I., 205, 1967, pp 214-7.

106. Baker L.A., Warner N.A. and Jenkins A.E. Trans. A.I.M.E., 230, 1964, 1228.

107. Roberts O.C., Robertson D.G.C. and Jenkins A.E. Trans. A.I.M.E., 245, 1969, pp 2413-2420.

108. Caryll D.B. and Ward R.G. J.I.S.I., Jan. 1967, pp 28-31.

109. Booth A.R. and Charles J.A. Iron Steel, London., 42, 1969, p 298.

110. Knights C.F. and Perkins R. Trans. I.M.M., Sept. 1970, C197-206.

111. Distin P.A., Whiteway S.G. and Masson C.R. Can. Met. Quart., Vol. 10, (1), P 13.

112. "Techniques of Metals Research", New York: Wiley-Interscience, 1970, Vol. IV, part 1, Chap. 4B.

113. Diaz C.M. and Richardson F.D., Inst. Min. Metall., 76, 1967, p 196.

114. Mah A.D. et al. Rep. Invest. U.S. Bur. Mines 7026, 1967, 20 p.

115. Kellogg H.H. J. Chem. Eng. Data., 14, (1), 1969, pp 41-44.

116. Warner J.S., I.N.C.O. Report, 1968.

117. Steele B.C.H. In "Electromotive Force Measurements in High Temperature Systems", Alcock C.B., ed., I.M.M., London 1968.

118. Kubaschewski O., Evans E., Alcock C.B. "Metallurgical Thermochemistry" Pergamon Press, 1967.

119. Phillips C.S.G. and Williams R.J.P. "Inorganic Chemistry", Clarendon Press, 1965.

120. Wells A.F.""Structural Inorganic Chemistry", Clarendon Press, 1962.

121. JANAF Thermochemical Tables, the Dow Chemical Company, Midland, Michigan, 1965.

122. Edwards R.K. and Brodsky M.B. Amer. Chem. Soc., 78, 1956, p 2983.

123. Elford L. Muller F. and Kubaschewski O. Berichte der Bunsengesellschaft, 73, Nr. 6, 1969, p. 601.

124. Hultgren, Orr, Anderson and Kelley. "Selected Values of Thermodynamic Properties of Metals and Alloys". John Wiley and Sons Inc., New York, 1963.

125. Hultgren R. and Pramod D. INCRA Monograph 1.

126. Kulkarni A.D. and Johnson R.E. Met. Trans., 4, July 1973, pp 1723-1727.

127. Graph from Masson C.R. J. Am Chem. Soc., 51, (3), pp 134-143.

128. Smith I.B. and Masson C.R. Can. J. Chem., 49, (5), 1971, pp 683-690.

129, Bell H.B. J.I.S.I., Feb. 1963, pp 116-121.

130. Seshadri S.K. Ph.D. Thesis, London, 1973.

131. Ray H.S. Indian J. Technol.,1, (6), 1969, pp 188-94.

132. Lange A. In "Advances in Extractive Metallurgy", (London: Inst. Min. Metall., 1968) pp 206-223.

133. N.B.S. Technical Notes 270-3 and 270-4., National Bureau of Standards, Washington D.C.

134. O'Bryan H.M., Monforte F.R. and Blair R., J. Am. Ceram. Soc., 48, (11), 1965, p 579

135. Gadella A.M.M. and White J. Trans. Brit. Ceram. Soc., 65, (1), 1966, pp 1-17.

136 Huang P-Y. and Hayward C.R. Am. Inst. Min. Metall. Eng. Tech. Pub. No. 2140, 19 p.

137. Kulkarni A.D. Met. Trans. 4, July 1973, pp 1713-1721.

138. Tankins E.S. Can. Met. Quart., 9, 1970, pp 353-57.

Guide to Experimental Runs. TABLE 3.1

Alloy	Code	Slag	CO_2/CO	Temp. Range °C
10% Au/Cu	CB(a)	B	2.028	1300-1450
"	CB(b)	B	20.53	"
"	CC(a)	C	1.732	"
"	CC(b)	C	8.471	"
"	CC(c)	C	36.09	"
"	CD(a)	D	1.741	"
"	CD(b)	D	8.447	"
"	CD(c)	D	21.45	"
"	CD(d)	D	25.93	"
"	CE(a)	E	1.736	"
"	CE(b)	E	5.040	"
10% Ni/Cu	N10C(a)	C	2.00	1350-1500
"	N10B(a)	B	5.00	"
"	N10B(b)	B	12.0	"
"	N10E(a)	E	5.00	"
20% Ni/Cu	N20B(a)	B	2.27	1350-1500
"	N20B(b)	B	5.00	"
"	N20C(a)	C	8.36	"
"	N20E(c)	B	16.4	"
"	N20E(a)	E	2.26	"
"	N20E(b)	E	5.00	"
"	N20E(c)	E	8.62	"
35% Ni/Cu	N35C(a)	C	2.00	1350-1500
"	N35B(a)	B	5.00	"
"	N35B(b)	B	12.0	"
"	N35E(a)	E	5.00	"
50% Ni/Cu	N50C(a)	C	8.55	1350-1500
"	N50E(a)	E	8.52	"